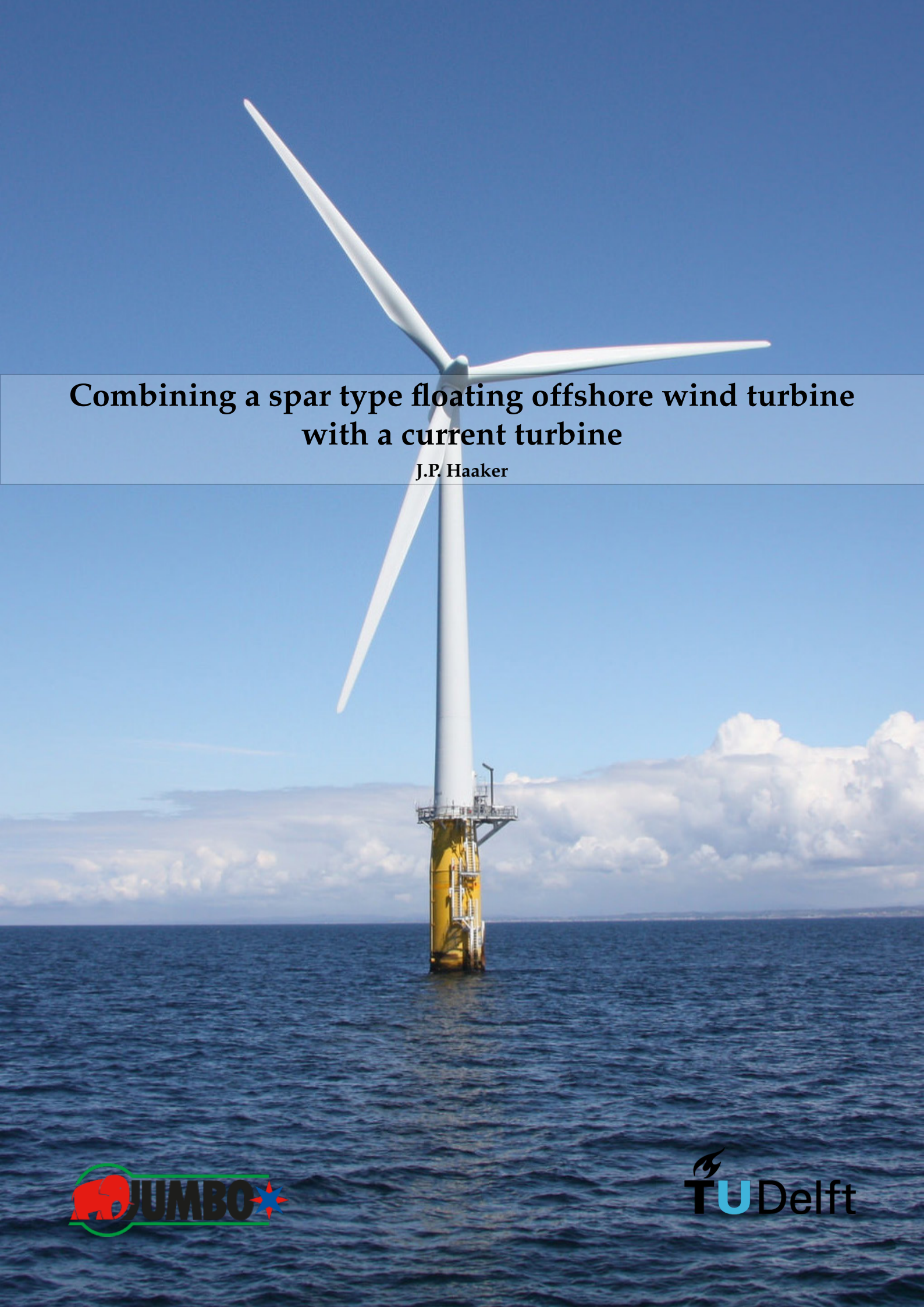

Combining a spar type floating offshore wind turbine with a current turbine

J.P. Haaker

JUMBO

TUDelft

Combining a spar type floating offshore wind turbine with a current turbine

by

J.P. Haaker

to obtain the degree of Master of Science

at the Delft University of Technology,

to be defended publicly on Thursday April 19, 2018 at 02:00 PM.

Student number:	4087925	
Project duration:	May 8, 2017 – April 19, 2018	
Thesis committee:	Prof. dr. ir. A. P. van 't Veer,	TU Delft, supervisor
	Ir. J. den Haan,	TU Delft
	Dr. ir. H. Polinder,	TU Delft
	Ir. K. van der Heiden,	Jumbo Maritime, supervisor

This thesis is confidential and cannot be made public until June 19, 2018.

TU Delft

Preface

This master thesis is submitted as part of the requirement for obtaining the degree of Master of Science in Offshore Engineering at the Delft University of Technology. The supervision from the Delft university of technology has been done by Prof.dr.ir. A.P. van 't Veer and Ir K. van der Heiden has been the supervisor from Jumbo Maritime.

Looking back from when I started, I must say that these past 11 months have been an enormous experience. I would like to express my gratitude towards Jumbo Maritime for hosting me these past 11 months. A special thanks to Kasper van der Heiden, my daily supervisor at Jumbo Maritime, for supporting me throughout my time at Jumbo. Sitting opposite of me and answering my endless stream of questions, Kasper thank you very much! I would also like to thank my fellow graduate students Michel, Sjoerd, Lex, Duke and Nicky for their positivity and the countless laughs we had during our various coffee breaks. Thank you to Joost den Haan, for helping me throughout my thesis and being part of my graduation committee. Thank you to Niels, for our discussions at the coffee breaks at the university. Thank you to Jeffrey for reading and remarking my thesis. Thank you to Henk Polinder for being part of my graduation committee. And finally a very special thank you to my family for their continuous support throughout my thesis.

Joeri Haaker

Delft, April 2018

Abstract

With the shift towards a more sustainable energy society, the increase in the electricity produced by renewable energy sources is steadily rising. However the cost of renewable energy sources still remains high compared to the traditional fossil fuel based energy sources. With the total worldwide energy demand also rising, combining renewable energy sources helps to reduce the cost through a shared infrastructure and increase in energy production. This thesis investigates the feasibility of a combination of floating offshore wind and marine current energy. As a basis the Hywind spar type floating offshore wind turbine is used. This 5 MW system is combined with a 1 MW marine current turbine. The characteristics of the current turbine will be examined with the program Aerodyn and the blades are designed with the program Harp_opt. As a cost reduction, the effect of scaling down the weight of the mooring system in combination with reversing the thrust of the current turbine is also investigated.

The program ANSYS AQWA is used to investigate the dynamic behavior of the combined system. The thrust forces of the wind and current turbines are calculated via an external python server and added to the simulation in AQWA. The structure is modeled in a rigid body approximation, assuming no structural deformations. The behavior of the combined system is investigated in 3 operational and 1 survival load case. The operational load cases represent the environmental conditions of the cut-in, rated and cut-out wind speed of the wind turbine. In the fourth load case the system is subjected to survival conditions and the direction of the thrust of the current turbine is reversed. The environmental conditions are simulated with a steady wind velocity and the sea state is modeled using the JONSWAP wave spectrum. In all 4 load cases the system is subjected to a strong current.

By using a levelized cost of energy prediction model, a first estimation of the levelized cost of energy of the combined system is obtained. Adding a current turbine to the Hywind spar increases the cost of the initial investments and operational cost of the system, but also increases the total energy generation. Compared to the original Hywind spar, adding a current turbine to the system lowers the levelized cost of energy from 149.4 €/MWh to 142.3 €/MWh. Scaling down the weight of the mooring system lowers the levelized cost of energy to 141.9 €/MWh.

From the results of the simulations it is found that using the current turbine during survival conditions has a positive effect on the motions and maximum tension in the lines. It is concluded that by using the thrust of the turbine the weight of the mooring system could be scaled down, but the effect on the levelized cost of energy is minimal and doesn't justify the increased risk of failure.

Contents

Preface **i**

Abstract **ii**

1 Introduction **1**
1.1 Background . . . 1
1.2 Thesis objective . . . 2
1.3 Thesis approach . . . 2
1.4 Thesis structure . . . 3

2 Marine Current **4**
2.1 Marine current energy . . . 4
2.2 Marine Current Turbines . . . 5
2.3 Rotor design . . . 5
2.3.1 Blade Element Momentum Theory . . . 5
2.3.2 Blade design . . . 6
2.4 Calculations turbine . . . 7
2.4.1 Turbine characteristics . . . 7

3 Offshore wind **10**
3.1 Offshore wind foundations . . . 10
3.2 NREL Hywind spar . . . 11
3.3 Tower structural properties . . . 12
3.4 NREL 5 MW reference wind turbine . . . 13

4 Environmental Loads **14**
4.1 Aerodynamic loading . . . 14
4.1.1 Aerodynamic loading structure . . . 14
4.1.2 Aerodynamic loading rotor . . . 15
4.2 Hydrostatic loading . . . 18
4.3 Hydrodynamic loading . . . 20
4.3.1 Oscillating loads . . . 20
4.3.2 Wave exciting loads . . . 21
4.3.3 Viscous drag . . . 24
4.3.4 Hydrodynamic loading rotor . . . 24
4.4 Load cases . . . 25
4.4.1 Operational mode . . . 27
4.4.2 Survival mode . . . 27

5 Model description **28**
5.1 Model parameters . . . 28
5.1.1 Geometry . . . 28
5.1.2 Mass properties . . . 29
5.1.3 Viscous drag . . . 29

5.1.4 Mesh . . . 30
5.2 Hydrodynamic added mass and damping coefficients . . . 30
5.2.1 Additional damping matrix . . . 31
5.3 Wind coefficients . . . 32
5.4 External python server . . . 32
5.5 Mooring system . . . 33
5.5.1 Mooring configuration 1 . . . 34
5.5.2 Mooring configuration 2 . . . 36
5.5.3 Cable dynamics . . . 37

6 Results & Discussion **39**
6.1 Operational mode . . . 39
6.2 Survival mode . . . 41
6.2.1 Load case 4, mooring configuration 1 . . . 42
6.2.2 Load case 4, mooring configuration 2 . . . 43
6.3 Levelized Cost of Energy . . . 45
6.3.1 LCOE breakdown . . . 46
6.3.2 Levelized Cost of Energy . . . 50
6.4 Discussion . . . 50

7 Conclusion & Recommendations **52**
7.1 Conclusion . . . 52
7.2 Recommendations . . . 54

A Wind coefficients **55**

B External python server **59**

C SERI 8PT Hydrofoil **62**

D Results Load case 1 **64**

E Results Load case 2 **68**

F Results Load case 3 **72**

G Results Load case 4 **76**

H Levelized Cost of Energy model **83**

Bibliography **93**

List of Figures

2.1 The blade is divided into several segments (elements) (Viré, 2016) . . . 5
2.2 Lift L and drag D (Viré, 2016) . . . 6
2.3 Normal and tangential forces (Viré, 2016) . . . 6
2.4 The power coefficient against TSR . . . 8
2.5 The coefficients of power C_p, and thrust C_t . . . 9

3.1 Different foundation types for offshore wind turbines (Kumar et al., 2016) 10
3.2 Impression of the Hywind spar foundation (Jonkman, 2010) . . . 12
3.3 Thrust and power characteristics (Jonkman et al., 2009) . . . 13

4.1 Pressure and velocity drop over disk (Viré, 2016) . . . 15
4.2 Actuator disk model (Viré, 2016) . . . 16
4.3 The effect of platform motions at hub height on relative wind velocity (Curfs, 2015) . . . 17
4.4 Thrust curve including different induction factors (Curfs, 2015) . . . 18
4.5 The position of centers of buoyancy and gravity (Khair Al-Solihat and Nahon, 2015) . . . 19
4.6 General wave characteristics (Journee, Massie, and Huijsmans, 2015) . . 21
4.7 Irregular sea created as a super position of regular waves (Journee, Massie, and Huijsmans, 2015) . . . 22
4.8 Irregular Wave, $H_{1/3}$ = 2.5m, T_p = 7s . . . 23
4.9 Drag factor of a cylinder (Male, 2017) . . . 24
4.10 Reversed thrust during survival mode . . . 25
4.11 Relation between $H_{1/3}$ and Beaufort wind scale (Journee, Massie, and Huijsmans, 2015) . . . 26
4.12 The direction of the wind and waves . . . 26

5.1 The geometry of the spar floater . . . 29
5.2 Panel mesh of the model . . . 30
5.3 Hydrodynamic added mass and damping coefficients . . . 31
5.4 Wind force coefficients, operational mode . . . 32
5.5 Wind moments coefficients, operational mode . . . 32
5.6 Delta configuration the Hywind spar (Steen, 2015) . . . 33
5.7 Mooring line schematic layout (Karimirad and Moan, 2012) . . . 36
5.8 Surge motions structure . . . 37
5.9 Sway motions structure . . . 38
5.10 Tension mooring line 1 . . . 38

6.1 Surge and Pitch motions, operational load cases . . . 40
6.2 Maximum tension mooring lines, operational load cases . . . 41
6.3 Maximum tension mooring lines, wind and current turbine parked . . . 42
6.4 Surge and Pitch motions, with and without the CT . . . 42
6.5 Maximum tension mooring lines, with and without the CT . . . 42

6.6 Surge and Pitch motions for the 2 mooring configurations 43
6.7 Maximum tension mooring lines for the 2 mooring configurations . . . 43
6.8 Ratio between min breaking load and max tension of the lines 44
6.9 Simplified explanation of the LCOE (EWEA, 2009) 45
6.10 LCOE cost break down for the base case of the reference case by Myhr et al. 46

A.1 Wind force coefficients, operational mode 56
A.2 Wind moments coefficients, operational mode 57
A.3 Wind force coefficients, survival mode 57
A.4 Wind moments coefficients, survival mode 57

D.1 The motions of the structure, load case 1, direction current 0° 64
D.2 Tension mooring lines, load case 1, direction current 0° 65
D.3 The motions of the structure, load case 1, direction current 180° 66
D.4 Tension mooring lines, load case 1, direction current 180° 67

E.1 The motions of the structure, load case 2, direction current 0° 68
E.2 Tension mooring lines, load case 2, direction current 0° 69
E.3 The motions of the structure, load case 2, direction current 180° 70
E.4 Tension mooring lines, load case 2, direction current 180° 71

F.1 The motions of the structure, load case 3, direction current 0° 72
F.2 Tension mooring lines, load case 3, direction current 0° 73
F.3 The motions of the structure, load case 3, direction current 180° 74
F.4 Tension mooring lines, load case 3, direction current 180° 75

G.1 The motions of the structure, load case 4, current turbine parked 77
G.2 Tension mooring lines, load case 4, current turbine parked 78
G.3 The motions of the structure, load case 4, current turbine operational . . 79
G.4 Tension mooring lines, load case 4, current turbine operational 80
G.5 The motions of the structure, load case 4, current turbine operational . . 81
G.6 Tension mooring lines, load case 4, current turbine operational 82

List of Tables

2.1 Turbine design criteria 6
2.2 Blade Layout 7

3.1 Floating Platform Structural Properties 12
3.2 NREL 5MW wind turbine properties 13

5.1 System mass properties 29
5.2 Additional linear damping 31
5.3 mooring system properties 34
5.4 6x36 mooring line 34
5.5 Mooring line specifications 36
5.6 Smaller mooring line setup 2 36
5.7 Mooring line specifications 37

6.1 Cost clump weights 47
6.2 Cost mooring lines 47
6.3 Cost mooring configuration normalized to cost per MW 48
6.4 CAPEX, original Spar 48
6.5 CAPEX, combined system, mooring configuration 1 49
6.6 CAPEX, combined system, mooring configuration 2 49

A.1 Wind coefficients operational condition 57
A.2 Wind coefficients Survival condition 58

List of Abbreviations

BEMT	Blade Element Momentum Theory
CAPEX	Capital Expenditures
COG	Center of Gravity
CM	Center of Mass
CSA	Cross Section Area
DECEX	Decommission Expenditures
DNV	Det Norske Veritas
DOF	Degree Of Freedom
EU	European Union
ECN	Energieonderzoek Centrum Nederland
EWEA	European Wind Energy Association
FWT	Floating Wind Turbine
FOWT	Floating Offshore Wind Turbine
FRA	Fixed Reference Axes
GPa	Gigapascal
GW	Gigawatt
GWEC	Global Wind Energy Council
HACT	Horizontal Axis Current Turbine
IEA	International Energy Agency
IWRC	Independent Wire Rope Core
JONSWAP	Joint North Sea Wave Project
kN	Kilonewton
LCOE	Levelized Cost of Energy
MCT	Marine current turbine
MPA	Megapascal
MSL	Mean Sea Level
MW	Megawatt
NASA	National Aeronautics and Space Administration
NREL	National Renewable Energy Laboratory
O&M	Operations and Maintenance
OPEX	Operating Expenditures
R&D	Research and Development
RPM	Revolutions Per Minute
SWL	Still Water Level
TSR	Tip Speed Ratio
UNFCCC	United Nations Framework Convention on Climate Change
WS	Warrington Seale
3D	3 dimensional

List of Symbols

a	Axial induction factor
$A_{i,j}$	Added mass coefficient
A	Area
A_W	Water line area
α	Wind profile component
$B_{i,j}$	Damping coefficient
β	Direction wind and waves
C_d	drag factor
C_p	Power coefficient
C_t	Thrust coefficient
D	Diameter
dA	Projected area
$\delta_{i,3}$	(i,3) component of the Kronecker-Delta function
Δ p	Pressure difference
E	Modulus of elasticity
E_T	Energy generation
η	Wave elevation
ϵ_n	Random phase angle component
F	Force
g	Gravity constant
γ	Peak enhancement factor
H	Wave height
$H_{1/3}$	Significant Wave height
h	Water depth
I	Water plane moment of inertia
I_t	Investments
k	Wave number
$K_{i,j}^{Hydrostatic}$	Hydrostatic stiffness matrix
λ	Tip Speed Ratio
λ_w	Wave length
m	Mass
M_t	Operation and maintenance cost
$\dot{m}$	Mass flow
∇	Displaced volume
ν	Kinematic viscosity
ω	Wave frequency
ω_p	Peak wave frequency
P	Power
r	Discount rate
S_ζ	Wave spectrum
σ	Spectral width parameter
ρ	Density

T	Thrust
T	Wave Period
t	Time
θ	Wind angle
U	Wind velocity
U_e	Wind velocity far away
U_r	Wind velocity at rotor
X_J	Degrees of freedom platform
Z	Height along tower
Z_r	Reference height
z_b	Distance center of buoyancy to still water level
z_g	Distance center of gravity to still water level
ζ_a	Wave amplitude

Chapter 1

Introduction

1.1 Background

On the 12th of December 2012 at the Paris climate conference, 196 countries around the world adopted the first ever legally binding global climate deal. This climate deal tries to reduce and mitigate the effects of global warming (UNFCCC, 2015). Before this agreement, the European parliament already defined their own objectives to lower the emission of green house gases. These objectives state that all European member states should have a reduction of 20% energy savings by 2020. These targets where updated in 2014 and replaced by the 2030 Framework (European Commission, 2014). This new framework states a 40% cut in green house gases, at least a 25% share of renewable energy and a further increase in energy efficiency of 25% by 2030.

Wind energy is currently the fastest growing clean and renewable energy source. Data provided by the global wind energy council state that the global cumulative installed capacity in 2016 was almost 500 GW, from which around 14 GW is installed offshore (GWEC, 2016). Although most installed wind power is still land based, offshore wind provides various advantages: a stronger and more stable wind climate, fewer restrictions in terms of noise and size, resulting in larger turbines.

The installed capacity of offshore wind is steadily rising. As of 2016 there is a total of 14 GW of installed offshore wind power capacity in 14 markets around the world. Of this global capacity, nearly 88% is located in waters off the coast of ten European countries (GWEC, 2016). The majority of the European offshore wind parks are located in the North Sea. With an average depth of 74 meters (Velema, 2010), large parts of the North Sea are shallow enough to make bottom-fixed foundations the most economical solution. However around 80% of all the European offshore wind resources are located in water depths of 60 meters and deeper. At this depth, floating wind foundations could be more economical than traditional bottom-fixed foundations (WindEurope, 2017).

Wind energy alone is not enough to achieve these ambitious goals. Other sources of renewable energy need to be developed and used. With a vast potential worldwide, marine current energy is one of the most attractive and promising renewable energy sources. One of the main advantages of using current energy, is the relatively high predictability of the (tidal) current resources, resulting in an accurate power production predictability.

Europe is currently leading in the development and testing of current (tidal) energy converters. More than 50% of all current (tidal) energy technology is located in European test centers and deployment sites. Despite recent progress, to date no tidal

energy projects have reached the level of being competitive with other forms of renewable energy. However, due to the high predictability, marine current technology remains an attractive and promising renewable energy source. To facilitate the development of this technology, the European Commission launched the Blue Energy Communication in January of 2014. This communication initiated the creation of the Ocean Energy Forum, a platform to bring ocean energy actors and stakeholders together to discuss issues and identify viable solutions for the development of ocean energy. This is done to realize the target, set by the European Commission, of having a combined wave and tidal capacity of 100 GW installed by 2050 (Magagna and Uihlein, 2015).

Due to the similarities of both techniques a combination between offshore wind and marine current seems logical. Knowledge gained from the offshore wind industry can be used to reduce the cost of marine current energy, because one of the problems is the relatively high cost of exploiting marine current energy. Combining multiple renewable energy sources helps to reduce the cost through a shared infrastructure and increase in energy production per platform.

1.2 Thesis objective

The objective of this thesis is to investigate the feasibility of a hybrid concept based on a combination of marine current and offshore wind energy production, in which the marine current turbine may be used as a form of station keeping. During normal operations both the wind and current turbines are used to generate electricity. During survival conditions, the wind turbine is shutdown to prevent damage and the direction of the thrust of the marine current turbine is reversed to help lower the resulting loads at the mooring system. Before the combined system is modeled, both systems will be investigated separately, to gain a better understanding into the behavior of a combination of both systems. After this investigation is done, both systems can be combined into a model which can be tested under various circumstances. With these results, a first estimation of the effect of adding a current turbine to the system on the levelized cost of energy is obtained. Lastly, as a cost reduction strategy the effect of scaling down the weight of the mooring system on the levelized cost of energy of the combined system will also be investigated.

1.3 Thesis approach

As mentioned in the beginning of this thesis, there is currently a shift from a fossil fuel based energy market to a more sustainable market. A literature study on different forms of renewable energy is done, from which offshore wind and marine current energy emerged as two promising ways to a more sustainable future. A combination of both offshore wind and marine current on one platform may be interesting, since marine current and offshore wind turbines use similar techniques to generate electricity. In order to understand the complex behavior of a combined wind and current energy platform, a model has to be created. Before this model is created, a understanding of the environmental conditions to which the model will be subjected to is needed.

After these conditions are known, a model of the combined system will be created. This model will be created within ANSYS AQWA. At first the model will only be subjected to hydrodynamical loading of the spar structure, which is used to check how the model behaves. Later the aerodynamic loading of the rotor and top structure will be included. Next, the hydrodynamic loading of the turbine under normal operating conditions and the effect of reversing the thrust direction during survival conditions will be investigated. After these results are known, an estimation of the effect of adding a current turbine to the levelized cost of energy is given.

1.4 Thesis structure

The first chapter gives background information about the need for increasing the exploitation of renewable energy sources. To achieve these goals, multiple sources of renewable energy are needed. The second chapter starts by explaining the benefits of using marine current energy. A rudimentary turbine is designed which is later used within the model. The third chapter gives a overview of the different foundations which are currently being used in the offshore wind industry. From these different foundations, the Hywind spar is chosen as a basis for this thesis. In order to describe the behavior of the model, a realistic environment needs to be created. Chapter 4 describes the different environmental loads the system will encounter. Chapter 5 describes the different parameters which make up the model within the program ANSYS AQWA. After a diffraction analyses, multiple simulations under different environmental conditions are done. The results of these simulation can be found in chapter 6 and will be used to give and estimation of the levelized cost of energy of the combined system. In the final chapter these results are used to give a conclusion about the combination of a floating offshore wind turbine with a current turbine. This will be followed by recommendations for further research.

Chapter 2

Marine Current

In this chapter a conceptual marine current turbine is designed and the properties of the turbine will investigated to see what the possibilities are for reversing the direction of the thrust of the turbine. This thrust will be used during survival conditions as a form of station keeping and it is investigated if this thrust can be used in combination with scaling down the weight of the mooring system as a cost reduction strategy. In the beginning of this chapter a brief introduction of the different forms of marine energy will be given. Next the rotor will be designed and the characteristics of the turbine are investigated. After the characteristics of the turbine are known, they can be added to the model in chapter 5 to create a hybrid system consisting of wind and current energy systems.

2.1 Marine current energy

As stated in chapter 1, one of the advantages of marine current is its high predictability. Marine currents mainly consist of the gravitational interaction of the Earth-Moon-Sun system, which causes the rise and fall of tides. These gravitational interactions make marine currents so predictable, but marine currents are also influenced by temperature and salinity differences and by the Coriolis effect (Bahaj, 2011). Current energy can be harvested at two different ways. One way of harvesting current energy is by building a dam or barrage across a bay. As the tide flows in and out, the dam creates a head difference on both sides. When this difference is high enough the sluice gates are opened and water flows through a turbine, which will generate electricity. This technique, which is limited with coastal area's with a specific set of requirements, has a huge impact on the local environment. Another way of harvesting current energy is by using marine current turbines (MCT). These current turbines, which are similar in technique to wind turbines, have some advantages over tidal barrage systems. Due to their relatively small size their environmental and visual impact is less and floating current turbines can also be used in deep water areas where building a barrage is not possible. The focus of this thesis lies on floating marine current turbines.

2.2 Marine Current Turbines

In recent years, various horizontal and vertical axis marine current turbines have been developed and reported in the literatures. Almost all turbines currently under development are superficially similar to wind turbines. Horizontal axis turbines represent the most common type of current energy converters and account for 76% of R&D efforts in the development of MCT's worldwide (Magagna and Uihlein, 2015). There are however some differences between wind and current turbines. Current turbine blades typically have smaller aspect ratio (chord/blade length) and greater thickness due to high root bending moments. Apart from these differences there is also the possible occurrence of cavitation and there are differences in the stall characteristics and in the Reynolds number (Batten et al., 2006).

2.3 Rotor design

For this master thesis a rudimentary design of the blades is iteratively obtained through the program HARP_Opt. This program, which stands for Horizontal Axis Rotor Performance Optimization, uses a multiple-objective (maximizing energy production or blade efficiency) algorithm and uses blade element momentum theory to design horizontal axis wind and current turbine rotor blades (Sale, 2010).

2.3.1 Blade Element Momentum Theory

Blade element momentum theory is a theory that is used to determine the forces acting on blades. In this theory, a blade is divided into several segments and the forces on each segment are calculated separately. Figure 2.1 shows the different shapes of a blade along the length of the blade. Each segment is shaped different and has different characteristics. For each segment the lift and drag forces are calculated. These forces are than used to determine the normal and tangential forces, which are used to calculate the subtracted power and thrust of the blade segment. The subtracted power by each blade element has to be equal and opposite to the change in momentum of the water particles and the total extracted power and thrust is found by by integrating over the length of the blade.

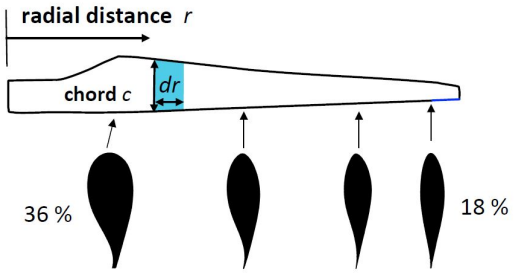

Figure 2.1: The blade is divided into several segments (elements) (Viré, 2016)

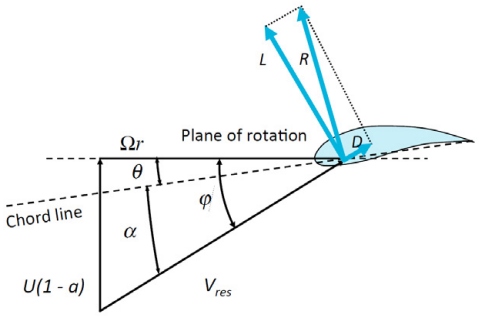

Figure 2.2: Lift L and drag D (Viré, 2016)

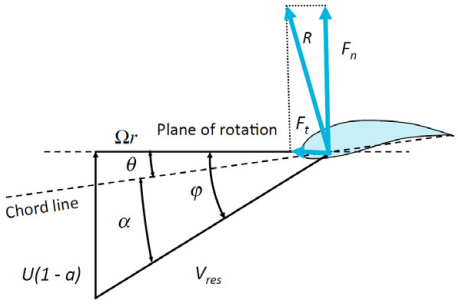

Figure 2.3: Normal and tangential forces (Viré, 2016)

2.3.2 Blade design

HARP_Opt determines the optimal blade shape (twist, chord and airfoil/hydrofoil distributions), for steady and uniform flows (no sheared or yawed flows). To determine the blade shape the following parameters need to be provided:

Table 2.1: Turbine design criteria

Number of blades	3
Number of blade segments	30
Rated power	1 MW
Rotor diameter	20 m
Minimum allowable rotor speed	6 RPM
Maximum allowable rotor speed	15 RPM
Rated tip speed ratio	4.2
ρ_w	1025 kg/m^3
ν_w	1.0e-6 m^2/s
Rated flow speed	2.5 m/s
Family of Hydrofoils	SERI 8PT
Hub height	30 below MSL

The optimization objective for designing this blade was set to most efficient and the available foil thickness where 24, 22, 21, 18 and 16. It should be noted that in a normal blade optimization multiple families of Hydrofoils and more thickness values are used. But such an optimization falls outside the scope of this thesis and the previously mentioned values are enough to create a rudimentary design for the rotor blades. HARP_Opt can interpolate between the thickness values if need be. An example of one of the used Hydrofoils can be found in Appendix C. After iteration HARP_Opt designed a rotor blade with the following properties:

Table 2.2: Blade Layout

Radius	Twist	Chord	hydrofoil
1.15	19.2	0.895	S8xx0861
1.45	29.2	1.09	S8xx0493
1.75	29.2	1.09	S8xx0299
2.05	29.2	1.29	S8xx0209
2.35	29.2	1.38	S8xx0175
2.65	27.4	1.38	S8xx0170
2.95	25.7	1.32	S8xx0166
3.25	24.2	1.25	S8xx0161
3.55	22.8	1.16	S8xx0160
3.85	21.4	1.08	S8xx0160
4.15	20.0	1.00	S8xx0160
4.45	18.8	0.925	S8xx0160
4.75	17.5	0.875	S8xx0160
5.05	16.3	0.794	S8xx0160
5.35	15.2	0.735	S8xx0160

Radius	Twist	Chord	hydrofoil
5.65	14.1	0.683	S8xx0160
5.95	13.1	0.634	S8xx0160
6.25	12.2	0.589	S8xx0160
6.55	11.3	0.548	S8xx0160
6.85	10.4	0.508	S8xx0160
7.15	9.62	0.472	S8xx0160
7.45	8.89	0.436	S8xx0160
7.75	8.24	0.404	S8xx0160
8.05	7.66	0.371	S8xx0160
8.35	7.16	0.341	S8xx0160
8.65	6.72	0.310	S8xx0160
8.95	6.37	0.281	S8xx0160
9.25	6.08	0.252	S8xx0160
9.55	5.89	0.224	S8xx0160
9.85	5.80	0.196	S8xx0160

2.4 Calculations turbine

Now that the rotor has been designed, the turbine needs to be tested under various circumstances. In order to simulate these various circumstances, the program aerodyn is used. The program AeroDyn was originally developed for modeling wind turbine aerodynamics, but equally applies to the hydrodynamics of marine current turbines. AeroDyn can calculate the aerodynamic loads on both the blades and tower. Aerodynamic calculations within the program are based on the principles of actuator lines. In this principle three dimensional flow around a body is approximated by local two dimensional flow at each section. The pressure and shear stresses are approximated by the lift forces and drag forces at each segment. The total hydrodynamic loads are found, by integrating the two dimensional loads along the length of the blade (Jonkman et al., 2015).

2.4.1 Turbine characteristics

The performance of a wind or current turbine is usually characterized with the non-dimensional thrust coefficient C_t and the non-dimensional power coefficient C_p. C_t relates to thrust, a force which the turbine applies to the flow, whilst C_p relates to the the amount of power the turbine can extract from the flow. The mathematical expressions of these coefficients can be found in chapter 4.

As stated in the turbine design criteria, the blade is designed to be optimal for a flow speed of 2.5 m/s, but can also operate at an even wider range of flow speeds. In order to achieve this the turbine needs to be a variable speed turbine. This means that when the flow speed changes, the rotor speed must also change. The ratio between the rotational speed of the turbine and the speed of the flow is normally described by the tip-speed ratio λ, where the tip-speed is the rotational velocity of the tip of the turbine blade.

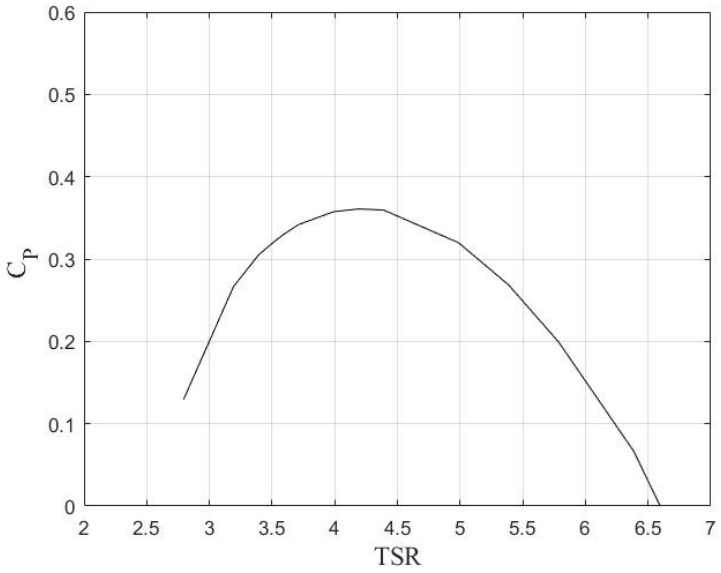

Figure 2.4: The power coefficient against TSR

The figure above shows that the tip-speed ratio is related to efficiency. To generate the optimum power, and keep $C_p = C_{p_{max}}$, the rotational speed of the turbine needs to be adjusted. To control the rotational speed of the turbine, the blades are turned around their longitudinal axis increasing or decreasing the surface area of the blades to the flow. This is called blade pitching. When the speed of the flow is decreased, the blades are pitched to expose more surface area to the flow, and when the speed of the flow increases, the blades are pitched to exposes less surface area to the flow. Changing the pitch of the turbine and subsequently the speed of the turbine, will result in a changed thrust. Thrust is the force a turbine adds to a flow to conserve momentum. The mathematical explanation of thrust can be found in chapter 4. If the blades are pitched far enough the direction of the resulting thrust will flip. This means that the turbine adds energy to a flow instead of subtracting it.

The figures below show the influence of the pitching of the blades of the turbine. The flow speed is kept at 2.5 m/s. The first figure shows the current turbine operating under normal operational conditions. The rotational speed of the turbine is kept at 10 RPM and the blades are pitched to different angles. In this figure the power coefficient is shown against different blade pitch angles. During normal operating conditions, the power coefficient is 0.35 and thrust coefficient is 0.40.

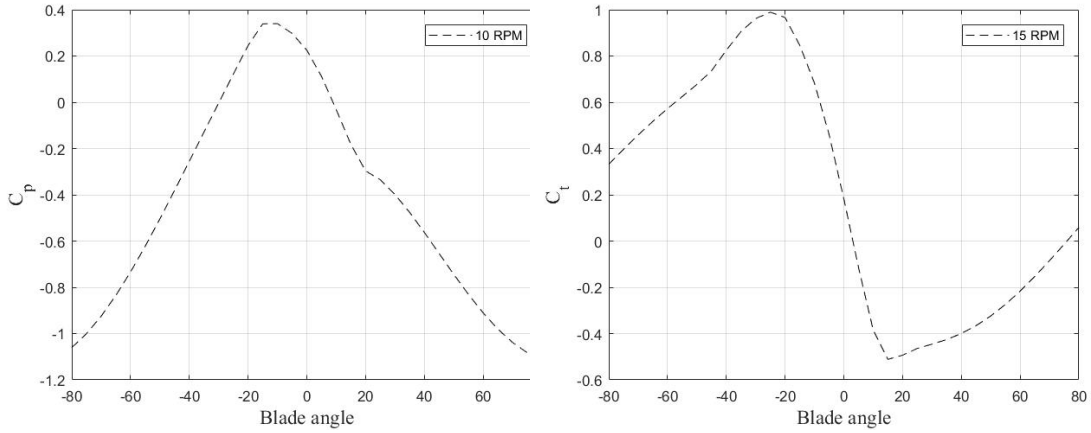

Figure 2.5: The coefficients of power C_p, and thrust C_t

The second figure shows the thrust coefficient of the turbine. In this figure the flow speed is kept at 2.5 m/s but the rotational speed of the turbine is increased to 15 RPM. When the blades are pitched to an angle of 5°, no lift is generated and the resulting thrust will be zero. If the blades are pitched to an angle above 5°, as shown in the figure, the direction of the thrust is flipped. In order to flip this direction power needs to be added to keep the rotational speed of the current turbine constant. Under these circumstances the turbine now operates as a propeller. The highest value of this reversed thrust is at a blade angle of 15°.

Chapter 3

Offshore wind

The offshore wind industry is currently relaying on bottom founded foundations in relatively shallow water. With around 80% of all the European offshore wind resources located in water depths of 60 meter and deeper and with the expected increase in offshore wind generation more wind parks will be placed in deeper water, resulting in the need for new types of foundations. With knowledge gained from the oil and gas industry these new types of foundations are currently being developed. With the increasing water depth, a shift from bottom founded to floating foundations is likely to happen. The focus of this thesis lies on the use of these floating foundations. In the first part of the chapter different ways of stabilize floating foundations will be explained. The next section provides some background information about the first floating offshore wind park in Scotland and the consideration of using the Hywind spar as the basis for this thesis. In the end of the chapter, the characteristics of the tower, wind turbine and the spar are provided. These characteristics will later be used in chapter 5 to create the model of a hybrid system consisting of wind and current energy systems.

3.1 Offshore wind foundations

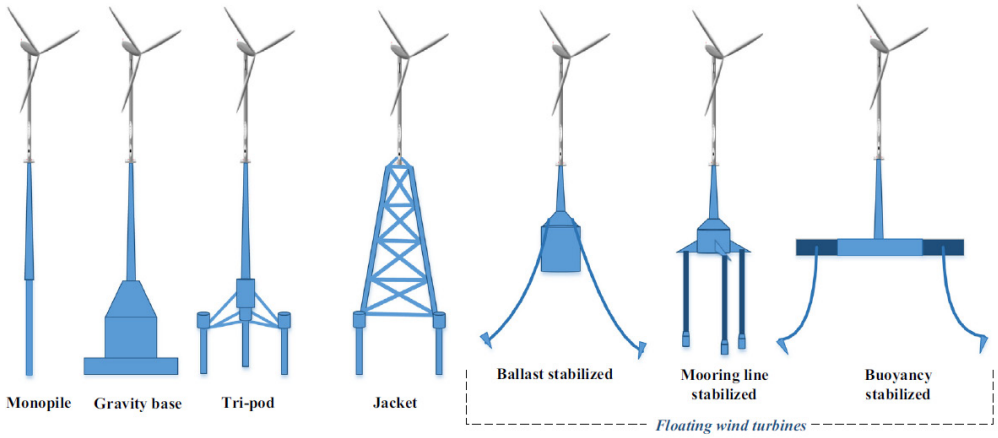

Figure 3.1: Different foundation types for offshore wind turbines (Kumar et al., 2016)

Figure 3.1 shows multiple ways of stabilizing wind turbines. These restoring mechanisms can be expressed by different kind of structures: the restoring by water plane

area moment can be represented by a shallow drafted barge. A deep draft spar represents vertical separation between the structure's center of gravity and the center of buoyancy and a tension leg platform represents restoring by the mooring system. Beside these described classes, it is also possible to have a design which includes the properties of several of these classes. An example of such a design is a semi submersible. This well known design from the oil and gas industry combines stabilization characteristics from both the spar and barge types.

As of October 2017, the world's first floating offshore wind park has started producing energy (Statoil, 2017). This offshore wind park is located 25 kilometers offshore from the town of Peterhead in Aberdeenshire, Scotland. The Hywind Scotland Pilot Park consists of 5 turbines with a turbine capacity of 6 MW per turbine and will power approximately 20,000 households. The floating foundation consists of a spar with a draft of approximately 80 meters (Steen, 2015).

For this research thesis only the deep draft spar foundation is considered. This concept is chosen for its simplicity in design and suitability to modeling. Another consideration for using the spar foundation is due to the fact that the deep draft foundation is the only foundations which is currently used in a floating wind farm. The basis for this thesis will be the 5MW Hywind spar type floating offshore wind turbine from the National Renewable Energy Laboratory (NREL). This system is rated at 5 MW, because for a floating offshore wind system in deep water to be cost effective, a wind turbine must be rated at 5 MW or higher (Musial et al., 2004). Another consideration of using this system comes from the fact that NREL provides all relevant data and works extensively with the wind industry to design and test cost effective wind systems and components (NREL, 2017).

3.2 NREL Hywind spar

As discussed in the previous section, the focus of this thesis lies in the use of the NREL Hywind spar. The NREL Hywind spar is a continuation of Statoil's Hywind demo spar floater (Statoil, 2008). This demonstration wind turbine with a rated power of 2.3 MW, was placed at the coast of Norway where it operated for 8 years helping gain vital insights in the problems regarding the operating of floating wind turbines. Statoil provided NREL with all relevant data to scale up their concept to house the NREL 5 MW reference turbine (Jonkman et al., 2009). The NREL Hywind spar consists of a steel hull of two cylindrical regions connected by a linearly tapered region. The diameter above the taper is more slender to reduce hydrodynamic loads near the free surface. An impression of the platform can be found in figure 3.2. The following properties describe the rest of the platform:

Table 3.1: Floating Platform Structural Properties

Platform draft	120 m
Elevation to Platform Top (Tower Base) Above SWL	10 m
Depth to Top of Taper Below SWL	4 m
Depth to Bottom of Taper Below SWL	12 m
Platform Diameter Above Taper	6.5 m
Platform Diameter Below Taper	9.4 m
Platform Mass, Including Ballast	7,466,330 kg
CM Location Below SWL Along Platform Centerline	89.92 m
Platform Roll Inertia about CM	4,229,230,000 kg*m^2
Platform Pitch Inertia about CM	4,229,230,000 kg*m^2
Platform Yaw Inertia about Platform Centerline	164,230,000 kg*m^2

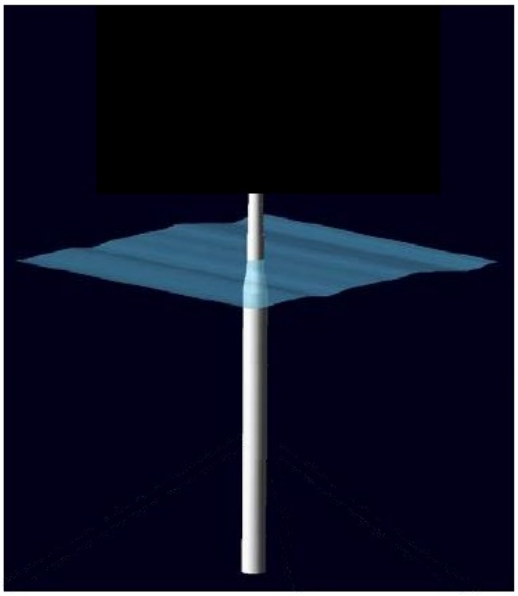

Figure 3.2: Impression of the Hywind spar foundation (Jonkman, 2010)

3.3 Tower structural properties

The base of the tower, which supports the wind turbine, is located at an elevation of 10 m above the still water level and is coincident with the top of platform. The top of the tower is located at a height of 90 meters above SWL. The diameters of the tower varies linearly from a diameter of 6.5 meters at the bottom of the tower, which is similar to the diameter of the platform, to a diameter of 4 meters at the top of the tower. The overall mass of the tower is 249,718 kg and the center of mass is located at 43.4 m along the tower centerline above the SWL (Jonkman, 2010).

3.4 NREL 5 MW reference wind turbine

On top of the tower a NREL 5 MW wind turbine is placed. This baseline wind turbine is a turbine designed by NREL to be applicable both on land as well as offshore (Jonkman et al., 2009). This turbine is a conventional three bladed upwind turbine and uses uses blade pitching as a way of controlling the speed of the turbine. The following information about the wind turbine is provided by NREL:

Table 3.2: NREL 5MW wind turbine properties

Rating	5 MW
Rotor & hub diameter	126 m, 3 m
Hub height	90 m
Cut-in, rated, cut-out speed	3 m/s, 11 m/s, 25 m/s
Rated tip speed	80 m/s
Rotor mass	110,000 kg
Nacelle mass	240,000 kg
Tower mass	249,718 kg
Location of CM	(-0.2m, 0.0m , 64 m)

Apart from these characteristics, NREL also provided power and thrust characteristics of the wind turbine over a wide range of wind speeds. These characteristics are shown in figure 3.3. The purple line at the bottom of the figure shows the thrust curve which is used in chapter 4 to determine the aerodynamic loading of the turbine at higher than rated wind velocities.

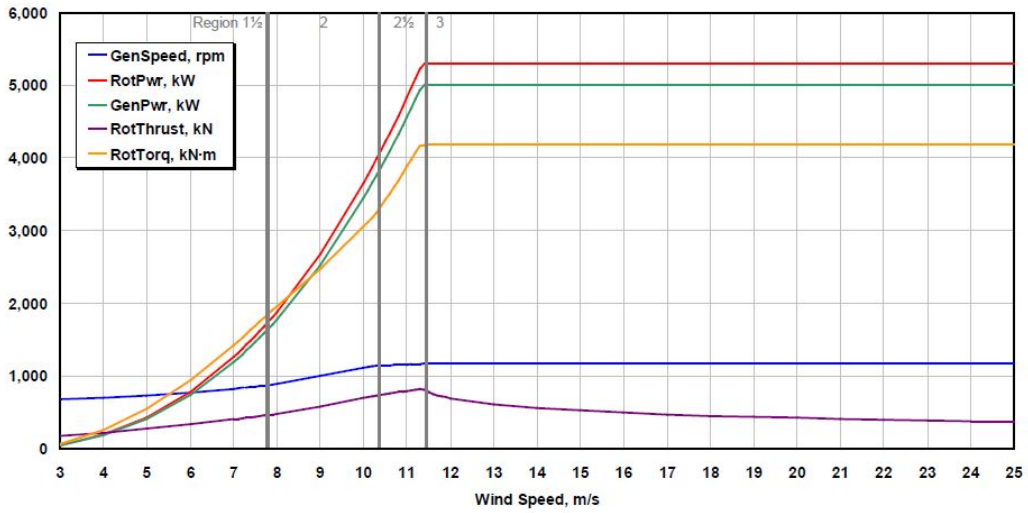

Figure 3.3: Thrust and power characteristics (Jonkman et al., 2009)

Chapter 4

Environmental Loads

Before the complex behavior of a floating spar type system can be understood, it is important to identify what environmental loading the system encounters. In case of the described spar equipped with a wind and current turbine, these loads will be a combination of hydro and aerodynamic loads. In this chapter these loads will be explained. The different load cases which the model will be subjected to will be described at the end of the chapter. These load cases will be a combination of different magnitudes and directions, and will cover both normal operation conditions as well as survival conditions.

4.1 Aerodynamic loading

The aerodynamic loading of a wind turbine is in itself a rather complex phenomenon which is influenced by many factors. Adding a floating foundation will increase the complexity of the aerodynamic loading, because the aerodynamic loading of the turbine is coupled to the dynamic behavior of the substructure (Karimirad, 2011). To stay within the scope of this thesis a more simplified approach of aerodynamic loading on the tower, nacelle and rotor will be used and explained.

4.1.1 Aerodynamic loading structure

The aerodynamic loads on the tower and nacelle are calculated with the following formula:

$$q_{aero}(z) = \frac{1}{2}\,\rho_{air}\,C_D\,U_z\,|U_z|\,dA$$

In this formula U_z is the wind velocity along the height of the structure. C_D is the dimensionless drag coefficient. ρ_{air} is the air density and dA is the projected area.

The variation of the wind velocity over height U_z is defined based on a reference wind speed at z = 90 m:

$$U_z = U_r * (\frac{Z}{Z_r})^{\alpha}$$

In this formula U_r is the wind speed at a reference height Z_r. The vertical coordinate Z varies along the height of the structure and the wind profile component α= 0.11 is based on the guidelines for offshore wind turbine design of DNV (DNV, 2014)

The diameter d of the tower varies from 6 meters at the bottom to 4 meters at the top. To calculate the loads on the tower, the tower is divided into several segments with a different diameter. The height of each segment dZ is 1 meter. The projected area dA is the diameter times the height of a segment. The value of the drag coefficient for the tower, C_D, is 1.2 (Zaaijer, 2017).

The wind speed at hub height is used to calculate the loads on the nacelle and the drag coefficient of a nacelle is approximately 1.2 (Zaaijer, 2017). The value of dA is the frontal area of the nacelle which is found to to be 36 m^2 (Vijfhuizen, 2008).

During survival mode the rotor is parked in a special position and the nacelle will follow the wind direction. In this position all blades are feathered to reduce the frontal area. The value of C_D is that of an airfoil, which is assumed to be 0.04 (NASA, 2015). The value of dA is the lateral area for the blades when feathered, which is 200 m^2 (Vijfhuizen, 2008).

4.1.2 Aerodynamic loading rotor

During normal operating mode the aerodynamic loading on the rotor depends on various circumstances. Among these circumstances are for instance the shape, orientation, rotational speed and size of the blades and the incoming wind velocity. All these circumstances will create a rather complex model which falls outside the scope of this thesis. An approximation for the loads, without the need for a complex model, is by using the actuator disk theory.

In the actuator disk theory the turbine is represented by an ideal cylindrical disk perpendicular to the flow of the medium, which exerts a force on the flow. This force called thrust, is equal to the pressure difference, Δ p , over the area of the disk.

$$T = \frac{\pi}{4} D^2 \, \Delta p$$

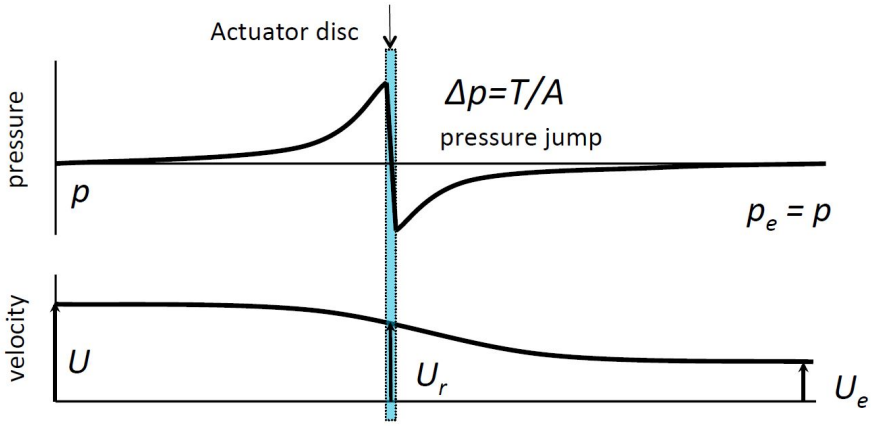

Figure 4.1: Pressure and velocity drop over disk (Viré, 2016)

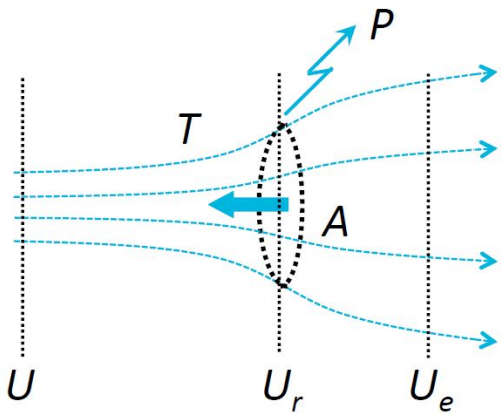

Figure 4.2: Actuator disk model (Viré, 2016)

The thrust force can also be expressed as the change of momentum of the flow:

$$T = \dot{m}\ (U - U_e)$$

Mass flow $\dot{m}$ through the disk is defined as:

$$\dot{m} = \rho_{air}\ U_r\ A$$

The velocity of the air at the disk is the average of the velocity of the incoming air and the air far downstream:

$$U_r = 1/2(U + U_e)$$

As seen in figure 4.2, some air is deflected away from the rotor which causes the air flowing through the disk to have a smaller velocity. The ratio between this velocity and the air velocity far away is called the induction factor a. It should be noted that the induction factor should be smaller than 0.5 for the momentum theory to stay valid:

$$a = (U - U_r)/U$$

After a is defined, it can be used to express the velocity of the flow at the disk and far downstream:

$$U_r = U\ (1 - a)$$
$$U_e = U\ (1 - 2a)$$

The induction factor can also be used to express both the thrust force and the non dimensional thrust coefficient as a function of the air velocity U:

$$T = \dot{m}\ (U - U_e)$$

$$T = \frac{1}{2}\,\rho_{air}\,U\,|U|\,A\,4\,a\,(1-a)$$

$$C_T = \frac{T}{\frac{1}{2}\,\rho_{air}\,U\,|U|\,A} = 4\,a\,(1-a)$$

Apart from describing the thrust, the induction factor can also be used to calculate the subtracted power from the flow and resulting power coefficient:

$$P = \frac{1}{2}\,\dot{m}\,(U^2 - U_e^2)$$

$$P = \frac{1}{2}\,\rho_{air}\,U^3\,A\,4\,a\,(1-a)^2$$

$$C_p = \frac{P}{\frac{1}{2}\,\rho_{air}\,U^3\,A} = 4\,a\,(1-a)^2$$

Now that we have defined a way to calculate the aerodynamic loading of the rotor, it must be coupled to the model. By using the actuator disk model, the aerodynamic loading is defined by the incoming wind velocity perpendicular to the disk. Due to the motions of the platform this disk will not be stationary and the disk will experience a relative wind speed. Figure 4.3 shows the effect of the motions of the platform at hub height. The relevant motions will the translational degree of freedom Surge(X_1) and the rotational degree of freedom Pitch(X_5) times L, the height of the hub from the CM. The resulting relative velocity at hub height will be:

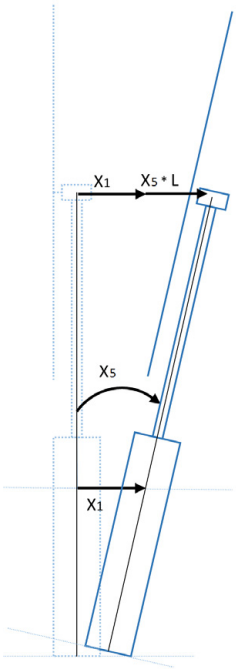

Figure 4.3: The effect of platform motions at hub height on relative wind velocity (Curfs, 2015)

$$U_{hub,rel} = U_{hub} - (\dot{X}_1 + \dot{X}_5 * L)$$

The resulting relative velocity is added to the formula of the thrust, which can than be used to calculate the aerodynamic loading of the rotor when the wind turbines operates.

$$T = \frac{1}{2}\, \rho_{air}\, U_{hub,rel}\, |U_{hub,rel}|\, A\, 4\, a\, (1-a)$$

As mentioned in the beginning of of this chapter, the aerodynamic loading of the rotor is a rather complex phenomenon, which can be simplified by using the actuator disk model. There is however one mayor drawback of using this theory. The theory does not hold over the entire range of wind velocities. At wind velocities higher than the rated wind velocity, the turbine blades will be pitched to ensure a stable power output, but will also lower the thrust. In the picture below the actual thrust curve of the turbine (Jonkman et al., 2009) is shown against the actuator disk model with different induction factors. To incorporate the thrust force at wind velocities higher than the rated wind velocity, an estimation is made which will be added to the model.

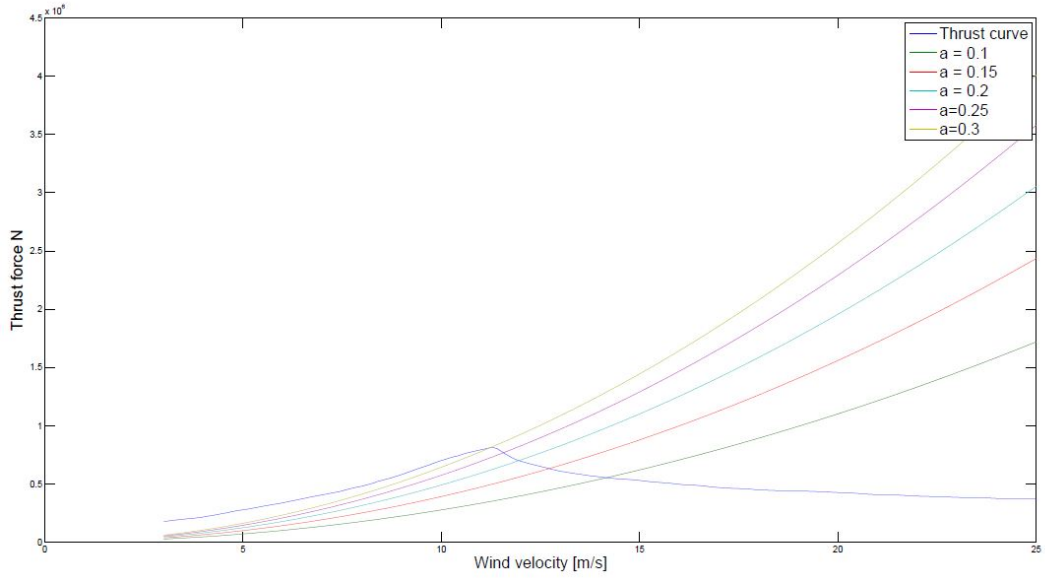

Figure 4.4: Thrust curve including different induction factors (Curfs, 2015)

4.2 Hydrostatic loading

The total load on the floating platform from linear hydrostatics:

$$F_i^{Hydrostatic} = \rho_w\, g\, \nabla_0\, \delta_{i,3}\ - K_{i,j}^{Hydrostatic}\, X_j$$

The first part of this equation represents the buoyancy force from Archimedes principle. which states that the buoyancy force directed vertically upward and equal to

the weight of the displaced fluid when the platform is in its undisplaced position. This term is nonzero only for the vertical heave-displacement. ρ_w is the water density, g is the gravitational acceleration constant, ∇_0 is the displaced volume of fluid when the platform is in its undisplaced position and $\delta_{i,3}$ is the (i,3) component of the Kronecker-Delta function, which is used to indicate that this force is limited to the heave motion only.

The second part of the equation represents the change in the hydrostatic force and moment as the platform is displaced. $K_{i,j}^{Hydrostatic}$ forms the (i,j) component of the hydrostatic restoring matrix formed by effects of the water plane area and center of buoyancy. X_J represent the degrees of freedom of the platform. Both i and J range from 1 to 6 (1 = surge, 2 = sway, 3 = heave, 4 = roll, 5 = pitch, 6 = yaw).

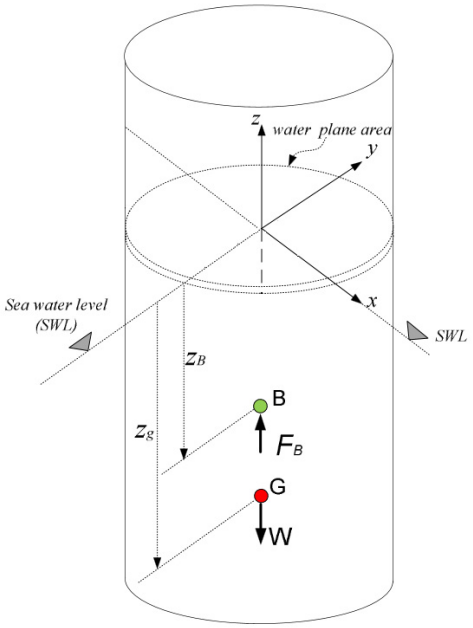

Figure 4.5: The position of centers of buoyancy and gravity (Khair Al-Solihat and Nahon, 2015)

The hydrostatic restoring forces in Surge, Sway and Yaw are zero. The restoring force in those degrees of freedom will come from the mooring system. The restoring force for a spar in Heave is:

$$K_{3,3}^{Hydrostatic} = \rho_w \; g \; A_w$$

In which ρ_w is the water density and figure 4.5 shows A_w, the water plane area of the floater. Due to the symmetry of the spar, the restoring moment in Roll and pitch is the same. The restoring moments in Roll and pitch includes the water plane area's moment of inertia and the position of both the centers of buoyancy and gravity (Journee, Massie, and Huijsmans, 2015). The restoring moments in Roll and Pitch are:

$$K_{4,4}^{Hydrostatic} = \rho_w \; g \; [I_{xx} \; + \; \nabla(z_b \; - \; z_g)]$$

$$K_{5,5}^{Hydrostatic} = \rho_w \, g \, [I_{yy} \, + \, \nabla(z_b \, - \, z_g)]$$

4.3 Hydrodynamic loading

Hydrodynamic loading of a structure in a marine environment is mainly caused by three categories of hydrodynamic loading. These categories are: the motions of the structure, the interactions between waves and the structure and the kinematics of water particles in waves. The oscillating motion of the structure will cause radiation forces and moments. The wave exciting loads originate from the interactions between waves and the structure and the drag loads are induced by the kinematics of water particles. All these different loads will be discussed in the section below.

4.3.1 Oscillating loads

Radiation forces and moments are induced by the harmonic oscillations of a structure moving in the undisturbed surface of a fluid. These oscillations will produce waves that propagate radially from the structure. These waves transport energy which is withdrawn from the oscillations, which will slowly damp out. This damping is called wave damping and is proportional to the velocity of the body. Its frequency dependent coefficient B has the dimensions of mass per unit of time. The other part of these forces is proportional to the acceleration of the structure. This force is caused by acceleration of the water particles near the structure. This part of the force does not dissipate energy and acts as a standing wave system near the structure. The frequency dependent coefficient A has the dimension of mass and is called the added mass of the system. These radially outgoing waves produce a fluctuating fluid pressures on the structure. Integrating this fluid pressure forces over the wetted surface of the structure gives:

$$F_i^{Radiation}(\omega) = -A_{i,j}(\omega) \, \frac{d^2 \, \eta_j}{d \, t^2} \, - \, B_{i,j}(\omega) \, \frac{d \, \eta_j}{d \, t}$$

In this equation a motion in the direction of j will contribute to a force in in the direction of i. The added mass and damping matrices will consist of j x i directions. Since j and i both consists of 6 DOF's, both added mass and damping coefficients matrices will consist of 36 coefficients:

$$A_{i,j}= \begin{bmatrix} A_{1,1} & A_{1,2} & A_{1,3} & A_{1,4} & A_{1,5} & A_{1,6} \\ A_{2,1} & A_{2,2} & A_{2,3} & A_{2,4} & A_{2,5} & A_{2,6} \\ A_{3,1} & A_{3,2} & A_{3,3} & A_{3,4} & A_{3,5} & A_{3,6} \\ A_{4,1} & A_{4,2} & A_{4,3} & A_{4,4} & A_{4,5} & A_{4,6} \\ A_{5,1} & A_{5,2} & A_{5,3} & A_{5,4} & A_{5,5} & A_{5,6} \\ A_{6,1} & A_{6,2} & A_{6,3} & A_{6,4} & A_{6,5} & A_{6,6} \end{bmatrix} \qquad B_{i,j}= \begin{bmatrix} B_{1,1} & B_{1,2} & B_{1,3} & B_{1,4} & B_{1,5} & B_{1,6} \\ B_{2,1} & B_{2,2} & B_{2,3} & B_{2,4} & B_{2,5} & B_{2,6} \\ B_{3,1} & B_{3,2} & B_{3,3} & B_{3,4} & B_{3,5} & B_{3,6} \\ B_{4,1} & B_{4,2} & B_{4,3} & B_{4,4} & B_{4,5} & B_{4,6} \\ B_{5,1} & B_{5,2} & B_{5,3} & B_{5,4} & B_{5,5} & B_{5,6} \\ B_{6,1} & B_{6,2} & B_{6,3} & B_{6,4} & B_{6,5} & B_{6,6} \end{bmatrix}$$

Both the coefficients of added mass and damping are frequency depending, so they are not directly applicable to a time domain analysis. In order to use both coefficients during a time domain analysis, a transformation from frequency to time domain is done by ANSYS AQWA.

4.3.2 Wave exciting loads

Wave excitation loads consist of forces and moments that act on the structure as if it were restrained. These loads are typically composed of the first order Froude-Kriloff and diffraction forces and the second order wave drift forces. Before these forces can be calculated a realistic representation of a wave climate is needed.

Regular Waves

The most simplest form of ocean waves are airy waves. The airy wave theory is based on the assumption of a homogeneous, incompressible, inviscid fluid and an irrotational flow. Furthermore, the wave amplitude is assumed to be small compared to the wave length and water depth. Figure 4.6 shows a harmonic wave from different perspectives. The origin of the coordinate system lies at still water level and the positive z-axis is directed upward. On the left the observer sees the wave profile as a function of the distance x at a fixed time t. On the right one can see a time record of propagating wave at a fixed point in x.

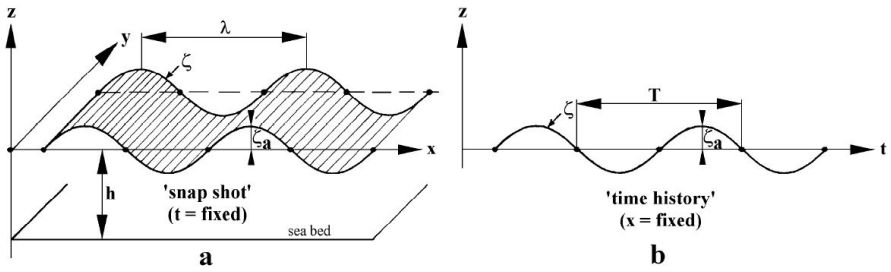

Figure 4.6: General wave characteristics (Journee, Massie, and Huijsmans, 2015)

The highest point of a sinusoidal wave is called the crest and the lowest part its through. The water depth h is measured between the sea bed and the still water level. The amplitude ζ_a is defined as the distance from crest to still water level and the wave height H is defined by:

$$H = 2\,\zeta_a$$

The wave length λ is defined as the horizontal distance between two successive wave crests. The distance of a single wave along the time axis is called the wave period and is indicated by T. In order to use the values of λ_w and T we needs to convert them to the wave number k and circular wave frequency ω:

$$k = \frac{2\,\pi}{\lambda_w}$$

$$\omega = \frac{2\,\pi}{T}$$

In airy wave theory it is defined that the wave period ω and the wave number k are related through the dispersion relation (Journee, Massie, and Huijsmans, 2015):

$$\omega^2 = g\ k\ tanh(k\ h)$$

The wave profile of a propagating regular wave in the positive x-direction can be expressed in terms of x and t in the following manner:

$$\zeta = \zeta_a\ cos(kx - \omega t)$$

Irregular Waves

Looking at regular harmonic waves of 4.6, one notices that they do not provide a realistic representation of a real life sea surface. A more realistic sea surface can be created by using irregular waves. It is possible to represent a irregular sea surface by using the super position principle which states that any irregular wave can be seen as a super position of many more simple regular harmonic waves, each with its on amplitude, wave frequency, wave number and direction of propagation. A visual representation of this principle can be seen in figure 4.7

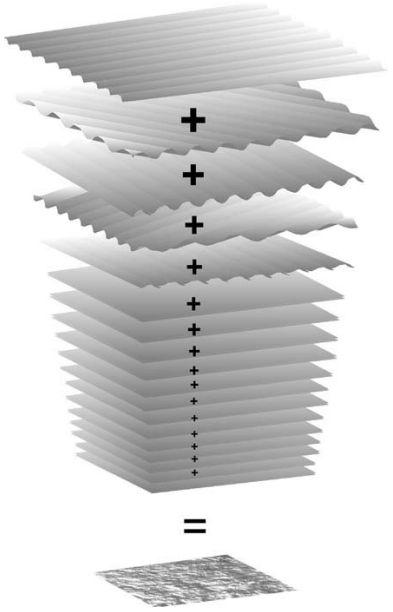

Figure 4.7: Irregular sea created as a super position of regular waves (Journee, Massie, and Huijsmans, 2015)

The relation between frequency and amplitude in this superposition of regular waves can be characterized by a wave-spectrum, which defines the distribution of wave energy over frequency which is representative for a certain sea-state. One of these wave spectra is the JONSWAP wave spectrum (Hasselmann et al., 1973), which is an extension of the Pierson Moskowitz spectrum (Pierson and Moskowitz, 1963) and can be represented in the following matter (DNV, 2011):

$$S_\zeta(\omega) = \frac{5}{16}\ H_{1/3}^2\ \omega_p^4\ \omega^{-5}\ exp(-\frac{5\ \omega_p^4}{4\ \omega^4})\ (1 - 0.287\ ln(\gamma))\ \gamma^A$$

with:

$$A = exp[-(\frac{(\omega - \omega_P)^2}{2\,\sigma^2\,\omega_P^2})]$$

γ = peak enhancement factor of 3.3
σ = 0.07 if $\omega < \omega_P$
σ = 0.09 if $\omega > \omega_P$

As mentioned in the beginning of this section and visualized in figure 4.7, an irregular sea state can be represented by a super position of regular harmonic waves. A time series of the wave elevation of a long crested irregular sea propagating in the positive x-direction can be described with:

$$\eta(x,t) = \sum_{n=1}^{N} \zeta_{a_n}\, cos(k_n x - \omega_n t + \epsilon_n)$$

Where the frequency dependent wave amplitude ζ_{a_n} is described by $\Delta\omega$ and the spectral density s_ζ

$$\zeta_{a_n} = \sqrt{2\; S_\zeta(\omega)\; \Delta\omega}$$

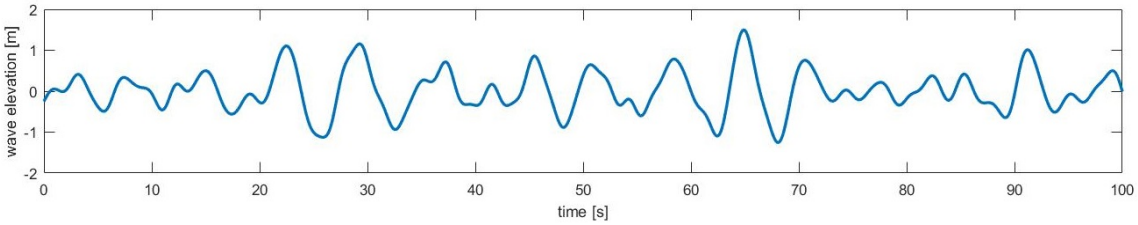

Figure 4.8: Irregular Wave, $H_{1/3}$ = 2.5m, T_p = 7s

Figure 4.8 shows an example of the wave elevation of a irregular wave created with a Jonswap spectrum.

Current

During the simulations of this model a relatively strong current is assumed. This current will interact with the waves and influences the wave characteristics. When the direction of the current and waves are in line with each other the interaction will increase the wave length and frequency of the waves, whilst a current with a opposing direction will decrease the wave length and wave frequency (Oh and Kim, 1992). The combined fluid particle velocity of currents and waves also effects the viscous drag forces on the structure. The diffraction and radiation forces on the floating structure are also affected by the presence of a current.

4.3.3 Viscous drag

During the calculation of the previously mentioned radiation and wave excitation forces water was assumed to be a non-viscous fluid. However water is not a non-viscous fluid, and the motion of water particles along the hull of the spar will cause friction. This friction is called viscous drag and is especially important in moderate to severe sea conditions. Viscous drag can be described using the following equation:

$$F_{drag} = \frac{1}{2}\,\rho_w\,C_D\,U_{rel}\,|U_{rel}|\,dA$$

In this equation C_D is defined as 0.6, which is a typical coefficient for a cylinder at higher Reynolds numbers as shown in figure 4.9. U_{rel} is the relative velocity between the the structure and the fluid velocity, and dA is the area where the fluid interacts with the structure.

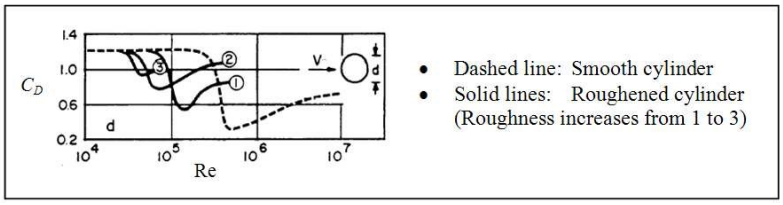

Figure 4.9: Drag factor of a cylinder (Male, 2017)

4.3.4 Hydrodynamic loading rotor

During normal operations when the current turbine is used to generate electricity, the hydrodynamic loading of the marine current turbine is similar to the aerodynamic loading of the wind turbine. There are of course some differences, ρ_w is the water density and the relative fluid speed, $U_{CT,rel}$ is calculated in the same way as the relative wind speed at the hub height of the wind turbine:

$$T = \frac{1}{2}\,\rho_w\,U_{CT,rel}\,|U_{CT,rel}|\,A\,4\,a\,(1-a)$$

During survival mode when the blades of the current turbine are pitched to flip the thrust, the previously mentioned equation will no longer be hold. To calculate this now reversed thrust, the program Aerodyn will be used. Figure 4.10 shows the thrust of the current turbine for a rotational speed of 15 rpm. This thrust curve is used to calculate the hydrodynamic loading of the turbine when the blades are pitched during survival mode:

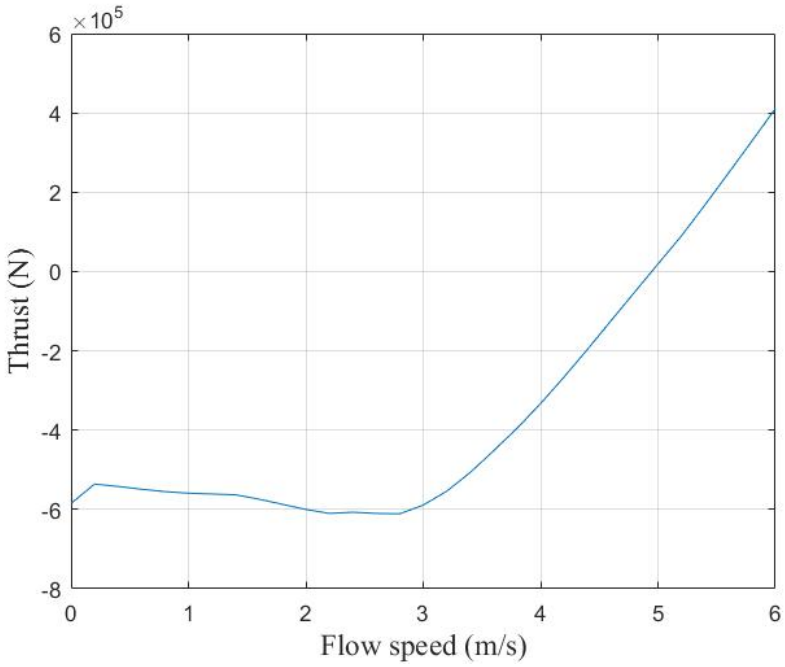

Figure 4.10: Reversed thrust during survival mode

4.4 Load cases

To investigate the dynamic behavior of the system under various circumstances, multiple load cases are considered. In these load cases, the system will be subjected to a combination of wind, waves and current. During normal operating mode, three different cases will be considered, whilst for survival mode the system will be exposed to one load case. The environmental values for the different load cases during operational mode are derived from the velocities of the cut in, rated and cut out speed of the wind turbine. The used wave spectrum is Jonswap and the peak wave period $T_P = 1.199\, T_1$ (Journee, Massie, and Huijsmans, 2015).

Wave Spectrum Parameter Estimates								
Scale of Beaufort	Wind Speed at 19.5 m above sea (kn)	Open Ocean Areas (Bretschneider)			North Sea Areas (JONSWAP)			
		$H_{1/3}$ (m)	T_1 (s)	T_2 (s)	$H_{1/3}$ (m)	T_1 (s)	T_2 (s)	γ (-)
1	2.0	1.10	5.80	5.35	0.50	3.50	3.25	3.3
2	5.0	1.20	5.90	5.45	0.65	3.80	3.55	3.3
3	8.5	1.40	6.00	5.55	0.80	4.20	3.90	3.3
4	13.5	1.70	6.10	5.60	1.10	4.60	4.30	3.3
5	19.0	2.15	6.50	6.00	1.65	5.10	4.75	3.3
6	24.5	2.90	7.20	6.65	2.50	5.70	5.30	3.3
7	30.5	3.75	7.80	7.20	3.60	6.70	6.25	3.3
8	37.0	4.90	8.40	7.75	4.85	7.90	7.35	3.3
9	44.0	6.10	9.00	8.30	6.10	8.80	8.20	3.3
10	51.5	7.45	9.60	8.80	7.45	9.50	8.85	3.3
11	59.5	8.70	10.10	9.30	8.70	10.00	9.30	3.3
12	>64.0	10.25	10.50	9.65	10.25	10.50	9.80	3.3

Figure 4.11: Relation between $H_{1/3}$ and Beaufort wind scale (Journee, Massie, and Huijsmans, 2015)

During all Load cases, the direction of the wind and waves are always in line with each other and come from the directions 0°, 30°, 60° or 90°. The direction of the current is set at 0° or 180°. Figure 4.12 shows the direction of the loading. In this figure the angle β shows the direction of the wind and waves with respect to the global coordinate system. A direction of 0° coincides with the positive X-axis and a direction of 90° coincides with the positive Y-axis.

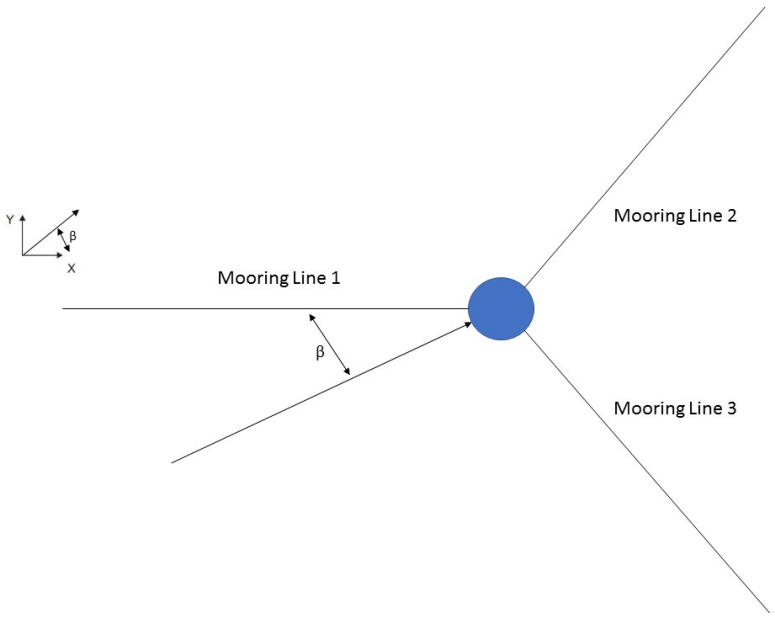

Figure 4.12: The direction of the wind and waves

4.4.1 Operational mode

During the operating load cases both the wind and current turbine are operating normally, their thrust will be calculated with the actuator disk theory and included in the AQWA model. The different environmental conditions are:

$H_{1/3}$ = 0.8m and T_P= 5.0s and a mean wind speed at hub height 3 m/s
$H_{1/3}$ = 1.8m and T_P= 6.0s and a mean wind speed at hub height 11 m/s
$H_{1/3}$ = 5.5m and T_P= 10.0s and a mean wind speed at hub height 25 m/s

During these load cases ocean currents are set to 2.5 m/s, this is done because for marine current turbines to be commercial viable, a current speed of at least 2 m/s is required (Batten et al., 2006).

4.4.2 Survival mode

During survival mode, the wind turbine will be shut down and the blades will be feathered. The blades of the current turbine will be pitched to flip their thrust. To include this thrust, the thrust curve of figure 4.10 will be used and included in the AQWA model. The environmental conditions during survival mode are:

$H_{1/3}$ = 14.5m and T_P= 19.0s and a mean wind speed at hub height 51 m/s

During the survival mode the velocity of the ocean current is set to 2.5 m/s.

Chapter 5

Model description

To investigate the complex behavior of the hybrid system during the various load cases, a model is created with the program ANSYS AQWA. This program can be used to investigate the effect of wind, waves and current on the behavior of floating and bottom founded marine structures. AQWA uses a three dimensional panel method to analyze the hydrodynamic behavior of a large structure in waves. The three dimensional panel method is based on fluid potential theory and represent the structure surface by a series of diffraction panels. The Morison's equation approach is used for slender body components and AQWA employs a hybrid method to model the large-volume components of a structure by diffracting panels and the small cross sectional components by Morison elements (Aqwa, 2013).

The first section describes the model parameters including the geometry and mass properties. In the next section the relevant hydrodynamic added mass and damping coefficients are shown. Section 5.3 describes the wind loads on the top structure and in section 5.4 the implementation of the hydrodynamical loading of the current turbine and the aerodynamic loading of the wind turbine during operations are described. In the final section of this chapter, the properties of the mooring system are provided.

5.1 Model parameters

To create the model in ANSYS AQWA, different parameters need to be implemented. The first parameters are the geometry and mass properties of the model. Special tube elements are used to capture the viscous drag in the model.

5.1.1 Geometry

As mentioned in chapter 3, the spar floater consists of two cylindrical regions connected by a linearly tapered region. Figure 5.1 shows the geometry which is used by AQWA. The diameter above the taper is 6.5 meter and below the taper 9.4 meter. The elevation to the tower base is 10 meter above SWL and the depth to the bottom of the platform(draft) is 120 meter below SWL.

Figure 5.1: The geometry of the spar floater

5.1.2 Mass properties

The properties of the overall system including rotor nacelle and tower:

Table 5.1: System mass properties

Overall Mass	8.06E+6 kg
CM Location Below SWL Along Centerline	78.61 m
System Roll Inertia about CM	2.13E+10 kg*m^2
System Pitch Inertia about CM	2.13E+10 kg*m^2
System Yaw Inertia about Platform Centerline	1.64E+8 kg*m^2

5.1.3 Viscous drag

In order to capture the viscous drag on the hull, Ansys AQWA recommends the use of Tube elements during time domain simulations. These circular non-panel elements, which can be placed within the hull of the model, have a drag and added mass coefficient. In order to not double up the effect of added mass which is computed by AQWA from the diffraction model, Ansys AQWA recommends creating the tube elements with a diameter 100 times smaller compared to the outside diameters of the spar. In order to include the viscous drag effects correctly the drag factor C_D is therefore multiplied by 100 (Aqwa, 2016). During the simulations two Morison elements are used, the first element has a diameter of 0.094 meter and the second element has a diameter of 0.065 meter.

5.1.4 Mesh

Before ANSYS AQWA can do a diffraction analysis, the surface of the model needs to be discretized with panels. Figure 5.2 shows the surface of the model discretized with quadrilateral panels. These zero thickness panels generate pressure and hydrostatic forces only. A total of 17,116 elements are used to generate the required mesh.

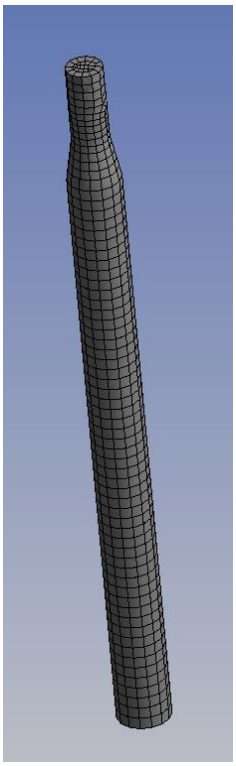

Figure 5.2: Panel mesh of the model

5.2 Hydrodynamic added mass and damping coefficients

The hydrodynamic coefficients, which are calculated during the diffraction analyses, of added mass and damping of the platform are shown as a function of frequency in figure 5.3. Only the upper triangular matrix elements are shown, because both matrices are symmetric due to the absence of forward speed. Because of the spar's symmetries, the coefficients A_{11} and B_{11} are identical to A_{22} and B_{22}, and A_{44} and B_{44} are identical to A_{55} and B_{55}. Other matrix elements not shown are zero valued.

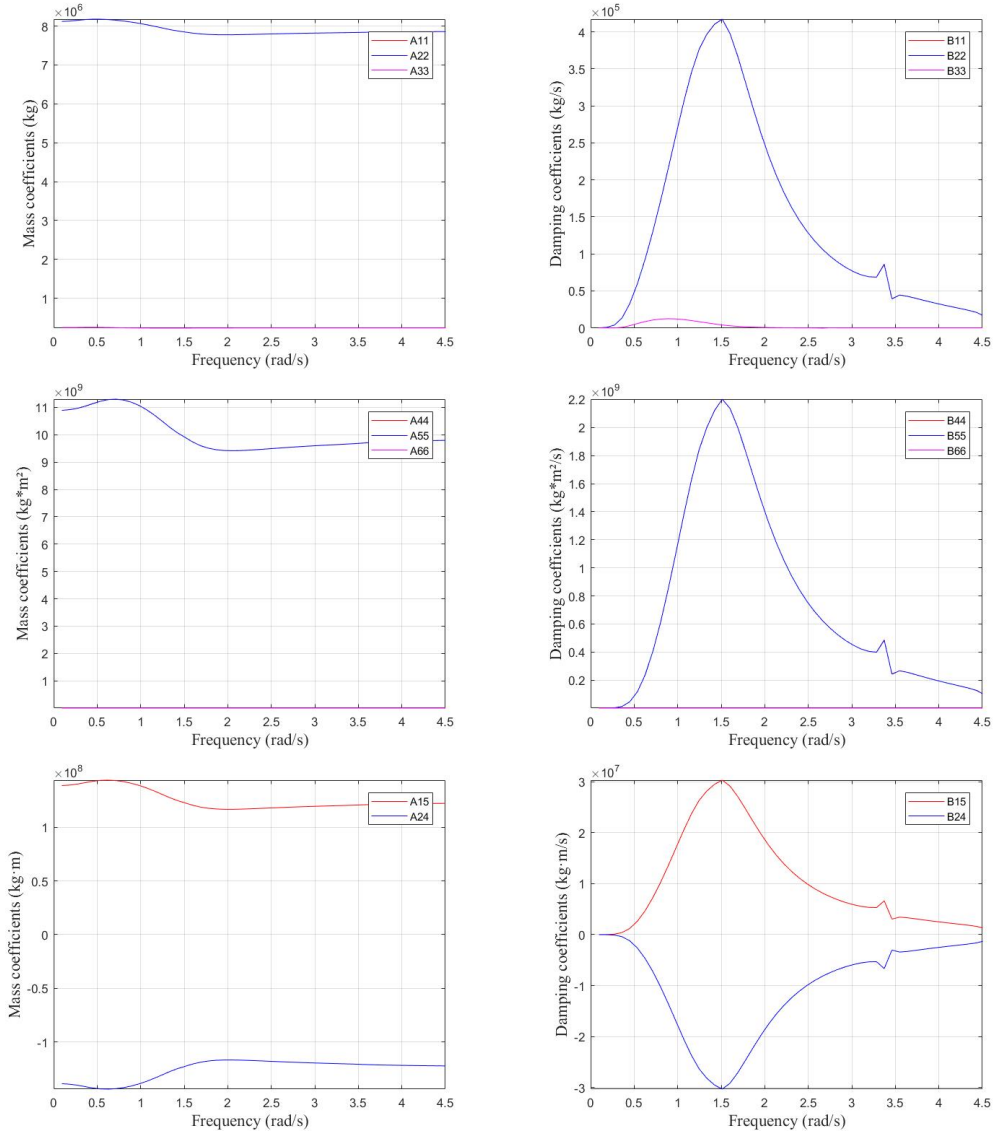

Figure 5.3: Hydrodynamic added mass and damping coefficients

5.2.1 Additional damping matrix

The linear radiation damping and the nonlinear viscous-drag damping of the model do not capture all of the hydrodynamic damping for the motions of the hywind spar. In order to capture all of the hydrodynamic damping, additional linear damping should be implemented. Additional damping in Surge , Sway, Heave and Yaw is needed. This additional damping is based on on still water free decay test. NREL recommended the following additional linear damping (Jonkman, 2010):

Table 5.2: Additional linear damping

Additional Surge damping	1.00E+5	N/(m/s)
Additional Sway damping	1.00E+5	N/(m/s)
Additional Heave damping	1.30E+5	N/(m/s)
Additional Yaw damping	1.30E+7	Nm/(rad/s)

5.3 Wind coefficients

To determine the wind loads on the top structure, AQWA makes use of wind coefficients. These wind coefficients are defined as a force or moment per unit velocity squared and are a summation of the aerodynamic loading of the top structure as a function of a reference wind velocity and wind direction. This summation consists of the aerodynamic loading on the tower, the nacelle and during survival mode when the wind turbine is parked the rotor. The loading on the top structure is calculated using the formulas described in chapter 4 and summed up as a function of the relative velocity between the incoming wind and the structure. During the simulations it is assumed that the nacelle will follow the direction of the wind and that the rotor will always be perpendicular to the incoming wind. In this way the loading of the top structure can always be decomposed into the directions of Surge, Sway, Roll and Pitch by using sines and cosines. It is not necessary to define every angle of the wind coefficients. AQWA is able to interpolate between angles. The figures below show the wind coefficients which are used during operational mode. A table with all wind coefficients and the wind coefficients which are used during survival conditions can be found in Appendix A.

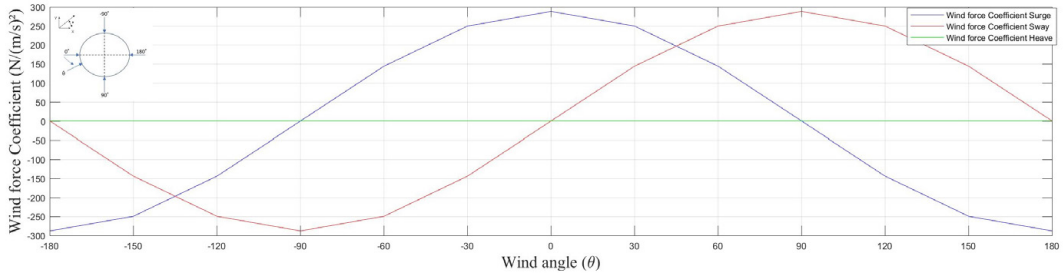

Figure 5.4: Wind force coefficients, operational mode

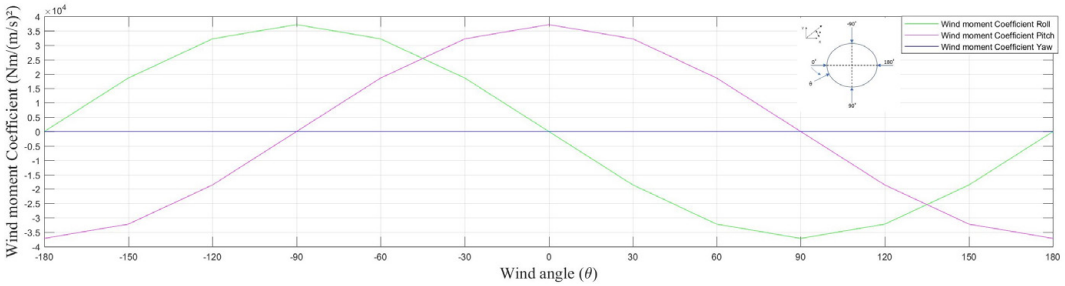

Figure 5.5: Wind moments coefficients, operational mode

5.4 External python server

AQWA can accept forces calculated from a process running on an external python server. The external server feature is activated by linking AQWA and the external process through a socket. A socket in this context refers to an internal endpoint for sending or receiving data. The server creates a socket, binds it to a free port number, and begins listening on that port. The feature requires the SUFC option to be activated in AQWA. AQWA provides the external server with the position and velocity of the

center of gravity in all DOF's, through the socket at each time step. Simultaneously, AQWA listens to the socket for the information generated by the external process and adds the calculated forces to the simulation (Aqwa, 2015). An example of the python code which is used during the simulations can be found in Appendix B.

During the simulation the thrust forces of the wind and current are calculated with the formula's described in chapter 4. To calculate the relative velocity the turbine encounters at hub height, the incoming wind velocity is decomposed into the structures directions of Surge and Sway by using sines and cosines. The python server uses radians as angles so a direction of 0° correspondents with 0 rad, a direction of 30° correspondents with $\pi/6$ rad, a direction of 60° correspondents with $\pi/3$ rad and a direction of 90° correspondents with $\pi/2$ rad. After the wind velocity is decomposed, the relative velocity which the turbine encounters is obtained by subtracting the structure velocity in surge and sway from the decomposed wind velocity in those directions.

5.5 Mooring system

To prevent the platform from drifting off, the original Hywind spar platform is moored by a system of catenary mooring lines which are connected to the spar by a delta configuration. Figure 5.6 shows an example of the delta configuration of the original Hywind spar.

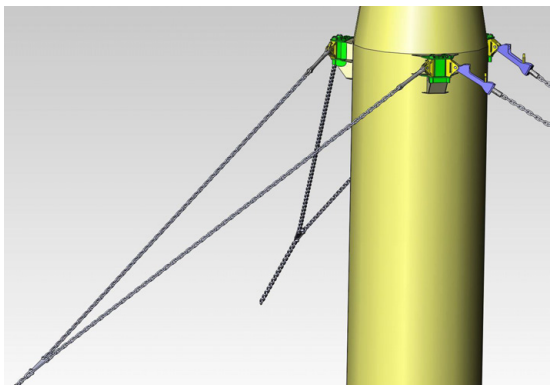

Figure 5.6: Delta configuration the Hywind spar (Steen, 2015)

NREL made some simplifications to the original mooring setup, which are listed below: The delta configuration is removed, but to create the same overall yaw spring stiffness an additional stiffness is added. This additional Yaw spring stiffness has been determined by NREL by creating two different mooring models. The first mooring model extended from the anchor to the apex of the delta and assumed the delta rigid. The second mooring model extended from the anchor to the spar. From these two models the difference in yaw stiffness was obtained. To check if this additional yaw spring stiffness was correct, the natural frequency in yaw was checked and confirmed with the free decay data of the yaw motion (Jonkman, 2015). In the second simplification, the original multi segment mooring line is replaced by a homogeneous line, with average values for the mass and stiffness, which are listed in table 5.3. The final simplifications during the simulations is that all damping related to the mooring

system is neglected (Jonkman, 2010). The following properties describe the mooring system:

Table 5.3: mooring system properties

Number of mooring lines	3
Angle between lines	120 °
Depth to fairleads below SWL	70 m
Radius to Anchors from platform centerline	853 m
Radius to fairleads from platform centerline	5.2 m
Section length	902 m
Mooring line diameter	0.09 m
Mass/unit length	77.7066 kg/m
Axial stiffness/unit length, EA	384,243,000 N
Additional Yaw spring stiffness	98,340,000 Nm/rad

5.5.1 Mooring configuration 1

As mentioned above, the information provided by NREL describes a homogeneous line with average values for the mass and axial stiffness. Information about the exact specifications of the lines where requested from NREL and Statoil, but where not provided due to company policy. Through the properties in 5.3 and by using the same mooring line setup as in (Karimirad and Moan, 2012), an estimation of the specifications of the original mooring properties is obtained. Information about the mooring system of the original Hywind demo spar is found in (Homb, 2013). The mooring system of the original Hywind demo spar consisted of a combination of steel wire rope mooring lines, small sections of mooring chain and clump weights. The mooring lines in (Karimirad and Moan, 2012), which has a similar platform to the one used in this thesis, consist of multiple line sections each having the same characteristics and a clump weight.

Mooring line

By using the provided values of the axial stiffness and the diameter of the uniform the mooring line, the characteristics of the original line can be calculated. Information about different mooring lines can be found in (Lankhorst Ropes, 2014), from this information a steel wire rope, 6x36 WS+IWRC mooring line of 90 mm^2 is chosen. This line has has the following properties:

Table 5.4: 6x36 mooring line

Line diameter	90 mm
Mass/unit length	33.1 kg/m
Minimal breaking load	5652 kN

The choice of for this line can be checked by comparing the properties of this line with the uniform line from NREL. Both lines have the same diameter, so the next step is to compare the modulus of elasticity of both lines. To determine the modulus of elasticity of the line, first the metal area of the line needs to be calculated. To calculate the metal area of a steel wire rope the following formula is used (CIMAF, 2013):

$$A = F\, d^2$$

A = metal area in mm^2
F = multiplication factor of 0.4715 for 6x36 with warrington seale and IRWC
d = nominal diameter of the wire rope in millimeters.

Which gives a metal area of 3819 mm^2. This metal area is needed when calculating the modulus of elasticity of the uniform mooring line. The modulus of elasticity of this line can be now be checked by dividing the provided value of EA of the uniform line with the metal area of the wire rope:

$$E = 384,243,000/A$$

Which gives a modulus of elasticity of 100 GPa. This value lies within the range of the modulus of elasticity of a 6x36 steel wire rope, which lies between 93 GPa and 102 GPa (CIMAF, 2013).

Clump weights

The clump weights will be modeled in the same manner as is done in (Karimirad and Moan, 2012), the clump weight will be modeled as a section of mooring line of 2 meters with a large mass per unit length and diameter compared to the wire rope sections. To achieve the proper weight, steel with a density of 7850 kg/m^3 is used. The mass of the clump weights is determined by calculating the weight of the original uniform line and subtracting the weight of the wire rope.

$$W_{clump} = ((77.7066 * 902) - (33.1 * 900))$$

Which gives a mass of 40,301 kg, this mass is divided over a section of 2 meters, so the mass per unit length of the clump weights will be 20,151 kg/m. To achieve this mass, steel is used. With a mass density of 7850 kg/m^3, a section of 1 meter clump weight will have a cross section area of:

$$CSA_{clump} = 20151/7850$$

Which gives a cross section area of 2.57 m^2, which is equal to a diameter of 1.80 meter.

Mooring line layout

Figure 5.7 shows the layout and different sections of the mooring line.

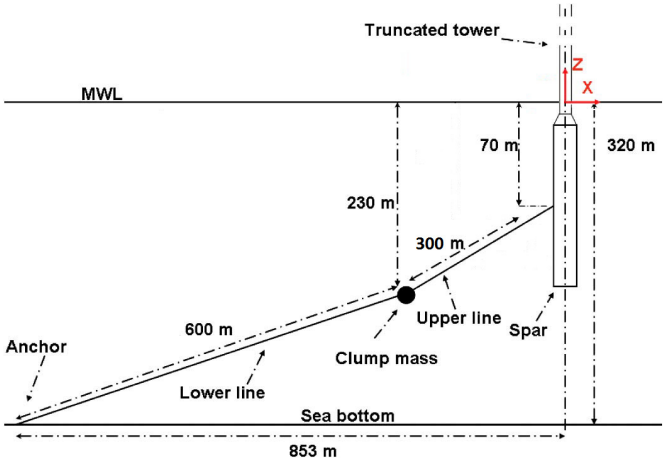

Figure 5.7: Mooring line schematic layout (Karimirad and Moan, 2012)

Table 5.5: Mooring line specifications

	Length (m)	Diameter (m)	Mass/length (kg/m)
Upper line	300	0.09	33.1
Lower Line	600	0.09	33.1
Clump weight	2	1.80	20,151

5.5.2 Mooring configuration 2

As mentioned in the beginning of this thesis, one of the objectives of this thesis is to investigate the reversing of the thrust of the current turbine to see if it is possible to scale down the weight of the mooring system. The second mooring setup that will be investigated has a mass which is 20% less compared to the previously mentioned mooring setup. This weight reduction will result in the use of a smaller cable and clump weight. From the list of Lankhorst ropes (Lankhorst Ropes, 2014), a cable with the following properties is chosen:

Table 5.6: Smaller mooring line setup 2

Line diameter	80 mm
Mass/unit length	26.2 kg/m
Minimal breaking load	4466 kN

The mass of the clump weight is:

$$W_{clump,2} = 0.8 * 40,301$$

Which gives a mass of 32,240 kg, this mass is divided over a section of 2 meters, so the mass per unit length of the clump weights will be 16,120 kg/m. The cross section area of 1 meter clump weight is:

$$\text{CSA}_{clump,2} = 16120/7850$$

Which gives a cross section area of 2.05 m^2, which is equal to a diameter of 1.61 meter. The layout of the mooring system is the same as the previous setup. The mooring line has the following specifications:

Table 5.7: Mooring line specifications

	Length (m)	Diameter (m)	Mass/length (kg/m)
Upper line	300	0.08	26.2
Lower Line	600	0.08	26.2
Clump weight	2	1.61	16,120

5.5.3 Cable dynamics

One of the simplifications which was used during the simulations of the original Hywind spar was the assumption that all damping related to the mooring lines could be neglected. To show the effect of dynamic effects on the mooring lines, AQWA has the option to calculate dynamic effects on the mooring lines during a simulation. When this option is chosen the effects of the line mass, the line drag forces and line elastic tension are considered, as well as their effect on the structures motion. To show the effect of using cable dynamics during a simulation, two simulations are done. The first simulation includes cable dynamics, whilst the second one does not. Both simulations are subjected to the same environmental conditions.These environmental conditions are the load conditions which are used in load case 4 and can be found in chapter 6. The direction of the current is 0° and the direction of the wind and waves is 30°

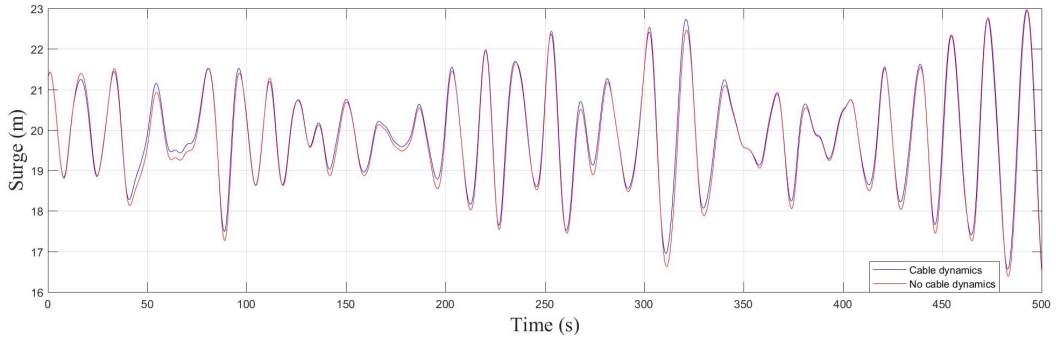

Figure 5.8: Surge motions structure

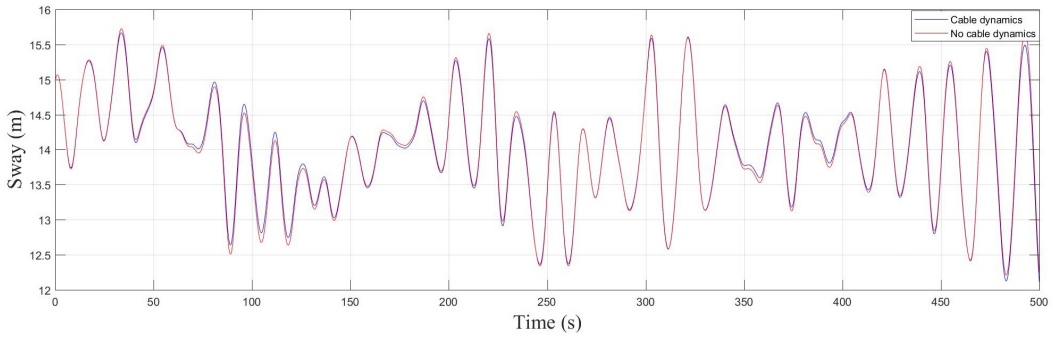

Figure 5.9: Sway motions structure

Figures 5.8 and 5.9 show the effect of using the cable dynamics on the motions of the structure in Surge and Sway. From these figures it can be observed that including the cable dynamics does not influence the motions of the structure by much.

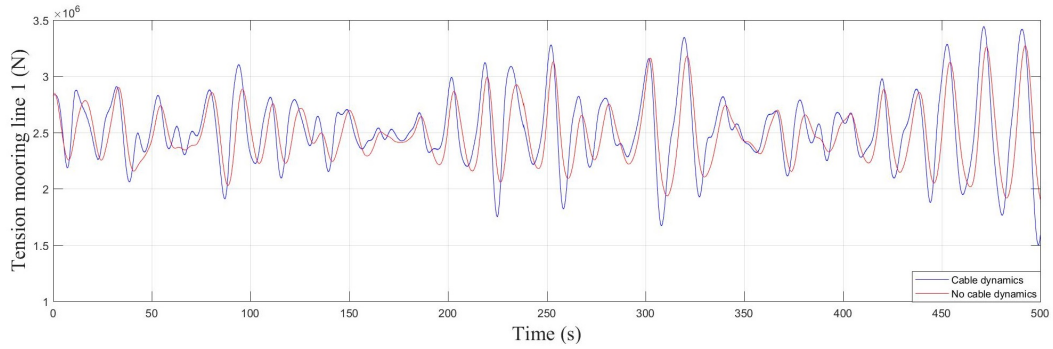

Figure 5.10: Tension mooring line 1

The effect of using the cable dynamics on the tension in mooring line 1 is shown in figure 5.10. From this figure it can be observed that there is a difference in the tension between both simulations, as one would expect, but the highest peak value of the tension for the line which has the cable dynamics turned on, is only 5% higher than the highest peak value in the line without cable dynamics.

To successfully include the dynamic effects of the mooring line, a small time step is required. During these simulations a time step of 0.001 seconds is used. Compared to the time step of 0.1 seconds which is the standard time step used during simulations in AQWA, these simulations take 100 times longer to calculate. If a larger time step is used the simulation will not converge and will give an error. To reduce the amount of computation time, the dynamic effects of the mooring line will therefore not be included in the simulations.

Chapter 6

Results & Discussion

In the first part of this chapter a selection of the results of the simulations is presented. All simulations have a run time of 10,000 seconds, but to show more detail, only the first 1,000 seconds of each simulation is shown in this chapter. The full length simulations can be found in the appendix. During the first simulations the system is subjected to the three operational load cases. In the fourth load case the system is subjected to survival conditions and the effect of reversing the thrust of the current turbine will be showed. The next step will be scaling down the weight of the mooring system in order to see if this is possible in combination with the current turbine.

After the simulations with AQWA, a first estimation of the effect of adding a current turbine to the system on the levelized cost of energy is obtained. The levelized cost of energy of the combined system will be compared to the original system to see the effect of adding the current turbine. Lastly the effect of scaling down the weight of the mooring system on the levelized cost of energy of the combined system will also be investigated.

6.1 Operational mode

The first three load cases simulate the system under normal operational conditions. These conditions simulate the cut in, rated and cut out wind velocities of the wind turbine. These wind velocities are 3 m/s, 11 m/s and 25 m/s. Together with the rated current velocity of 2.5 m/s, these load cases make up the workable range under which the system normally operates. From these load cases, the motions which result in the highest maximum tension in the mooring lines are presented in this section. This is the case when wind, waves and current are in line with each other and come from the direction of 0°. The results of the other simulations can be found in the appendices.

Figure 6.1 shows the relevant motions of the combined system when both the wind and current turbine are operational. From this figure it can be observed that the current has the largest influence on the mean offset in Surge, this is concluded by comparing the results of load case 1 with load cases 2 and 3, where a stronger wind is present. The influence of the wind loads on the top structure will increase with an increasing wind velocity, while the thrust forces of the wind turbine will be maximum at the rated wind speed. The influence of the thrust forces can be observed when looking at the Pitch angle of the structure in load case 2. With a mean value of 6.8°, this angle is higher than the mean value of 6.1° of load cases 3, due to the pitching of the blades in load case 3.

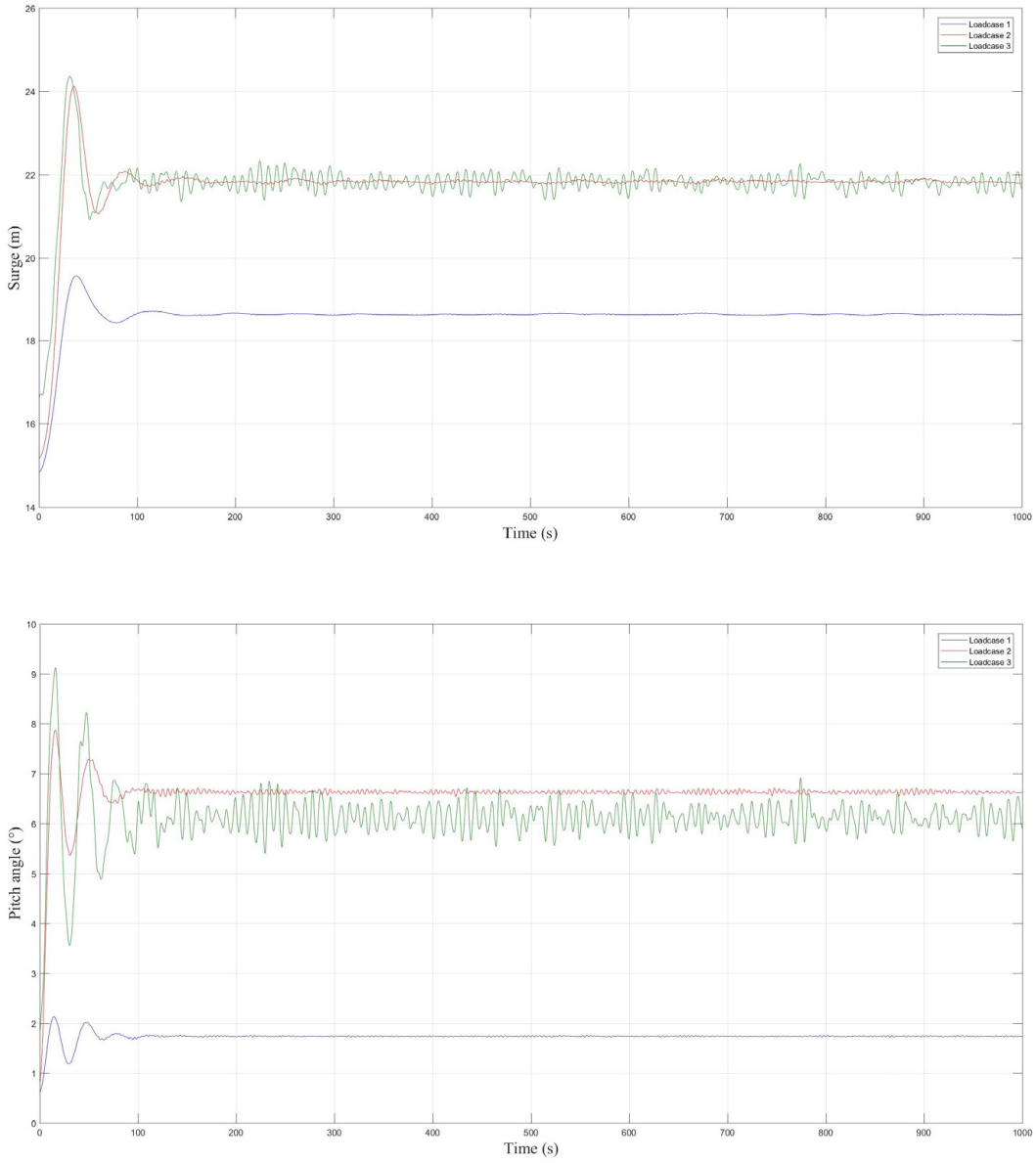

Figure 6.1: Surge and Pitch motions, operational load cases

Figure 6.2 shows the maximum tension in the mooring lines during each of the load cases. The mean values of the tension in the mooring lines are caused by both the drag forces on the hull and the wind loads on the top structure and the thrust forces of the wind and current turbine. While the oscillations around these mean values are caused by the periodic loading of the waves. These oscillations get bigger when the wave height increases, as can seen from load case 3.

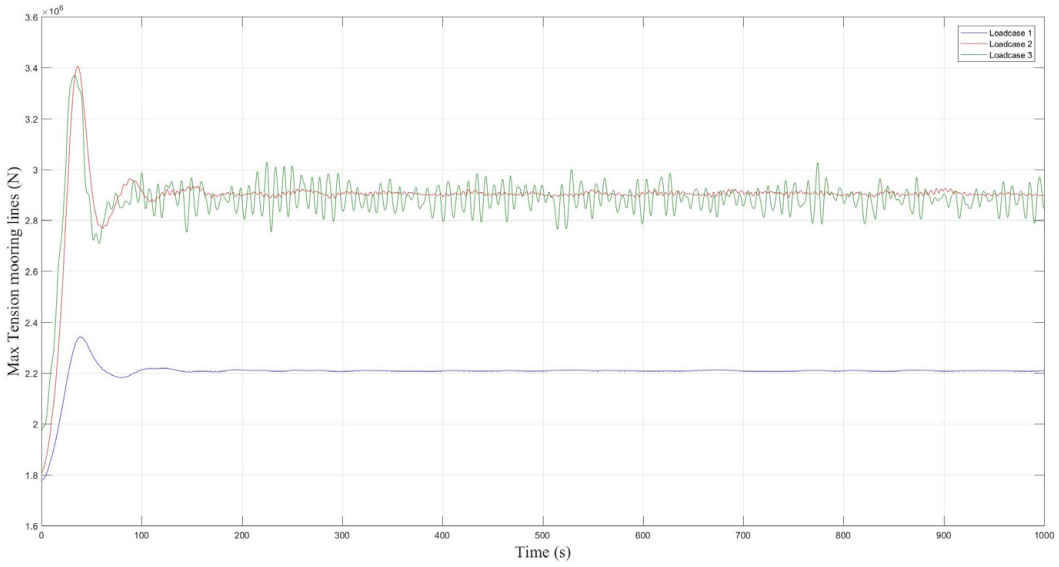

Figure 6.2: Maximum tension mooring lines, operational load cases

6.2 Survival mode

In the fourth load case the system is subjected to survival conditions. During survival conditions, with a wind velocity of 51 m/s the wind turbine is parked, so the wind turbine doesn't generate thrust forces and two possibilities for the current turbine are investigated. In the first possibility the current turbine is also parked and in the second possibility the blades of the current turbine are pitched to reverse the direction of the thrust.

In order to find the maximum loads on the mooring system, a number of different simulations under survival conditions need to be done. During each of the simulation a slightly different sea state is generated by AQWA using a random Seed. These different sea states result in a different wave loading on the system. Using the same seed value will result in the same sea state, so simulations can be reproduced. From these different sea states the one which will result in the highest tension in the mooring lines will be used during the simulations for survival conditions. Figure 6.3 shows the probability of exceedance of the maximum tension in the mooring lines. From this figure it can be concluded that the sea state with a seed value of 7 will result in the highest tension in the mooring lines. This seed value will therefore be used during the simulations of load case 4.

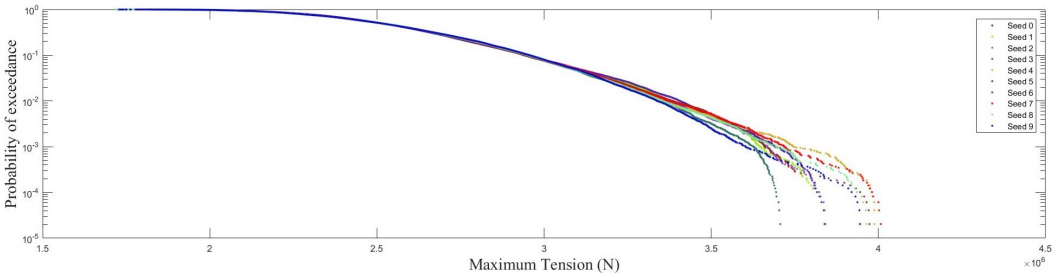

Figure 6.3: Maximum tension mooring lines, wind and current turbine parked

6.2.1 Load case 4, mooring configuration 1

Figure 6.4 shows the effect of reversing the direction of thrust of the current turbine on the motions of the structure. By comparing the results of the full length simulations it can be concluded that reversing the direction of the thrust leads to a lowering of the mean offset in Surge by 17.8 %, and a lowering of the maximum value by 10.0 %. The thrust of the current turbine also has a positive effect on the pitch motion of the structure lowering the mean angle by 20.4% and the maximum value by 11.7%

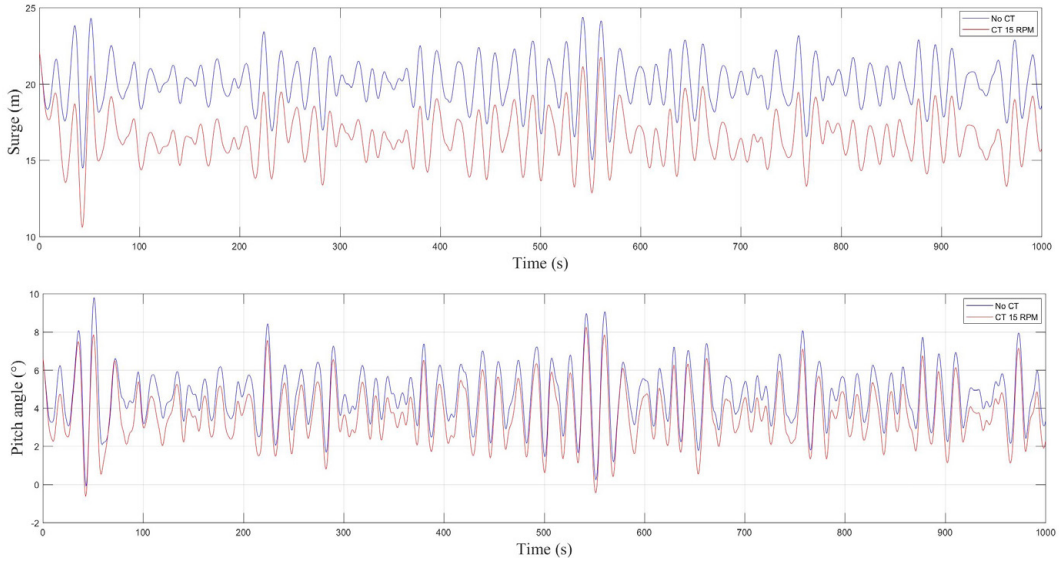

Figure 6.4: Surge and Pitch motions, with and without the CT

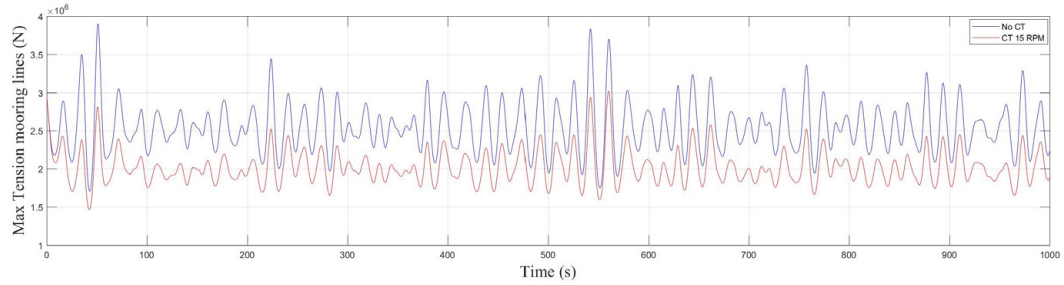

Figure 6.5: Maximum tension mooring lines, with and without the CT

Figure 6.5 shows the maximum tension in the mooring lines. When the results of the full length simulations are used, it can be concluded that adding the current turbine results in a lowering of the maximum tension with 19.3%, while the mean value is lowered by 20.7 %

6.2.2 Load case 4, mooring configuration 2

To see the effect of scaling down the weight of the mooring system on the maximum tension and behavior of the system, mooring configuration 2 will be compared to mooring configuration 1 for this load case. Figure 6.6 shows the difference in motions of the system. Figure 6.7 shows the difference in the tension of the mooring lines.

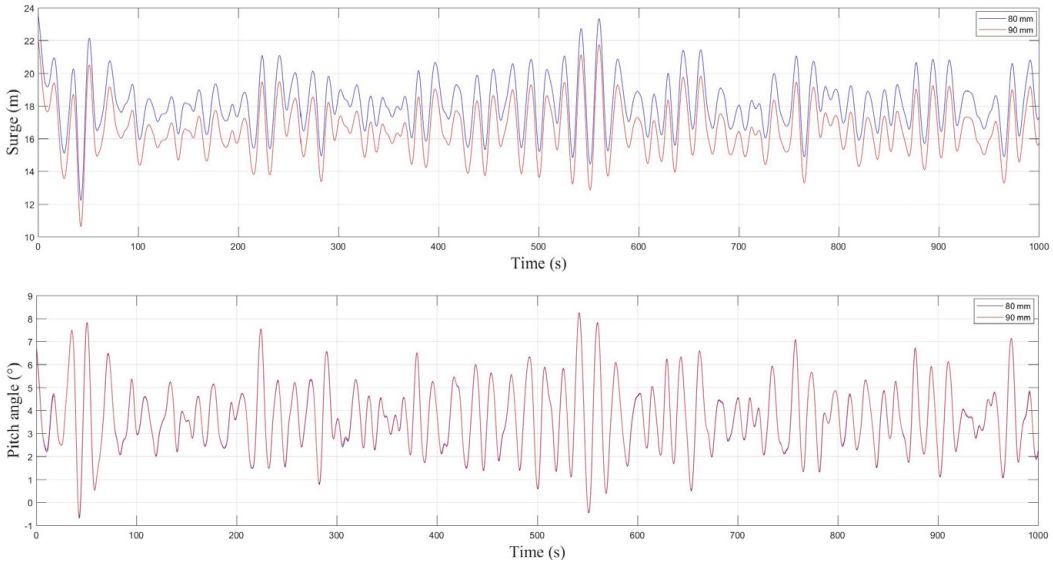

Figure 6.6: Surge and Pitch motions for the 2 mooring configurations

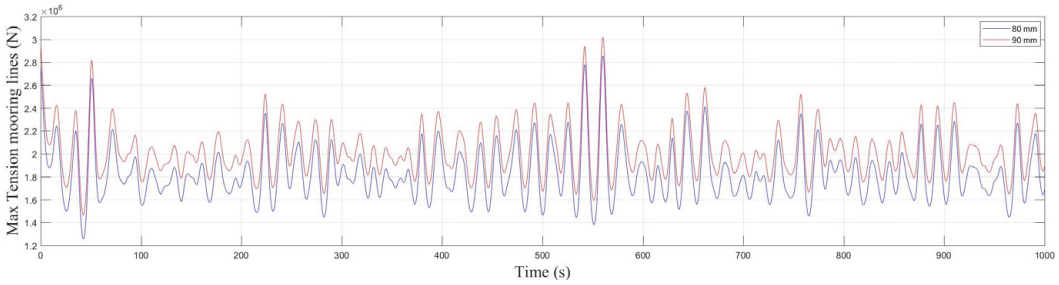

Figure 6.7: Maximum tension mooring lines for the 2 mooring configurations

From the results of the full length simulations it can be concluded that scaling down the weight of the mooring system lowers the maximum tension in the mooring lines. However, the smaller 80 mm mooring cables also have a lower minimum breaking load, meaning the line will fail earlier compared to the larger 90 mm mooring line. The probability of exceedance of the ratio between the minimum breaking load and the maximum tension of the full length simulations is plotted in figure 6.8, for a mooring line to be considered safe, a safety factor of 1.67 (MSL, 2001) or higher should always

be maintained. It can be observed that the ratio of mooring configuration 1 with a line diameter of 90 mm is always higher than the safety factor, whereas mooring configuration 2 with a line diameter of 80 mm exceeds the safety factor to a minimum of 1.45

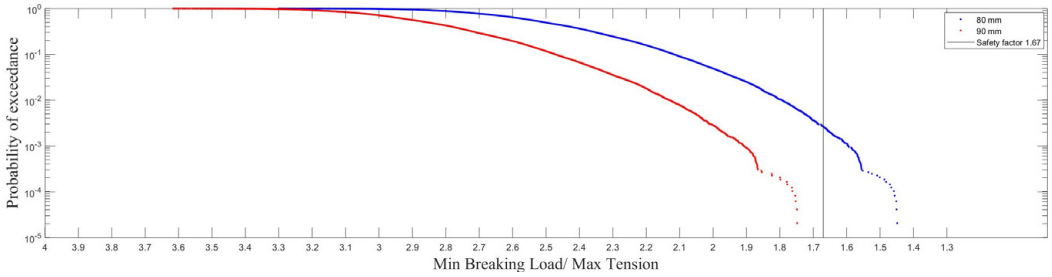

Figure 6.8: Ratio between min breaking load and max tension of the lines

6.3 Levelized Cost of Energy

The levelized cost of energy (LCOE) is an economic assessment of the average total cost to build and operate a power generating energy system over its lifetime divided by the total energy output of the system over that lifetime. The total costs are divided into three categories: Capital Expenditures (CAPEX), Operating Expenditures (OPEX) and Decommission Expenditures (DECEX). Capital Expenditures are expenses or investments used to upgrade or obtain physical assets in order to create a future benefit. Among these expenses are for instance the expenses related to designing, constructing and installing of components for the energy system. Operating expenses are expenses related to normal operations, including maintaining and operating an energy system. Decommissioning expenditures are expenses related to the decommissioning of the energy system at the end of its lifetime. Figure 6.9 shows a simplified explanation of the levelized cost of energy.

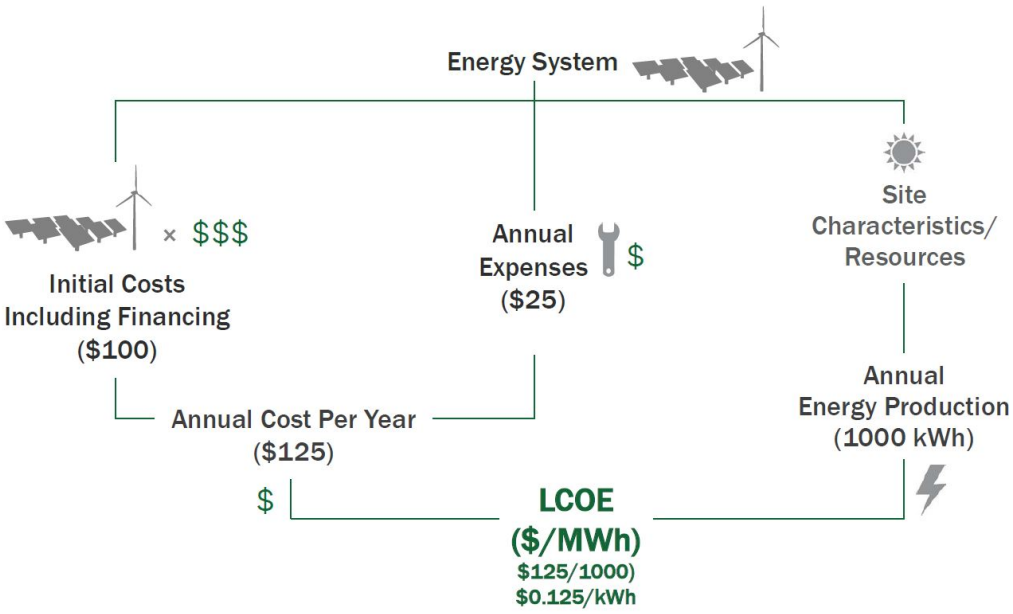

Figure 6.9: Simplified explanation of the LCOE (EWEA, 2009)

The following equation is used to calculate the LCOE:

$$\text{LCOE} = \frac{\sum_{t=0}^{n} \frac{I_t + M_t}{(1+r)^t}}{\sum_{t=0}^{n} \frac{E_t}{(1+r)^t}}$$

Where I_t denotes investments at time t, M_t denotes operation and maintenance costs at time t, E_t denotes energy generation at time t, r denotes the evaluation discount rate and t denotes the time ranging from zero to n.

As a basis for calculating the levelized cost of energy, the values found in the paper by Anders Myhr, Catho Bjerkseter, Anders Ågotnes and Tor Nygaard titled: levelized cost of energy for offshore floating wind turbines in a life cycle perspective (Myhr

et al., 2014) will be used. In this paper the levelized cost of energy of different floating wind turbines is calculated and compared to a baseline bottom founded wind farm. Among the different floating wind turbines investigated by Myhr et al., is the Hywind spar, which is used as a basis for this master thesis. To provide scope for this thesis, only the base case of the LCOE range is considered. The best and worst case scenarios are left out. Figure 6.10 shows the breakdown values of the LCOE of the base case scenario for the different concepts:

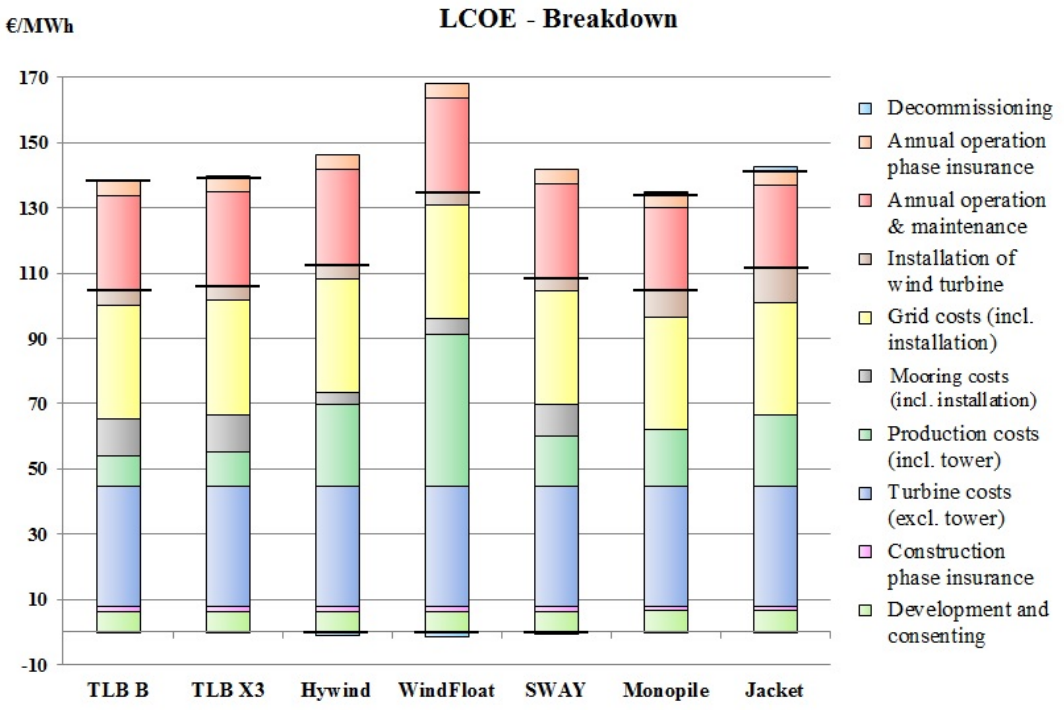

Figure 6.10: LCOE cost break down for the base case of the reference case by Myhr et al.

6.3.1 LCOE breakdown

From the figure it can be observed that the the LCOE values of the Hywind spar are dominated by CAPEX costs, denoted by the different breakdown values between the X axis and the first black line. To have an estimation of the effect of adding a current turbine to the system, a simple model is used to calculate the Levelized Cost of Energy per MW. This model is created by the Crown Estate (Howard, 2012) to allow users to test their own cost reduction assumptions. The same model is used by Myhr et al and can be found in Appendix H. The model has some predefined values which are used in this thesis. The expected operational lifetime of the project is 20 years with a discount rate of 8.2%. The preliminary development and construction phase takes 4 years and the decommission time takes 1 year. Which gives a total project time of of 25 years. The model is used to calculate the LCOE for 1 unit of 5 MW for the original spar and 6 MW for the combined system. Increasing the amount of units will likely lower the LCOE, but falls outside the scope of this thesis.

Adding a current turbine to the Hywind spar will have an effect on the levelized cost of energy, but not all breakdown values will be influenced. It is assumed that

the cost of construction insurance, support structure, grid costs, decommissioning, installation and mooring remain the same for the combined system.

The water depth used by Myhr et al. during their comparison is assumed to be 200 meters. The water depth in this thesis is 320 meters, so a different mooring system is used. The details and cost of the mooring system used in this thesis are derived below and added to the models of both the original and combined system. The values of the CAPEX, OPEX and DECEX provided by Myhr et al are normalized to values given per MW. The total cost can be calculated by multiplying the different values by 5 because the rated power of the wind turbine is 5 MW. The rated power of the current turbine is 1 MW, to account for the extra production of the current turbine, some values will be scaled by $\frac{5}{6}$ to remain the same for the combined model. The remaining breakdown values will be effected by the adding of the current turbine and the additional CAPEX and OPEX will be introduced below and will be added to the model. Lastly the effect of scaling down the weight of the mooring system will be investigated by using mooring configuration 2.

Mooring cost

The total mooring cost of the original hywind spar calculated by Myhr et al. is €635,000 for the baseline case with a water depth of 200 meters. This value is a combination of the cost of the mooring lines, anchors and installation cost. The cost of the 3 anchors is estimated to be €342,000 based on numbers provided by Vryhof Anchors (Myhr et al., 2014) and the cost of installation of the mooring system is assumed to be €167,000. Which leaves a cost of €126,000 for the mooring lines. The values for the installation and the anchors are assumed to remain similar, but the cost of the mooring lines will increase, due to an increased water depth and a slightly different mooring setup. The cost of the mooring cables and clump weights is calculated in the following way:

The cost of the clump weights is assumed to be linked to the steel price. These prices are volatile and change regularly, but as a baseline price €1,000 per ton is used.

Table 6.1: Cost clump weights

Configuration	Weight (ton)	Price per clump (€)
1	40.301	€40,301
2	32.240	€30,240

To calculate the cost of the mooring lines information is obtained from Lankhorst ropes (Lankhorst Ropes, 2018). Which gave an estimated cost of €105.15 per meter for the 90mm line and an estimated cost of €83.10 per meter for the smaller 80mm line.

Table 6.2: Cost mooring lines

Configuration	Length (m)	Price per line (€)
1	900	€94,635
2	900	€74,790

Combined with the prices of the anchors and installation cost this leads to a cost of €913,808 for mooring configuration 1 and a cost of €824,090 for mooring configuration 2. Table 6.3 shows the values of the mooring configurations when normalized to the cost per MW.

Table 6.3: Cost mooring configuration normalized to cost per MW

Configuration	original 5 MW	combined 6 MW	Total cost
1	€182,761	€152,301	€913,808
2	-	€137,348	€824,090

CAPEX

The following CAPEX breakdown values where computed by Myhr et al and will be used as a basis for the combined system. The value used for the mooring costs is the previously calculated value normalized to a value per MW. The values for the original 5 MW system are:

Table 6.4: CAPEX, original Spar

CAPEX	per MW
Development and consenting	€208,000
Construction phase insurance	€50,000
Turbine cost	€1,281,000
Support structure (inc. tower)	€888,000
mooring (inc. installation)	€182,761
Grid cost	€1,097,000
Installation cost	€157,000
Total CAPEX per MW (€)	€3,863,761

As mentioned in the previous section, adding a current turbine to the hywind spar will influence some of these breakdown values, but not all. An estimation of the cost of a 1 MW current turbine is obtained through literature. In the paper 'Evaluation and comparison of the levelized cost of tidal, wave, and offshore wind energy' by S. Astariz, A. Vazquez, and G. Iglesias (Astariz, Vazquez, and Iglesias, 2015), an estimation of the CAPEX of a current turbine is given. In the paper it is stated that the development cost of commercial current energy farms is similar to the development cost of offshore wind farms due to their similar environment. The development cost of the current turbine are assumed to be €208,000 per MW.

Furthermore it is assumed that the device cost per MW for a horizontal axis tidal turbines is similar to the device cost per MW of offshore wind turbines, which seems reasonable due to their similarities in design. The cost of the current turbine is assumed to be €1,281,000

After successfully scaling the cost of the other CAPEX, the following values are used in the combined model to calculate the levelized cost of energy with mooring configuration 1:

Table 6.5: CAPEX, combined system, mooring configuration 1

CAPEX	per MW
Development and consenting	€208,000
Construction phase insurance	€42,000
Turbine cost	€1,281,000
Support structure (inc. tower)	€740,000
mooring (inc. installation)	€152,301
Grid cost	€914,000
Installation cost	€130,000
Total CAPEX per MW (€)	€3,467,301

Using mooring configuration 2 results in a lower cost of the mooring system. The following values are used in the model to calculate the levelized cost of energy with mooring configuration 2:

Table 6.6: CAPEX, combined system, mooring configuration 2

CAPEX	per MW
Development and consenting	€208,000
Construction phase insurance	€42,000
Turbine cost	€1,281,000
Support structure (inc. tower)	€740,000
mooring (inc. installation)	€137,348
Grid cost	€914,000
Installation cost	€130,000
Total CAPEX per MW (€)	€3,452,348

OPEX

Myhr et al. gave an estimation of the annual operational cost of €131,000 per MW for the Hywind spar. Accurately estimating the cost of operating and maintenance of a current turbine is difficult to predict, due to the lack of long term operational data. A higher cost for O&M is expected due the complexity and location of the turbine under water. Literature shows some values for this cost, which is based on the experience from other offshore installations such as wind and oil platforms, but a large level of uncertainly still remains. The International Energy Agency predicts a value of €250,000 per MW of the annual operational cost of commercial scale current energy projects (IEA, 2015).

To have an estimation of the annual cost of operation and maintenance of the combined system these two values are combined with a weighted factor, where the weight

of O&M cost of Spar is 5 times higher than the weight of the O&M of the current turbine. This results in the annual operational cost of € 150,000 per MW for the combined system.

Annual Energy production

To determine the annual energy production of of the combined system an estimation of the energy production of the combined system needs to be made. The total annual energy production is a combination of the annual production of the wind and current turbine. This annual production is determined by the load factor, which is the ratio between the realized grid output and theoretical production.

The load factor of the wind turbine used in this thesis is assumed to be 44%, this value is a combination of the capacity factor and various losses. These losses consist of electrical array losses, aerodynamic losses and wind farm availability losses.

Determining the load factor of the current turbine is rather difficult. Depending on the configuration and location of the turbine, there is a wide range of different load factors found in literature. A value of 40% is assumed plausible by Ocean Energy Europe (Ocean Energy Europe, 2017), whilst values found in (NZ Electricity Commission, 2005) show a range from 40% to 50% and values found in (Batten et al., 2007) show a range that runs from 23% to 58%. To simplify the calculations of the annual energy production, the load factor of both the current and wind turbine is assumed to be 44%. With a theoretical annual production of 8760 MWh per MW this leads to a net annual energy production of 3854 MWh per MW

6.3.2 Levelized Cost of Energy

Implementing the values of CAPEX, OPEX and DECEX in the model results in a levelized cost of energy of the original 5 MW system of 149.4 €/MWh. This cost is calculated in Appendix H and is comparable to the LCOE calculated by Myhr et al.

Implementing the various values of CAPEX, OPEX and DECEX for the combined 6 MW system results in a levelized cost of energy of 142.3 €/MWh. Using mooring configuration 2 lowers the levelized of cost of energy to 141.9 €/MWh.

6.4 Discussion

The results of the simulations show the behavior of the system under various environmental conditions. During the modeling of the wind and current turbine some assumptions and simplifications are made to limit the complexity of the system. These limitations will influence the results of the simulations and will be addressed below. The last part of this section mentions some of the difficulties when using the levelized cost of energy model.

The first limitation has to do with the way the the wind turbine is modeled. The actuator disk model, which is used to calculate the thrust of the wind turbine, is only applicable up until the rated wind speed of the wind turbine, it cannot take into account the pitching of the blades. This pitching of the blades results in a lower thrust for an increasing wind velocity, this thrust curve can be observed in figure 4.4. To

have an estimation of the thrust at higher wind velocities, the previously mentioned thrust curve is used. However this thrust curve is for a land based turbine and for steady wind velocities. To account for the effects of the motions of the system a slightly higher thrust value is used. Although this thrust value gives an indication of the thrust at higher wind velocities it has some drawbacks. As mentioned in chapter 4 the aerodynamic loading of the rotor will influence the dynamic behavior of the system and the motions of the spar will influence the aerodynamic loading of the turbine. By using a constant value for the thrust, this coupling effect is not taken into account.

A second limitation lies in the assuming of a steady current velocity when calculating the thrust of the current turbine. ANSYS AQWA does not provide the external python server with the fluid velocity it uses during the simulation. During the simulation AQWA calculates the fluid velocity as a superposition of the current velocity and the horizontal particle velocity due to the motions of the waves. AQWA only provides the external python server with the resulting velocity of the structure during each time step. This velocity is used to calculate the relative velocity between the incoming fluid velocity and the velocity of the structure. During the calculations in the external subroutine this incoming velocity is assumed to be 2.5 m/s and the effect of the horizontal particle velocities induced by the waves at a depth of 30 meters is neglected. It should be noted that for short and relatively small waves this influence deep under water may be neglected, but for higher and longer waves this influence will play a significant role and should be taken into account.

The third limitation of this model is the influence of the rotational motions of the spar during the thrust calculations. While the platform motions are taken into account for the relative velocity during the thrust calculations, the influence of the rotational motions of the spar on the angle of the blades is not. As stated in the first limitation of the model, the actuator disk model cannot take into account the effect of an angling of the blades. This angle of the blades may influence the resulting thrust of the wind turbine under situations where the control system of the turbine is not able to adjust to the rotation of the platform.

A first estimation of the levelized cost of energy of the combined system is obtained, but a large level of uncertainly still remains. Accurately determining the the additional CAPEX and OPEX due to the adding of the current turbine is difficult. Due to a lack of industry data, there is a wide range of different values found in literature. Although currently still a problem, the more the floating wind and current energy industry matures, the more data will be available, making future estimations of the levelized cost of energy more accurate.

Chapter 7

Conclusion & Recommendations

7.1 Conclusion

With the shift towards a more sustainable energy society, the increase in the electricity produced by renewable energy sources is steadily rising. However the cost of renewable energy sources still remains high compared to the traditional fossil fuel based energy sources. With the total worldwide energy demand also rising, combining renewable energy sources helps to reduce the cost through a shared infrastructure and increase in energy production. In this thesis the feasibility of a combination of offshore wind and marine current energy is investigated. The effect of seizing down the weight of the mooring system in combination with reversing the direction of the thrust of the current turbine is also investigated as a further cost reduction.

The program ANSYS AQWA is used to investigate the dynamic behavior of the combined system. The thrust forces of the wind and current turbines are calculated via an external python server and added to the simulation in AQWA. The structure is modeled in a rigid body approximation, assuming no structural deformations.

There are four different load cases considered for this thesis. These load cases represent the environmental conditions which the system is subjected to. To model these environmental conditions several assumptions are made. The wind velocity in all load cases is assumed steady and the waves are modeled using the JONSWAP wave spectrum. The first load case represents the cut in wind speed for the wind turbine which is the lowest possible wind speed where the wind turbine can operate in. The second load case represents the rated wind conditions for the wind turbine and the third load case represents the upper most region in which the wind turbine can operate. Load case four represents survival mode for the system. Under these conditions, the wind turbine is parked and the blades of the current turbine are pitched to reverse the direction of the thrust. During each of these 4 load cases the system is subjected to a strong current.

In the operational load cases the mean value of the tension in the mooring lines is caused by both the drag forces on the hull and the wind loads on the top structure and the thrust forces of the wind and current turbine. While the oscillations around these mean values are caused by the periodic loading of the waves. These oscillations get bigger when the wave height increases.

In the survival load case the effect of reversing the direction of the thrust of the current turbine on the motions of the structure is investigated. It is concluded that using the current turbine has a positive effect on the motions of the structure, lowering the mean offset in Surge by 17.8 % and lowering the maximum value by 10.0 %. Furthermore,

the mean pitch angle is lowered by 20.4 % and the maximum value by 11.7%. These reductions lead to a lowering of the mean tension in the mooring lines of 20.7 % and a lowering of the maximum peak value of 19.3 %.

When the current turbine is used in combination with the the original mooring configuration the maximum tension in the mooring lines is 3232 kN. With a minimum breaking load of 5652 kN, the ratio of the minimum breaking load and maximum tension is 1.75. This value is higher than the safety factor of 1.67, which is required for floating production systems in the traditional offshore industry. Mooring configuration 2 has a maximum tension of 3082 kN. With a minimum breaking load of 4466 kN, this leads to a ratio of 1.45, which is lower than the safety factor of 1.67, but not by much. Mooring configuration 2 is chosen to be 20% lighter, to see the effect of scaling down the weight of the mooring system on both the dynamic behavior of the system and the levelized cost of energy. Meaning a properly designed mooring system can probably be lighter than the original setup and remain within the safety factor, if the current turbine is used.

Adding a current turbine to the system will increase the cost of the system, but the trade off is the extra generated electricity from the current turbine. To see if adding a current turbine has a positive effect on the levelized cost of energy, a first estimation is obtained by using an adapted LCOE model. The combined 6 MW wind and current system is compared to the original 5 MW Hywind spar, which has been used as a basis for the combined system. To have a realistic comparison between both systems some predefined values in the model remain the same. In both cases the expected operational lifetime of the project is 20 years with a discount rate of 8.2%. The preliminary development and construction phase takes 4 years and the decommission time takes 1 year. This gives a total project time of 25 years.

During the calculations of the LCOE of the combined system it is assumed that the extra cost related to the adding of the current turbine are for the development, maintenance and for the turbine itself. The cost related to the installation, construction insurance, support structure, grid costs and decommissioning are assumed to remain similar. The mooring cost are assumed similar at first to calculate the effect of adding the current turbine to the system. After estimating the increased energy production of the current turbine, a levelized cost of energy of 142.3 €/MWh is calculated for the combined system. The levelized cost of energy of the original system is 149.4 €/MWh, so adding a current turbine has a positive effect on the levelized cost of energy. The next step will be simulating the effect of scaling down the weight of the mooring system on the LCOE. The mooring cost will be lowered and added to the LCOE model. Unfortunately, the effect of downscaling the weight of the mooring system only has a marginal effect on the LCOE. The LCOE for the second mooring configuration is 141.9 €/MWh, compared to the 142.3 €/MWh of the first mooring configuration this difference doesn't justify the increased risks of failure.

Although still considered relatively high, the LCOE of the investigated system is comparable to the LCOE of dutch wind farms. The Borssele 2015 wind farm has for instance a LCOE of 149.0 €/MWh, if the grid cost is taken into account (ECN, 2015). With time and more industry data, further ways of lowering the levelized cost of energy could be investigated making this combination more successful and comparable to fossil fuel based energy sources, which have an average LCOE of approximately 70 €/MWh (VGB PowerTech, 2015) .

7.2 Recommendations

A first estimation of the effect of combining offshore wind and current energy on a floating platform is obtained. Future work should be done to accurately describe the system under realistic conditions to gain more knowledge of the effects of this combination. Some recommendations for future research and cost reduction strategies are made below:

The actuator disk theory is a quick way to give an estimate of the thrust forces of a wind and current turbine, but has some drawbacks. The actuator disk theory cannot take into account the effect of an angling of the blades, which is of importance due to the motions of the platform and to accurately calculate the thrust forces at flow speeds above rated wind or current velocity. To overcome this drawback it is recommended to use Blade Element Momentum Theory in an environment with more control for the user than ANSYS AQWA.

A rudimentary blade is designed in this thesis. Future research should be done into optimizing blades for the dual use of the current turbine. It may be of interest to see what the possibilities are of optimizing blades which can also be used as propulsion during storm conditions.

The cost of O&M is estimated using values found in literature, but accurately determining the cost of O&M is of importance. In the calculations of the LCOE, the cost of O&M remains the same over the entire project lifetime, which may be a high estimation. Further technological developments should be implemented in O&M estimations, which may lower the cost of O&M considerably. A lowering of the annual O&M cost by €100,000 will for instance result in a lowering of the levelized cost of energy from 142.3 to 138.0 €/MWh.

Future research should be done to investigate ways of lowering the CAPEX of the combined system. A way of lowering these cost is to increase the amount of deployed units of the system. Large-scale production will most likely result in lower production cost of both the substructure and turbines. These cost make up a large part of the total CAPEX, so lowering these cost will result in a further reduction of the levelized cost of energy of the system.

Appendix A

Wind coefficients

In order to add the loads due to wind forces on the structure, AQWA makes use of wind coefficients. These wind coefficients are defined as the force or moment per unit velocity squared. The moment is about the center of gravity and the forces are a function of the relative velocity between the structure and wind. AQWA uses a reference wind speed and direction to calculate the aerodynamic loading off the top structure.

A.1 Reference wind speed

The variation of the wind velocity over height U_z is defined based on a reference wind speed at z = 90 m:

$$U_z = U_r * (\frac{Z}{Z_r})^{\alpha}$$

In this formula U_r is the wind speed at a reference height Z_r. The vertical coordinate Z varies along the height of the structure and the wind profile component α= 0.11 is based on the guidelines for offshore wind turbine design of DNV (DNV, 2014)

α = 0.11

U_r = reference wind speed (m/s)

Z_r = 90 m

A.1.1 Tower loads

The aerodynamic loading on the tower can be calculated with the formula below. The diameter d of the tower varies from 6 meters at the bottom to 4 meters at the top, this is implemented by creating segments with a different diameter. The height of each segment dZ is 1 meter. The value of the drag coefficient C_D is assumed to be 1.2 (Zaaijer, 2017).

$$\text{Fw.tower} = \frac{1}{2}\ \rho_{air}\ C_D\ U_z^2\ dA$$

ρ_{air} = 1.2041 kg/m^3

C_D = 1.2

dA = d*dZ (m^2)

dZ = 1 m

A.1.2 Nacelle loads

The drag coefficient of a nacelle is assumed to be 1.2 (Zaaijer, 2017). Furthermore, the value of dA is found to be 36 m^2 (Vijfhuizen, 2008).

$$\text{Fw.nacelle} = \frac{1}{2}\,\rho_{air}\,C_D\,U_{hub}^2\,dA$$

ρ_{air} = 1.2041 kg/m^3

C_D = 1.2

dA = 36 m^2

A.1.3 Rotor loads

During survival mode the rotor is parked in and the nacelle will follow the wind direction. In this position the blades are feathered to reduce the frontal area. The value of C_D is that of an airfoil, which is assumed to be 0.04 (NASA, 2015). The value of dA is the lateral area for the blades when feathered, which is 200 m^2 (Vijfhuizen, 2008).

$$\text{Fw.rotor} = \frac{1}{2}\,\rho_{air}\,C_D\,U_{hub}^2\,dA$$

ρ_{air} = 1.2041 kg/m^3

C_D = 0.04

dA = 200 m^2

A.1.4 Wind Coefficients

These are the resulting wind coefficients in all degrees of freedom:

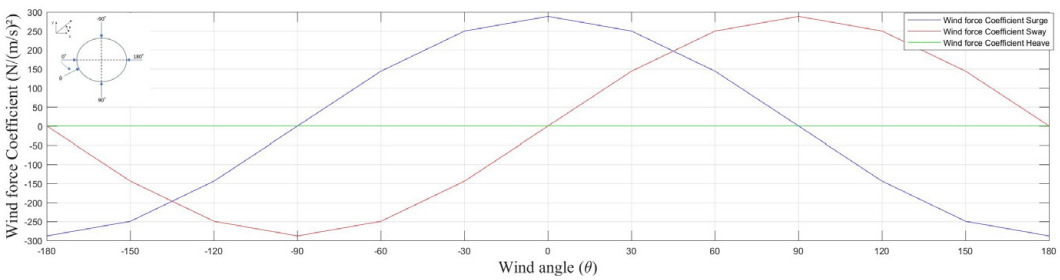

Figure A.1: Wind force coefficients, operational mode

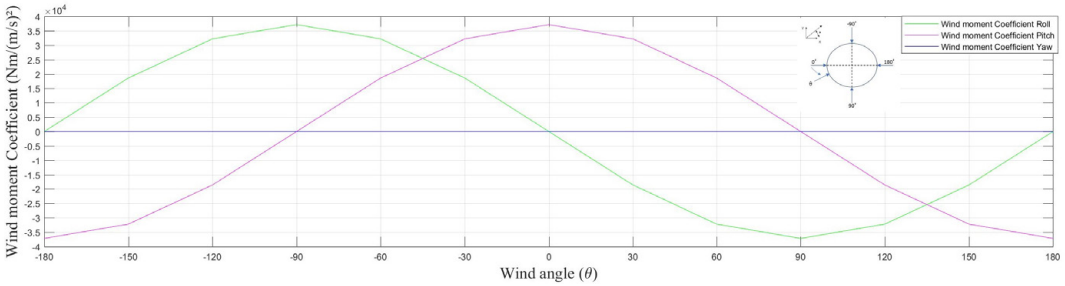

Figure A.2: Wind moments coefficients, operational mode

Table A.1: Wind coefficients operational condition

Direction	Surge	Sway	Heave	Roll	Pitch	Yaw
°	$N/(m/s)^2$	$N/(m/s)^2$	$N/(m/s)^2$	$Nm/(m/s)^2$	$Nm/(m/s)^2$	$Nm/(m/s)^2$
-180	-288	0	0	0	-37208	0
-150	-249.42	-144	0	18604	-32223.07	0
-120	-144	-249.42	0	32223.3	-18604	0
-90	0	-288	0	37208	0	0
-60	144	-249.42	0	32223.3	18604	0
-30	249.42	-144	0	18604	32223.07	0
0	288	0	0	0	37208	0
30	249.42	144	0	-18604	32223.07	0
60	144	249.42	0	-32223.07	18604	0
90	0	288	0	-37208	0	0
120	-144	249.42	0	-32223.07	-18604	0
150	-249.42	144	0	-18604	-32223.07	0
180	-288	0	0	0	-37208	0

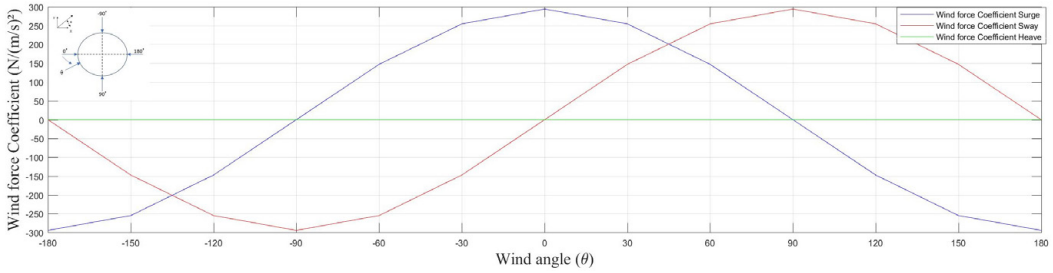

Figure A.3: Wind force coefficients, survival mode

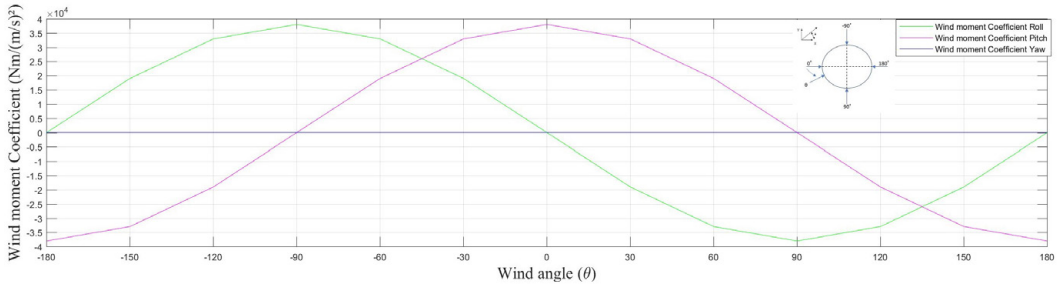

Figure A.4: Wind moments coefficients, survival mode

Table A.2: Wind coefficients Survival condition

Direction	Surge	Sway	Heave	Roll	Pitch	Yaw
°	$N(m/s)^2$	$N(m/s)^2$	$N(m/s)^2$	$Nm(m/s)^2$	$Nm(m/s)^2$	$Nm(m/s)^2$
-180	-294	0	0	0	-38017	0
-150	-254.61	-147	0	19008.5	-32923.69	0
-120	-147	-254.61	0	32923.69	-19008.5	0
-90	0	-294	0	38017	0	0
-60	147	-254.61	0	32923.69	19008.5	0
-30	254.61	-147	0	19008.5	32923.69	0
0	294	0	0	0	38017	0
30	254.61	147	0	-19008.5	32923.69	0
60	147	254.61	0	-32923.69	19008.5	0
90	0	294	0	-38017	0	0
120	-147	254.61	0	-32923.69	-19008.5	0
150	-254.61	147	0	-19008.5	-32923.69	0
180	-294	0	0	0	-38017	0

Appendix B

External python server

AQWA can accept forces calculated from a process running on an external python server. The external server feature is activated by linking AQWA and the external process through a socket. A socket in this context refers to an internal endpoint for sending or receiving data. The server creates a socket, binds it to a free port number, and begins listening on that port. The feature requires the SUFC option to be activated in AQWA. AQWA provides the external server with the position and velocity of the center of gravity in all DOF's, through the socket at each time step. Simultaneously, AQWA listens to the socket for the information generated by the external process and adds the calculated forces to the simulation

During the simulation the thrust forces of the wind and current are calculated with the formula's described in chapter 4. To calculate the relative velocity the turbine encounters at hub height, the incoming wind velocity is decomposed into the structures directions of Surge and Sway by using sines and cosines. The python server uses radians as angles so a direction of 0° correspondents with 0 rad, a direction of 30° correspondents with $\pi/6$ rad, a direction of 60° correspondents with $\pi/3$ rad and a direction of 90° correspondents with $\pi/2$ rad. After the wind velocity is decomposed, the relative velocity which the turbine encounters is obtained by subtracting the structure velocity in surge and sway from the decomposed wind velocity in those directions.

The thrust forces of the current turbine are added in a similar way, but the direction of the current is 0° or 180°. An example of the used python code can be found below.

```
#########################################################################
from AqwaServerMgr import *

#########################################################################

# External force subroutine for load case 2 with a current
    direction of 180 degrees and a wind and waves direction of 60
    degrees
# Force is acting in Surge Sway, Roll and Pitch


def UF(Analysis,Mode,Stage,Time,TimeStep,Pos,Vel):
    AddMass = BlankAddedMass(Analysis.NOfStruct)
    Force   = BlankForce(Analysis.NOfStruct)
    Error   = 0
```

```
    # User defined code here
    for s in range(Analysis.NOfStruct):

Force[s][0] =( 0.5*1.2*pi*63*63*(cos(pi/3)*11
-(Vel[s][0]+170*Vel[s][4]))*(cos(pi/3)*11-(Vel[s][0]
+170*Vel[s][4]))*0.3*4*0.7)
- 0.5*1025*pi*100*(2.5+(Vel[s][0]+50*Vel[s][4]))*(2.5+
(Vel[s][0]+50*Vel[s][4]))*0.40

Force[s][1] =( 0.5*1.2*pi*63*63*(sin(pi/3)*11
-(Vel[s][1]-170*Vel[s][3]))*(sin(pi/3)*11-(Vel[s][1]
-170*Vel[s][3]))*0.3*4*0.7)

Force[s][3] = -1*(170*Force[s][1])

Force[s][4] =(170*(0.5*1.2*pi*63*63*(cos(pi/3)*11
-(Vel[s][0]+170*Vel[s][4]))*(cos(pi/3)*11-(Vel[s][0]
+170*Vel[s][4]))*0.3*4*0.7)) - 50 *(0.5*1025*pi*100*(2.5
+(Vel[s][0]+50*Vel[s][4]))*(2.5+(Vel[s][0]+50*Vel[s][4]))*0.40)

    # Now return the results

    return Force,AddMass,Error


##########################################################################

Server = AqwaUserForceServer()

for UF in [UF]:
    try:
      print 'Now running user function "'+UF.__name__+'"'
      Server.Run(UF)
    except Exception as E: # If an error occurred, we print it but
        continue
        print "Caught error : ",E
        print "Skipping to next case"
```

```
##########################################################################
from AqwaServerMgr import *

##########################################################################

# load case where current turbine is used as propulsion. Current
    direction is 0 degrees and the wind and wave direction is 0
    degrees.
# Force is acting in Surge and Pitch.


def UF(Analysis,Mode,Stage,Time,TimeStep,Pos,Vel):
    AddMass = BlankAddedMass(Analysis.NOfStruct)
    Force   = BlankForce(Analysis.NOfStruct)
    Error   = 0
```

```
    # User defined code here
    for s in range(Analysis.NOfStruct):

Force[s][0] = (44.441*(2.5-(Vel[s][0]+50*Vel[s][4]))**9
    -1385.1*(2.5-(Vel[s][0]+50*Vel[s][4]))**8 +
    18058*(2.5(Vel[s][0]+50*Vel[s][4]))**7 -1.2717*10**5 *
    (2.5-(Vel[s][0]+50*Vel[s][4]))**6 + 5.214*10**5
    *(2.5-(Vel[s][0]+50*Vel[s][4]))**5 -1.2539*10**6
    *(2.5-(Vel[s][0]+50*Vel[s][4]))**4 + 1.72*10**6 *
    (2.5-(Vel[s][0]+50*Vel[s][4]))**3 +
      -1.2651*10**6 *(2.5-(Vel[s][0]+50*Vel[s][4]))**2 +
          4.1223*10**5 *(2.5-(Vel[s][0]+50*Vel[s][4]))
          -5.8385*10**5)

Force[s][4] = 50*(44.441*(2.5-(Vel[s][0]+50*Vel[s][4]))**9
    -1385.1*(2.5-(Vel[s][0]+50*Vel[s][4]))**8 +
    18058*(2.5-(Vel[s][0]+50*Vel[s][4]))**7 -1.2717*10**5 *
    (2.5-(Vel[s][0]+50*Vel[s][4]))**6 + 5.214*10**5
    *(2.5-(Vel[s][0]+50*Vel[s][4]))**5 -1.2539*10**6
    *(2.5-(Vel[s][0]+50*Vel[s][4]))**4 + 1.72*10**6 *
    (2.5-(Vel[s][0]+50*Vel[s][4]))**3 +
      -1.2651*10**6 *(2.5-(Vel[s][0]+50*Vel[s][4]))**2 +
          4.1223*10**5 *(2.5-(Vel[s][0]+50*Vel[s][4]))
          -5.8385*10**5)

    # Now return the results

    return Force,AddMass,Error


##########################################################################

Server = AqwaUserForceServer()

for UF in [UF]:
    try:
      print 'Now running user function "'+UF.__name__+'"'
      Server.Run(UF)
    except Exception as E: # If an error occurred, we print it but
        continue
        print "Caught error : ",E
        print "Skipping to next case"
```

Appendix C

SERI 8PT Hydrofoil

Reynolds number in millions = 2.5
Stall angle = 19°)
C_n slope for zero lift (dimensionless) = 0
C_n at stall value for positive angle of attack (dimensionless) = 0
C_n at stall value for negative angles of attack = 0°
Angle of attack for minimum C_D = 0°
Minimum C_D value = 0

α	C_l	C_d	C_{pmin}
-180	0.0000	0.0570	-1
-175	0.0255	0.0661	-1
-170	0.0510	0.0932	-1
-165	0.0765	0.1376	-1
-160	0.1020	0.1977	-1
-155	0.1275	0.2717	-1
-150	0.1530	0.3574	-1
-145	0.2822	0.4521	-1
-140	0.3752	0.5528	-1
-135	0.4368	0.6565	-1
-130	0.4700	0.7598	-1
-125	0.4771	0.8596	-1
-120	0.4604	0.9528	-1
-115	0.4220	1.0364	-1
-110	0.3645	1.1077	-1
-105	0.2905	1.1646	-1
-100	0.2030	1.2051	-1
-95	0.1051	1.2280	-1
-90	0.0000	1.2324	-1
-85	-0.1089	1.2181	-1
-80	-0.2185	1.1853	-1
-75	-0.3257	1.1351	-1
-70	-0.4277	1.0688	-1
-65	-0.5220	0.9882	-1
-60	-0.6069	0.8958	-1
-55	-0.6810	0.7943	-1
-50	-0.7437	0.6866	-1
-45	-0.7956	0.5759	-1
-40	-0.8385	0.4656	-1
-35	-0.8759	0.3588	-1
-30	-0.9143	0.2588	-1
-28	-0.9323	0.2213	-1
-26	-0.9532	0.1856	-1
-24	-0.9786	0.1519	-1
-22	-1.0104	0.1201	-1
-20	-1.0513	0.0906	-1
-19	-1.0919	0.0770	-11.699
-18.5	-1.0989	0.0702	-11.526
-18	-1.1050	0.0635	-11.315
-17.5	-1.0984	0.0585	-11.027
-17	-1.1048	0.0522	-10.858
-16.5	-1.1036	0.0470	-10.589
-16	-1.0968	0.0425	-10.277
-15.5	-1.0905	0.0381	-9.969
-15	-1.0824	0.0343	-9.617
-14.5	-1.0725	0.0307	-9.224
-14	-1.0631	0.0274	-8.947
-13.5	-1.0429	0.0244	-8.526
-13	-0.9972	0.0211	-8.027
-12.5	-0.9354	0.0186	-7.364
-12	-0.8974	0.0167	-6.966
-11.5	-0.8813	0.0153	-6.565
-10.5	-0.8449	0.0132	-5.855
-10	-0.8059	0.0125	-5.408
-9.5	-0.7618	0.0119	-4.947
-9	-0.7153	0.0113	-4.465
-8.5	-0.6662	0.0108	-4.016
-7.5	-0.5631	0.0099	-3.125
-7	-0.5095	0.0095	-2.707
-6.5	-0.4552	0.0092	-2.314
-6	-0.4007	0.0088	-1.94
-5.5	-0.3512	0.0079	-1.624
-5	-0.3061	0.0063	-1.342
-4.5	-0.2488	0.0060	-1.093
-4	-0.1909	0.0059	-0.945
-3.5	-0.1326	0.0058	-0.893
-3	-0.0742	0.0057	-0.842
-2.5	-0.0158	0.0056	-0.792
-2	0.0425	0.0056	-0.744
-1.5	0.1011	0.0055	-0.697
-1	0.1597	0.0055	-0.675
-0.5	0.2182	0.0055	-0.72
0	0.2765	0.0055	-0.767

α	C_l	C_d	C_{pmin}
0	0.2765	0.0055	-0.767
0.5	0.3348	0.0056	-0.814
1	0.3929	0.0056	-0.861
1.5	0.4506	0.0057	-0.911
2	0.5079	0.0058	-0.962
2.5	0.5646	0.0059	-1.013
3	0.6204	0.0061	-1.065
3.5	0.6749	0.0064	-1.116
4	0.7291	0.0066	-1.172
4.5	0.7829	0.0069	-1.247
5	0.8362	0.0072	-1.429
5.5	0.8881	0.0075	-1.626
6	0.9376	0.0080	-1.83
6.5	0.9843	0.0085	-2.039
7	1.0175	0.0097	-2.228
7.5	1.0406	0.0111	-2.402
8	1.0707	0.0119	-2.614
8.5	1.1060	0.0125	-2.847
9	1.1418	0.0132	-3.094
9.5	1.1775	0.0139	-3.376
10	1.2117	0.0147	-3.741
10.5	1.2440	0.0157	-4.07
11.5	1.3057	0.0178	-4.799
12	1.3326	0.0192	-5.188
12.5	1.3570	0.0204	-5.566
14	1.4339	0.0260	-6.665
14.5	1.4544	0.0284	-7.054
15	1.4726	0.0312	-7.459
15.5	1.4915	0.0340	-7.852
16	1.5059	0.0374	-8.256
16.5	1.5184	0.0411	-8.593
17	1.5309	0.0451	-8.923
17.5	1.5361	0.0499	-9.267
18	1.5440	0.0547	-9.625
18.5	1.5455	0.0605	-9.947
19	1.5463	0.0666	-10.239
19.5	1.5438	0.0733	-10.537
20	1.5366	0.0809	-10.714
21	1.4458	0.0950	-1
22	1.4033	0.1101	-1
24	1.3299	0.1420	-1
26	1.2687	0.1759	-1
28	1.2165	0.2118	-1
30	1.1711	0.2494	-1
35	1.0762	0.3500	-1
40	0.9948	0.4573	-1
45	0.9167	0.5683	-1
50	0.8360	0.6797	-1
55	0.7497	0.7881	-1
60	0.6563	0.8904	-1
65	0.5558	0.9837	-1
70	0.4490	1.0651	-1
75	0.3376	1.1323	-1
80	0.2238	1.1835	-1
85	0.1102	1.2171	-1
90	0.0000	1.2324	-1
95	-0.1038	1.2289	-1
100	-0.1977	1.2070	-1
105	-0.2786	1.1674	-1
110	-0.3432	1.1114	-1
115	-0.3883	1.0409	-1
120	-0.4110	0.9582	-1
125	-0.4084	0.8658	-1
130	-0.3776	0.7668	-1
135	-0.3157	0.6641	-1
140	-0.2189	0.5611	-1
145	-0.1915	0.4609	-1
150	-0.1642	0.3668	-1
155	-0.1368	0.2815	-1
160	-0.1094	0.2078	-1
165	-0.0821	0.1480	-1
170	-0.0547	0.1039	-1
175	-0.0274	0.0769	-1
180	0.0000	0.0677	-1

Appendix D

Results Load case 1

D.1 Direction current 0°

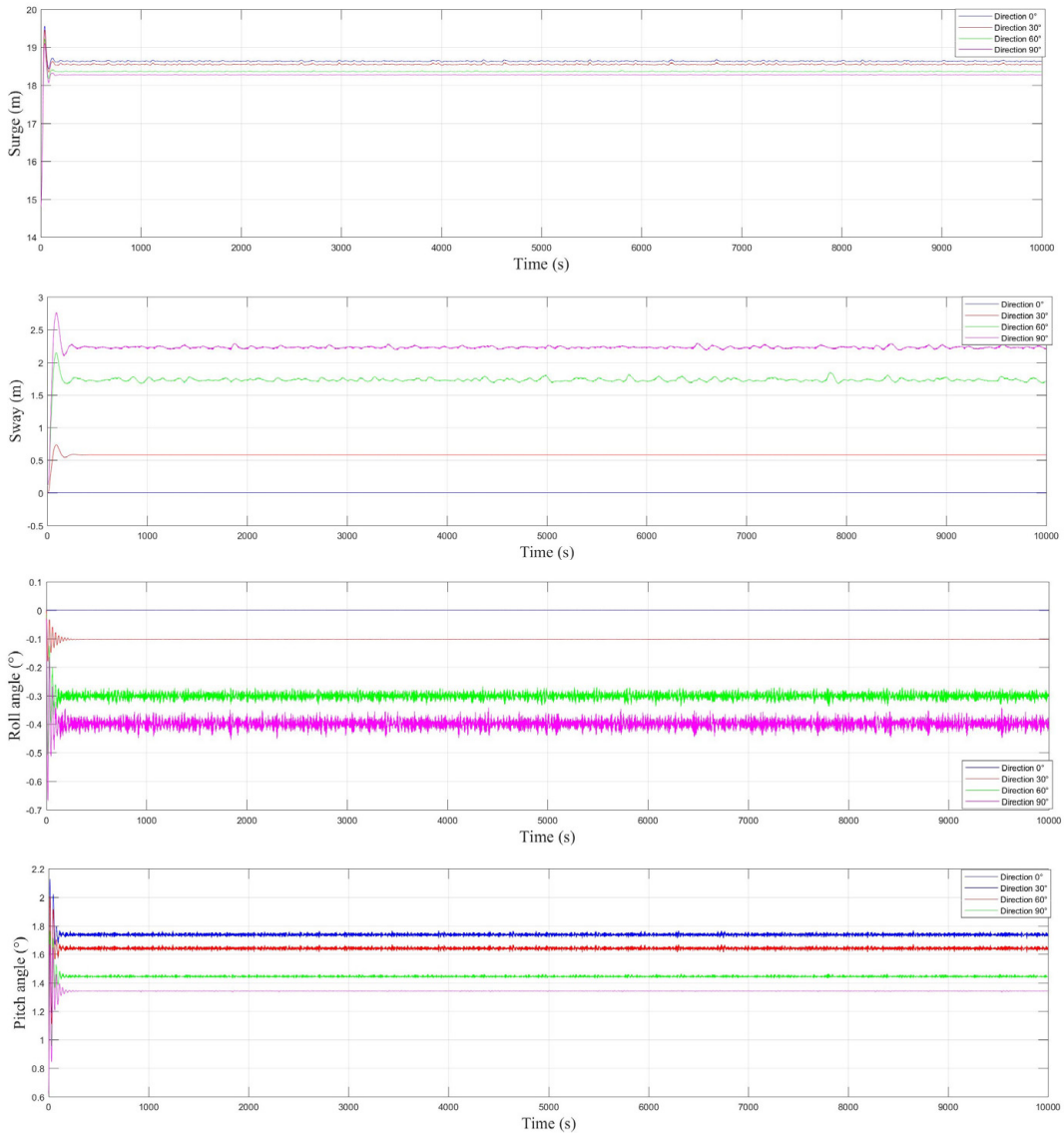

Figure D.1: The motions of the structure, load case 1, direction current 0°

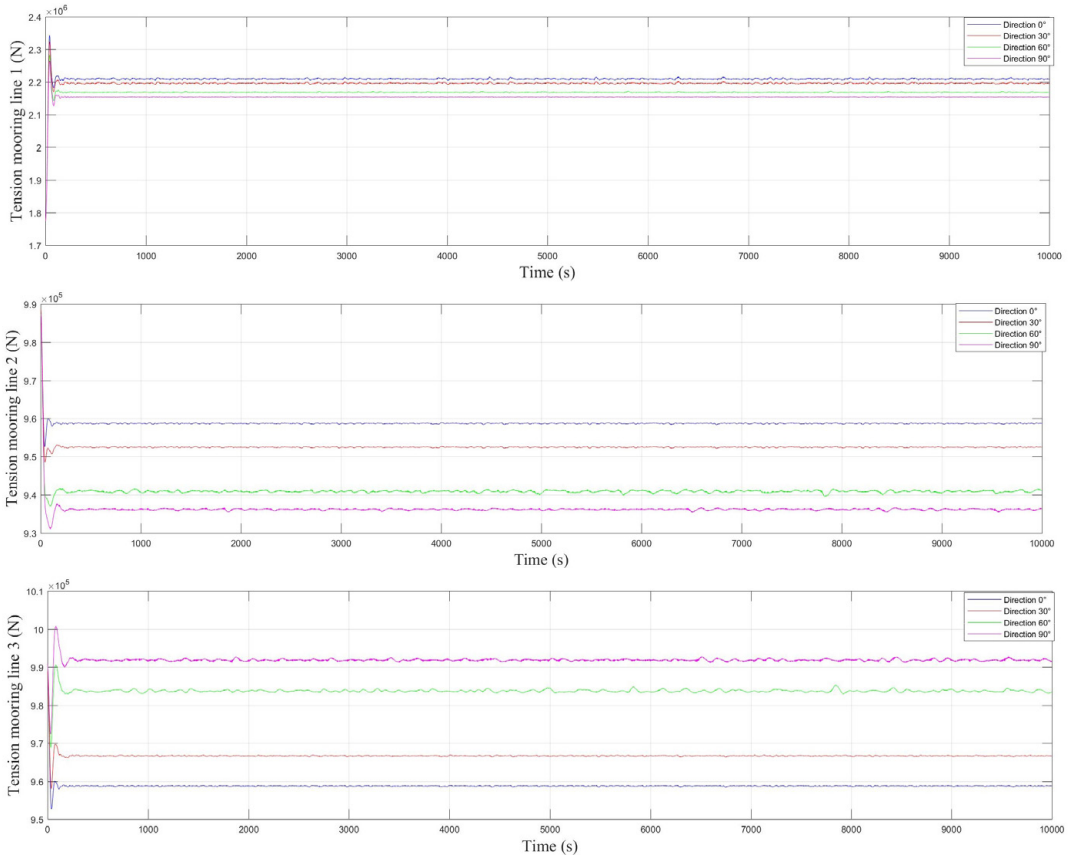

Figure D.2: Tension mooring lines, load case 1, direction current 0°

D.2 Direction current 180°

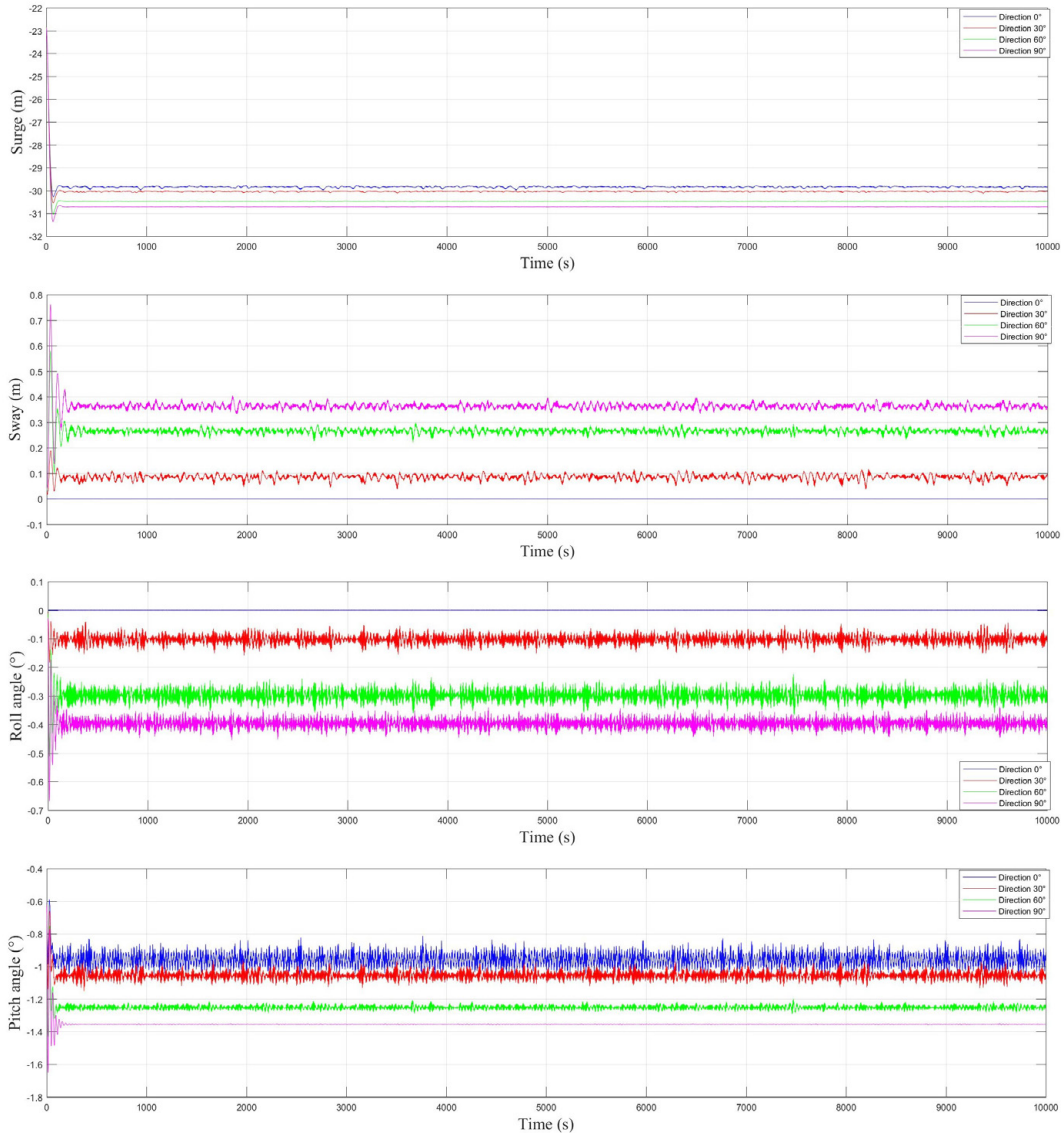

Figure D.3: The motions of the structure, load case 1, direction current 180°

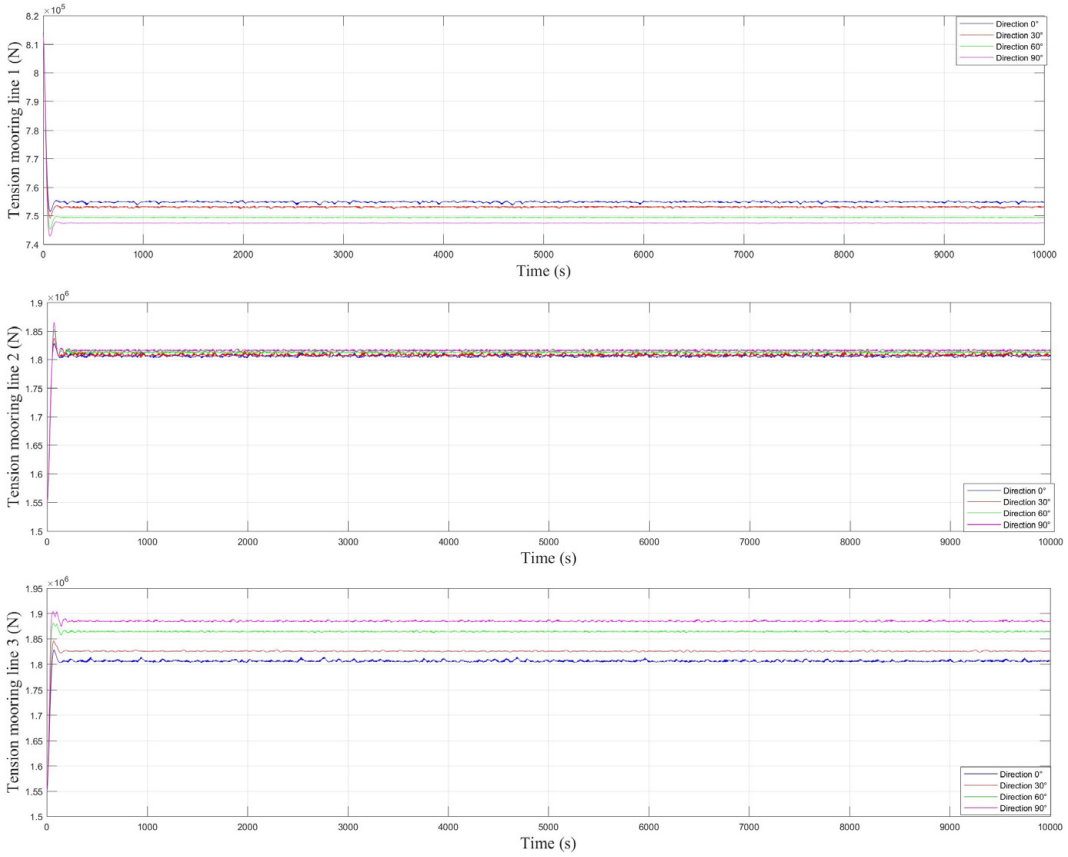

Figure D.4: Tension mooring lines, load case 1, direction current 180°

Appendix E

Results Load case 2

E.1 Direction current 0°

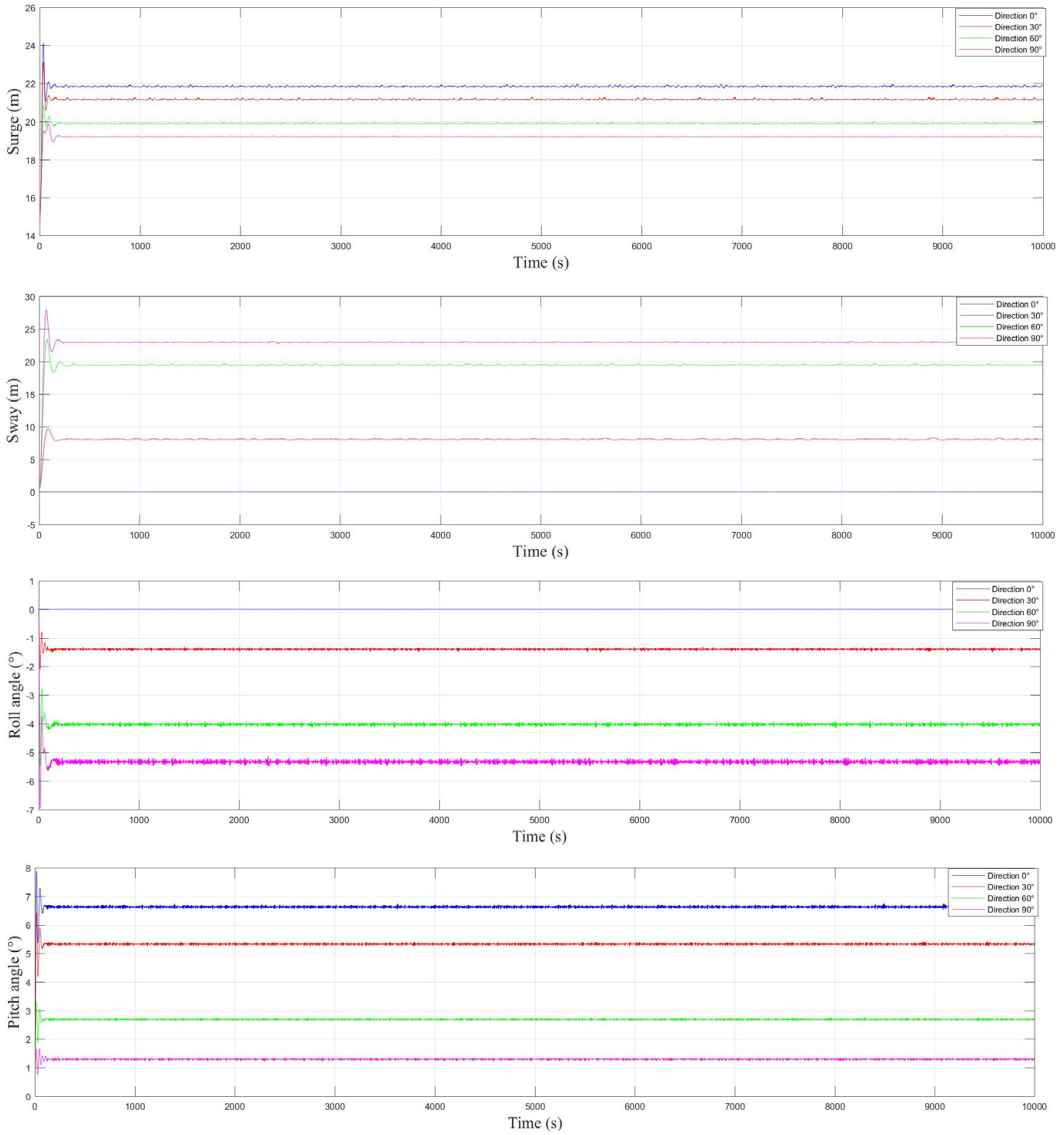

Figure E.1: The motions of the structure, load case 2, direction current 0°

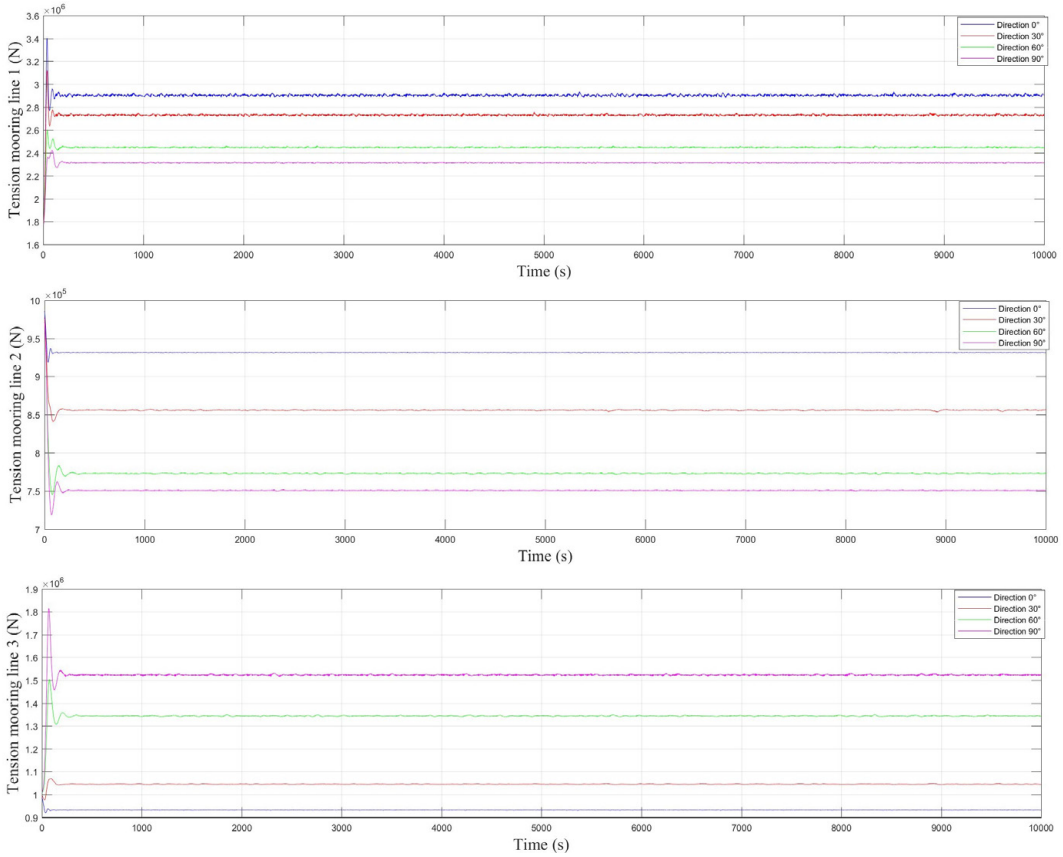

Figure E.2: Tension mooring lines, load case 2, direction current 0°

E.2 Direction current 180°

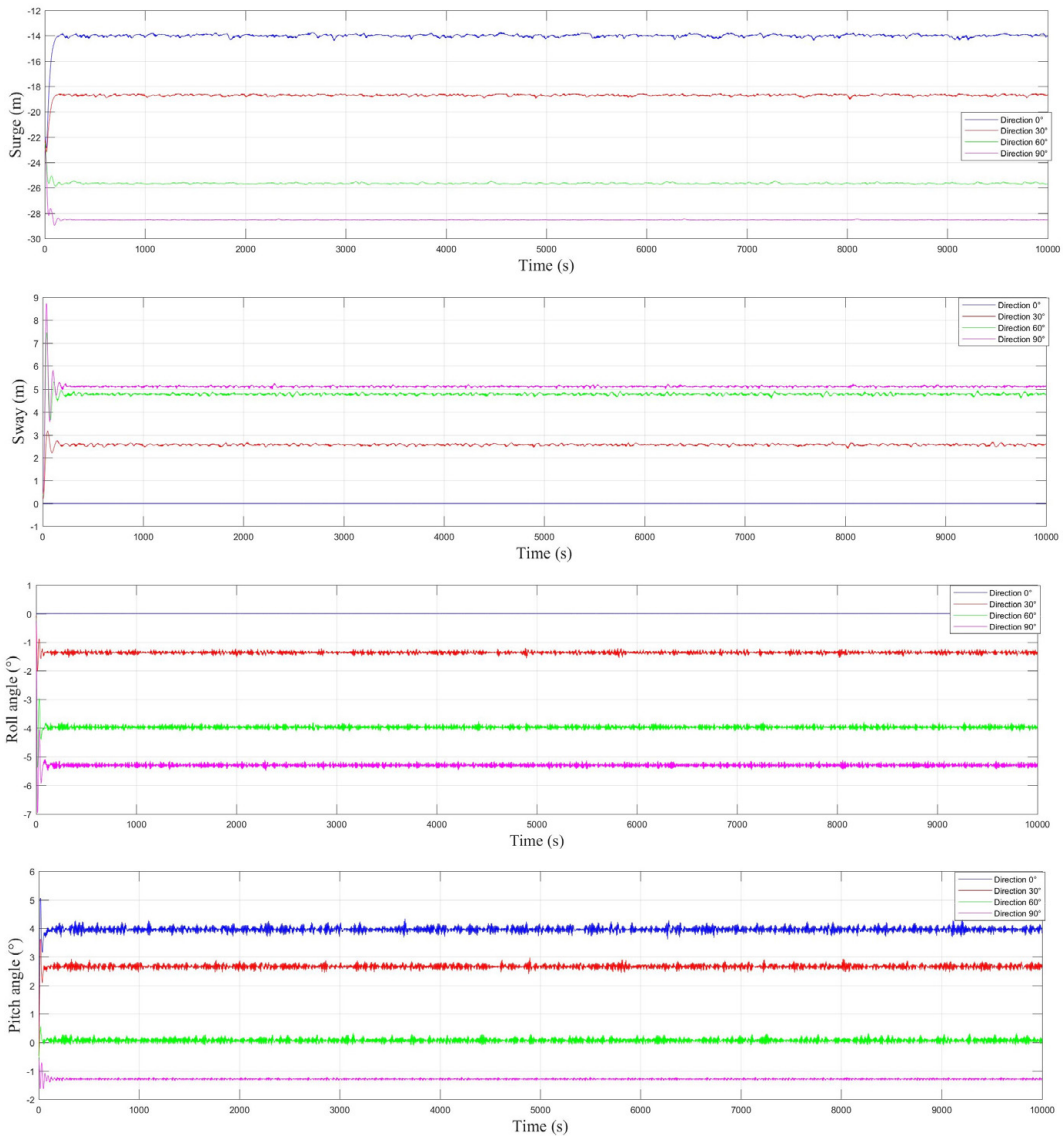

Figure E.3: The motions of the structure, load case 2, direction current 180°

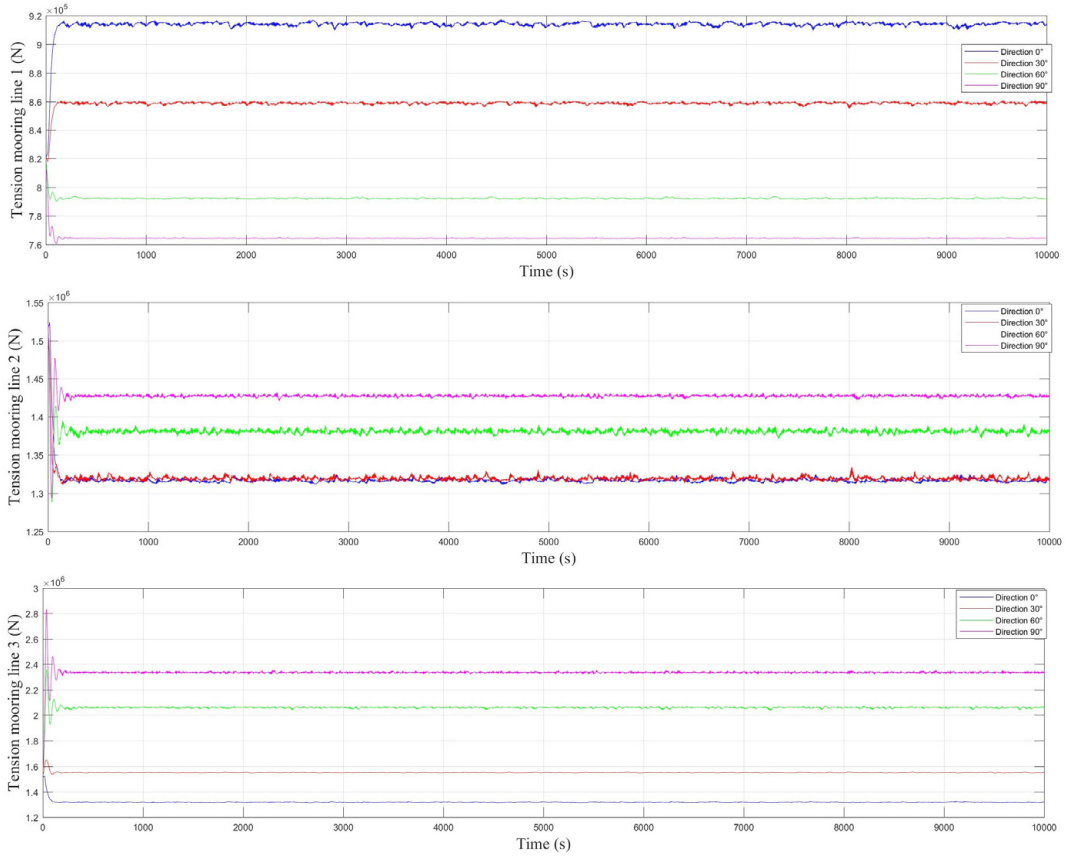

Figure E.4: Tension mooring lines, load case 2, direction current 180°

Appendix F

Results Load case 3

F.1 Direction current 0°

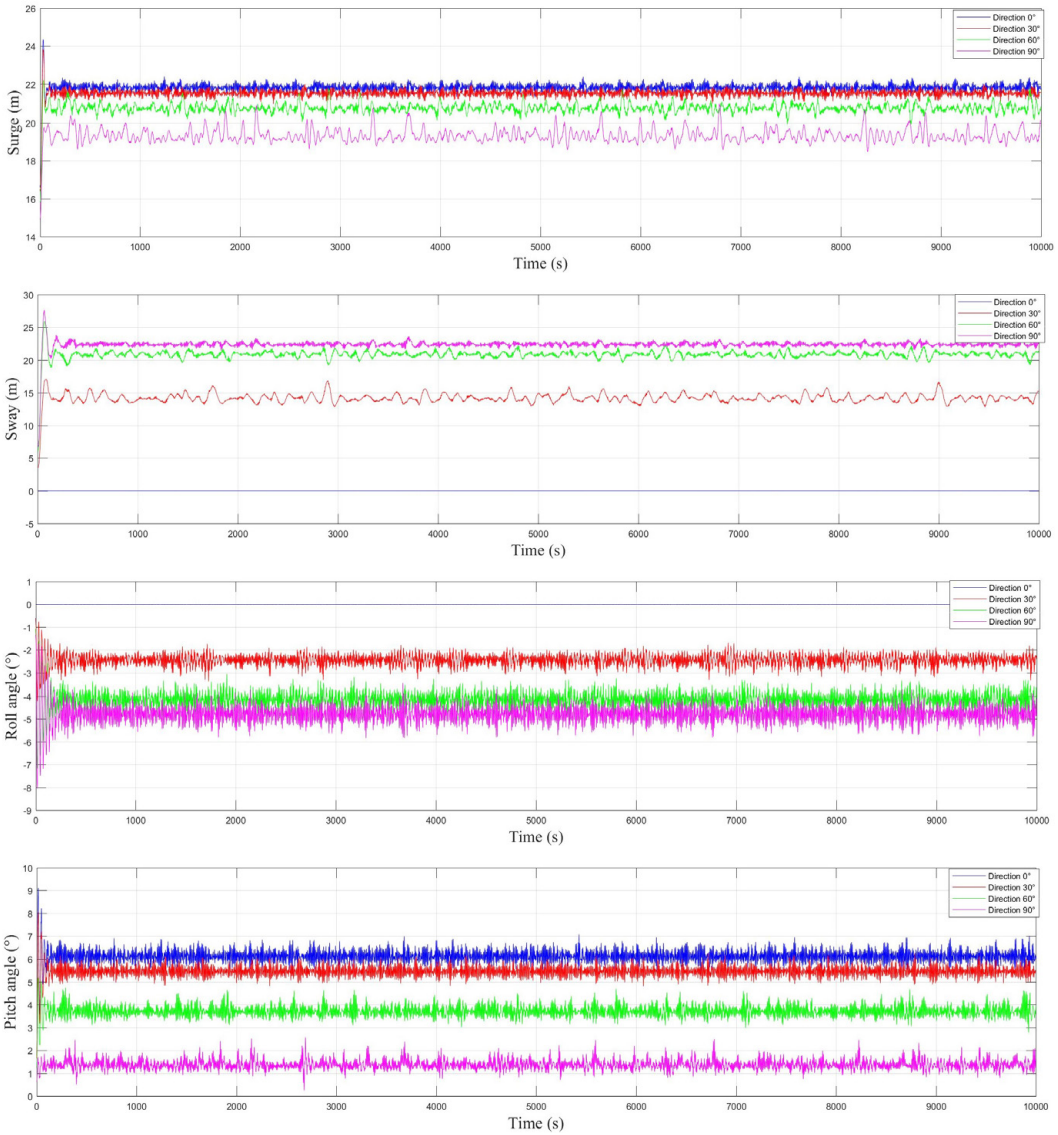

Figure F.1: The motions of the structure, load case 3, direction current 0°

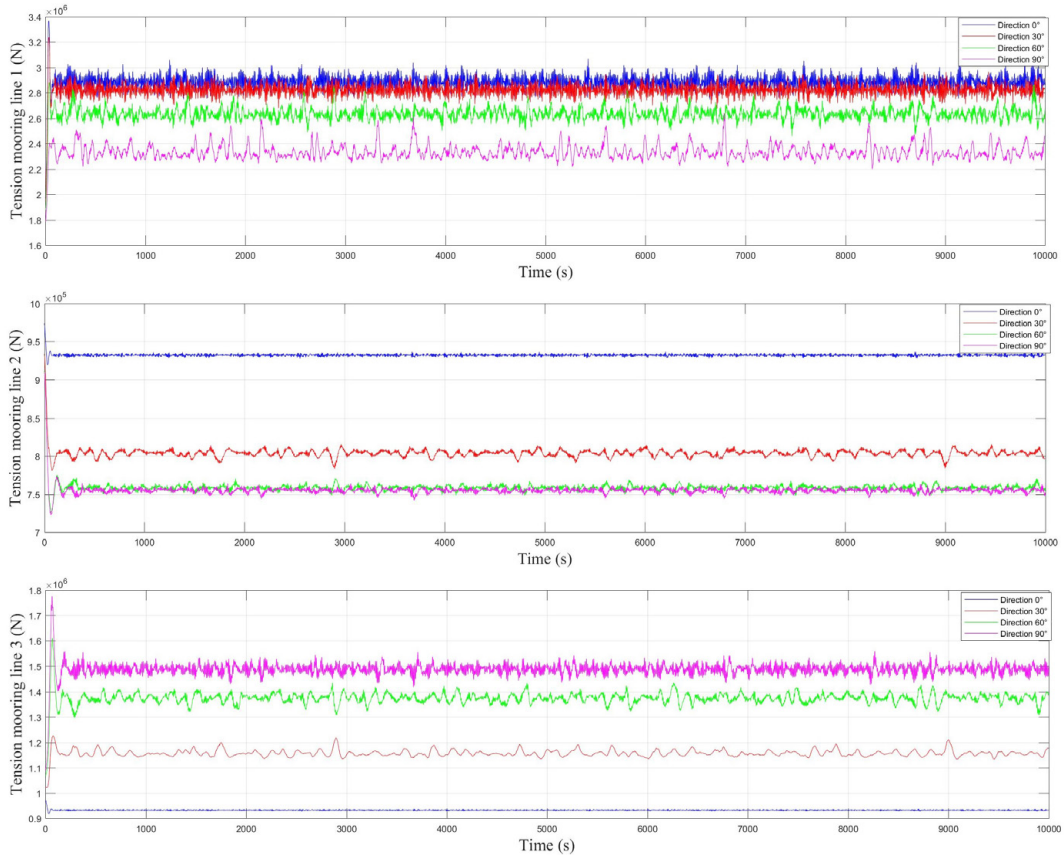

Figure F.2: Tension mooring lines, load case 3, direction current 0°

F.2 Direction current 180°

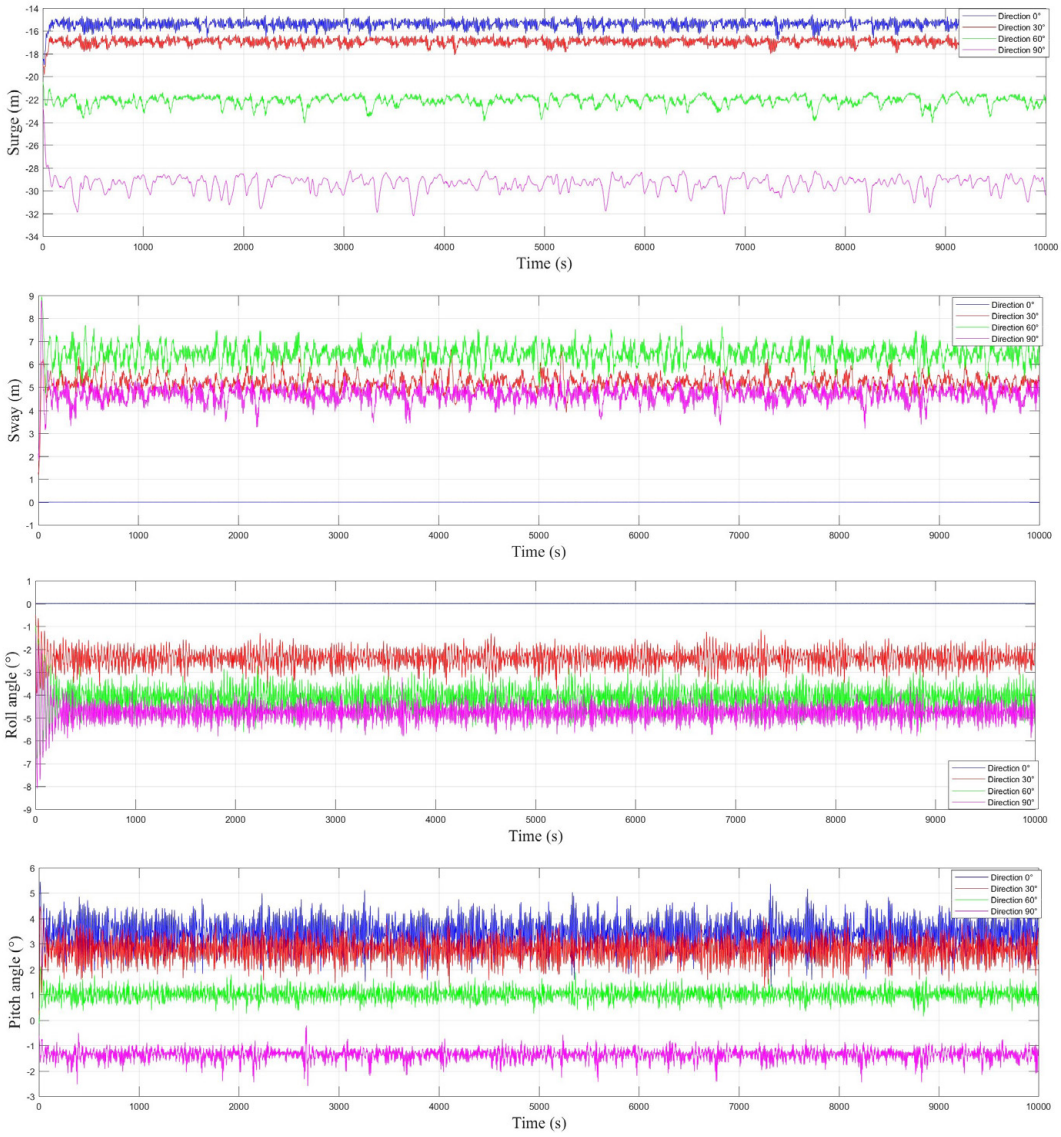

Figure F.3: The motions of the structure, load case 3, direction current 180°

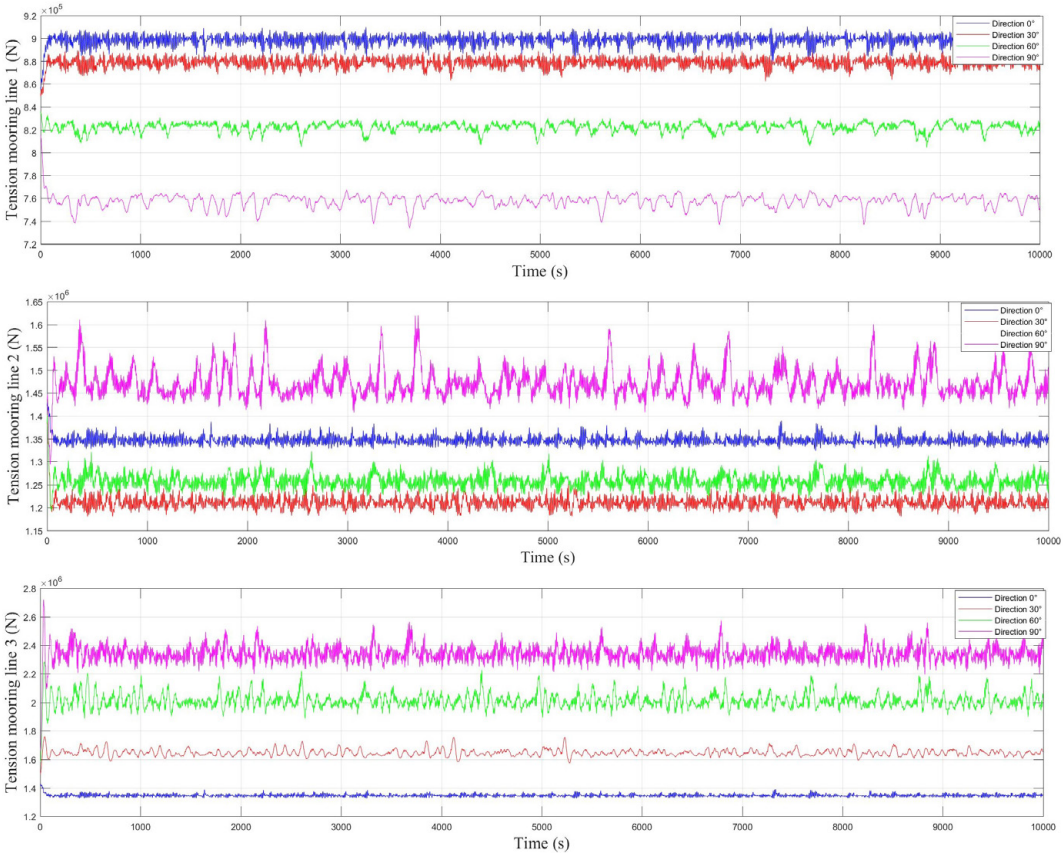

Figure F.4: Tension mooring lines, load case 3, direction current 180°

Appendix G

Results Load case 4

G.1 Mooring configuration 1

G.1.1 Current Turbine parked

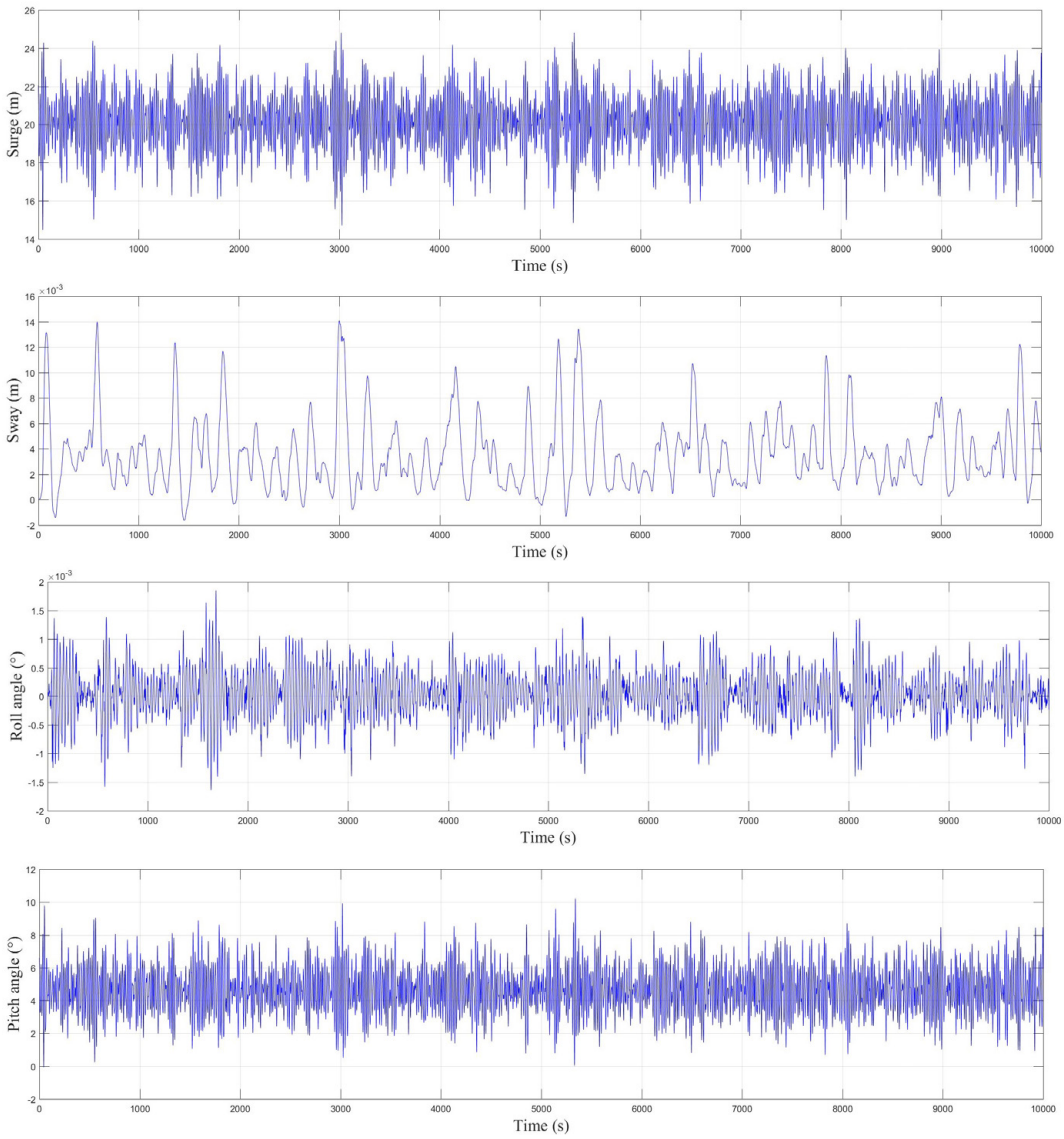

Figure G.1: The motions of the structure, load case 4, current turbine parked

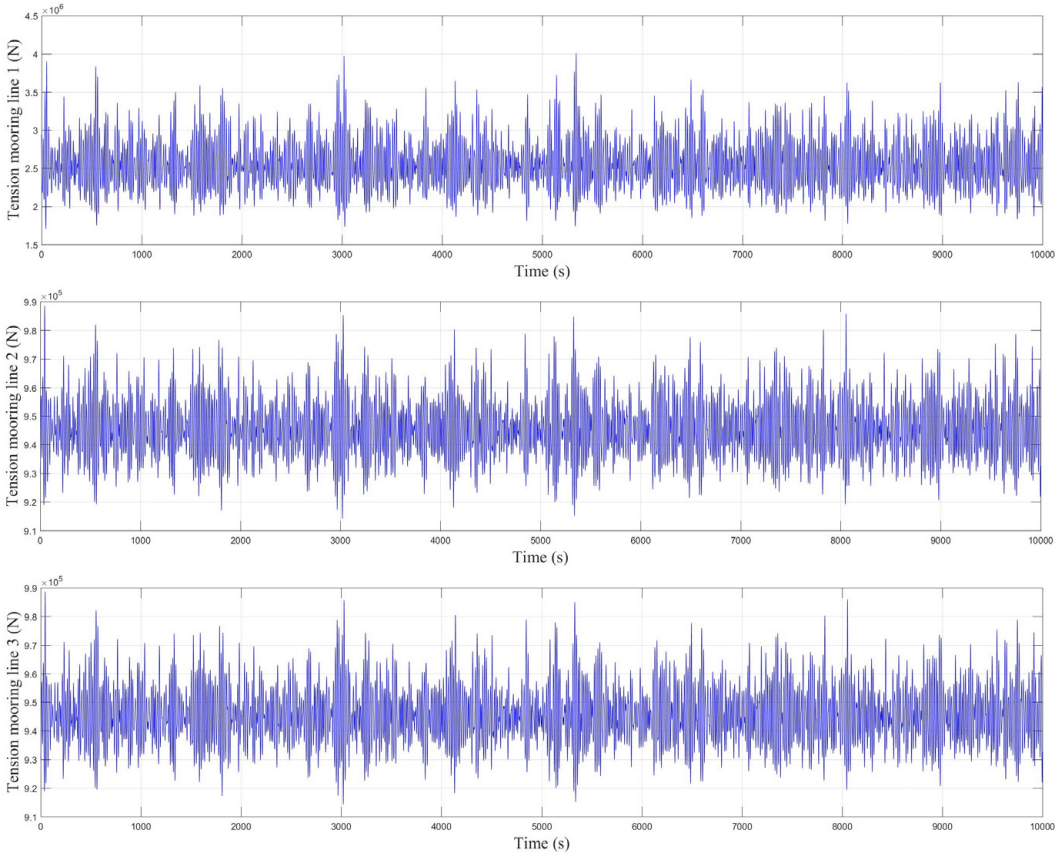

Figure G.2: Tension mooring lines, load case 4, current turbine parked

G.1.2 Current Turbine operational

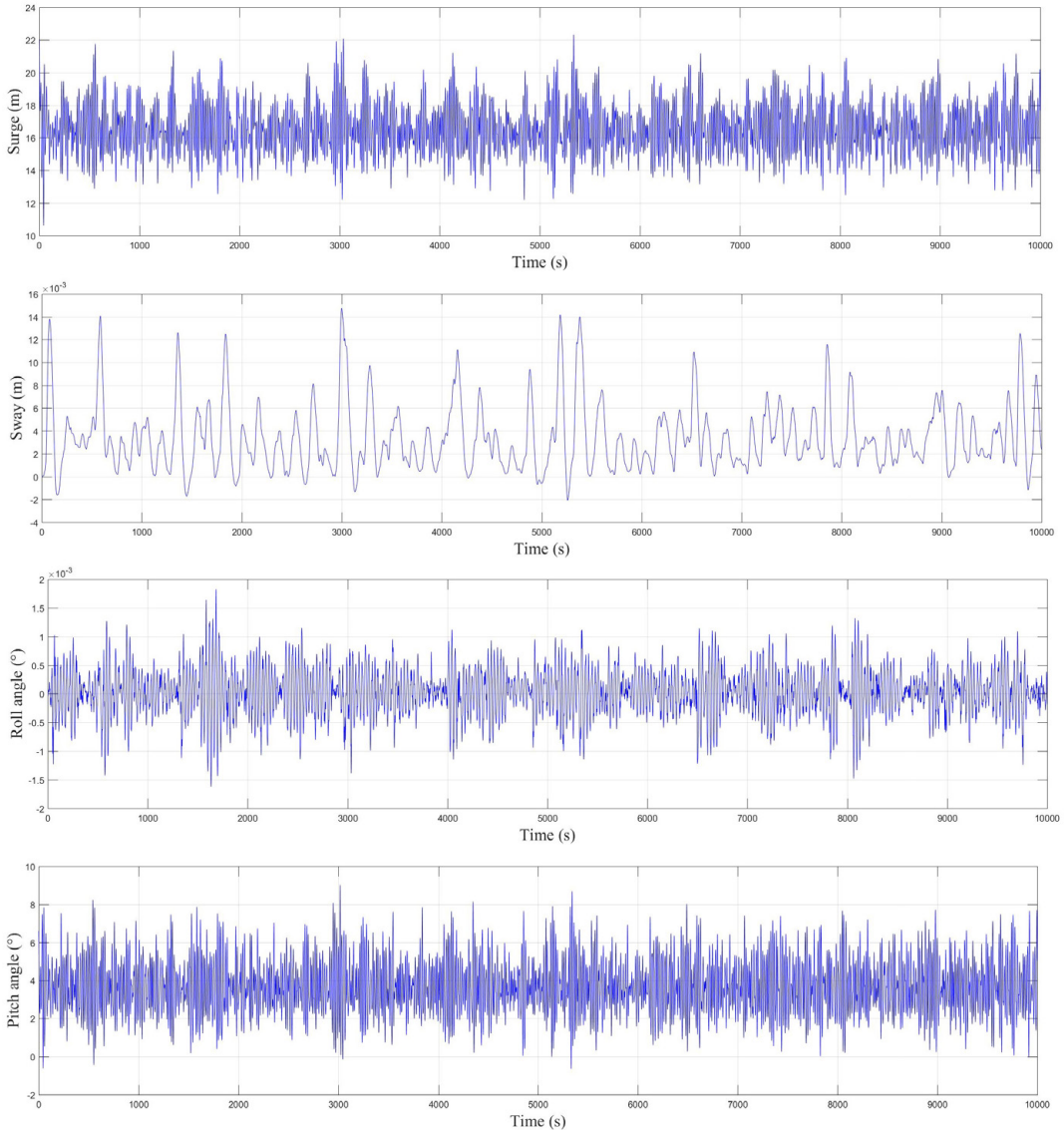

Figure G.3: The motions of the structure, load case 4, current turbine operational

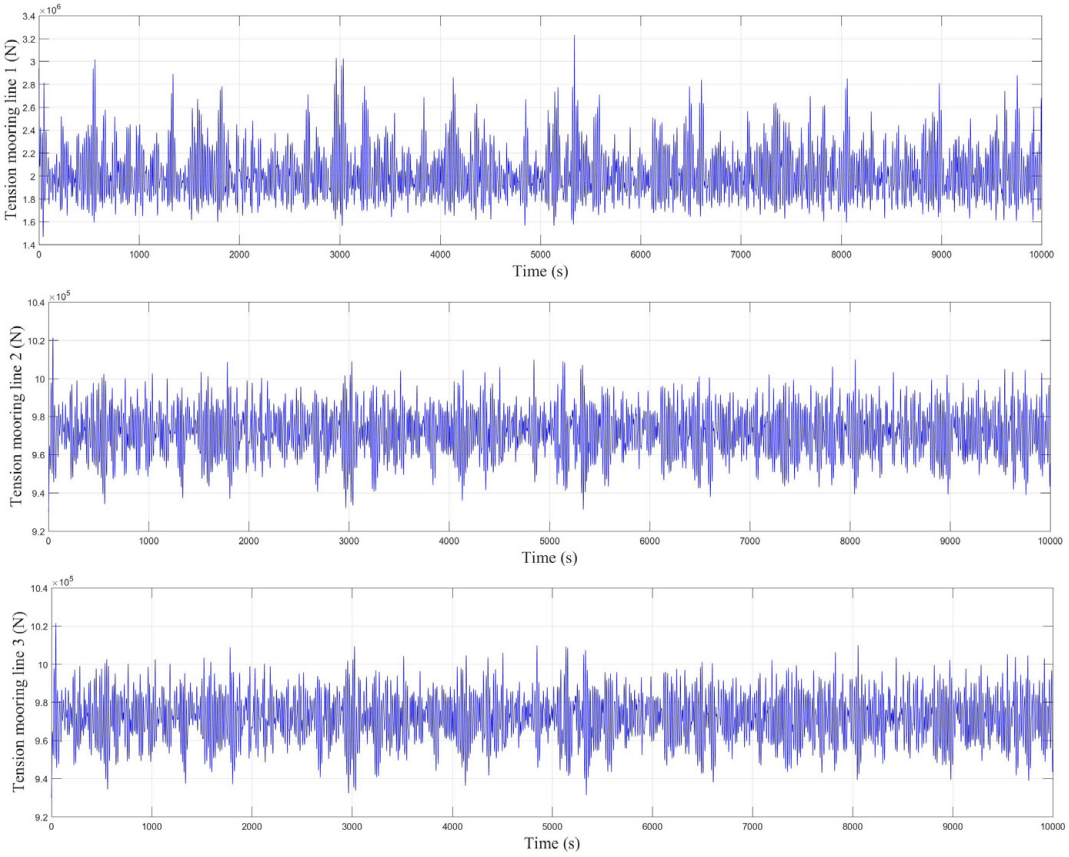

Figure G.4: Tension mooring lines, load case 4, current turbine operational

G.2 Mooring configuration 2

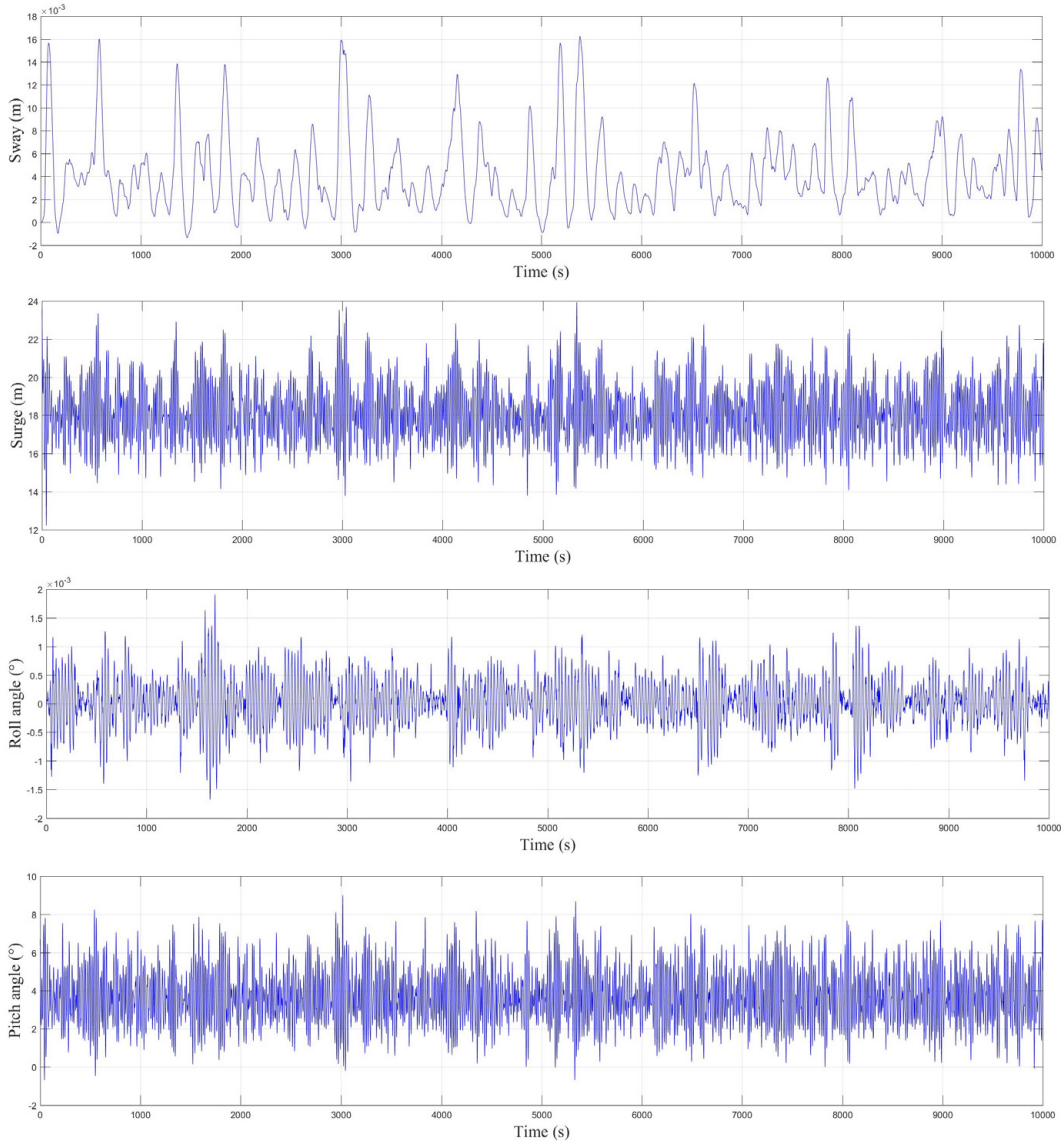

Figure G.5: The motions of the structure, load case 4, current turbine operational

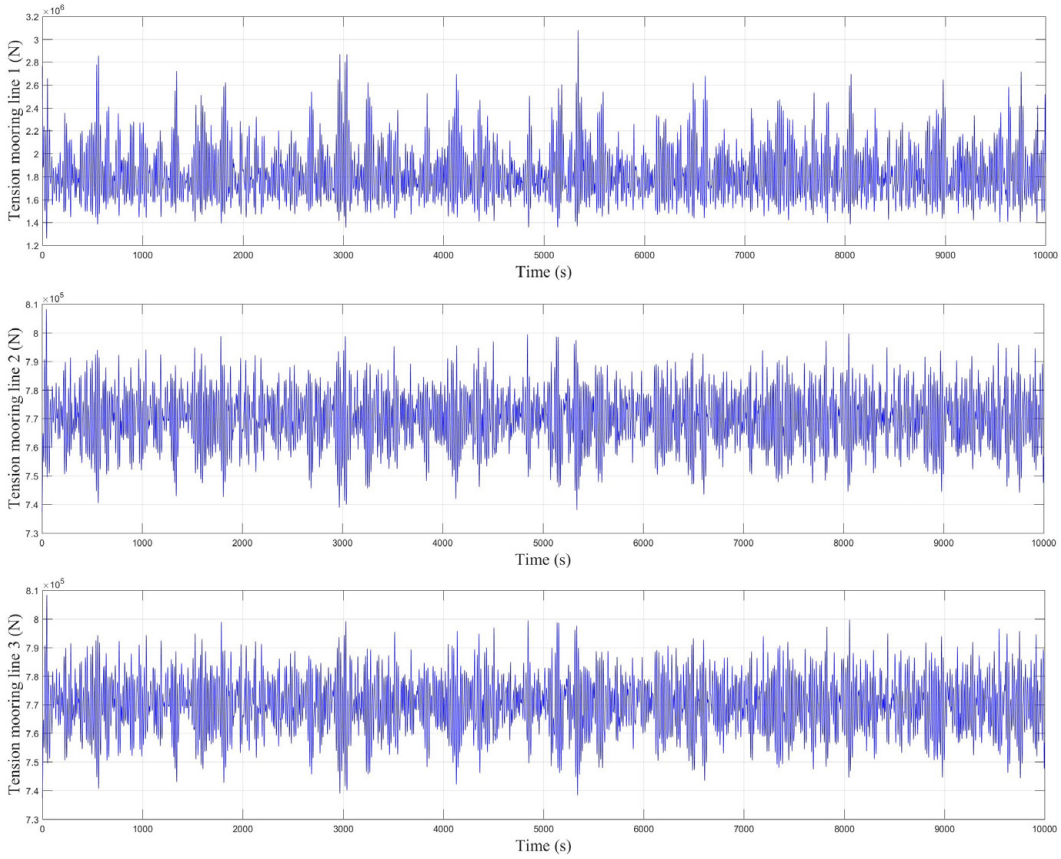

Figure G.6: Tension mooring lines, load case 4, current turbine operational

Appendix H

Levelized Cost of Energy model

In this appendix the calculations of the levelized cost of energy of the reference 5 MW Hywind Spar are compared to the combined 6 MW system. The model used in this appendix is created by the Crown Estate (Howard, 2012), and can be used as a tool to test cost reduction assumptions. The model has some predefined values which are used for this thesis. The expected operational lifetime of the project is 20 years with a discount rate of 8.2%. The preliminary development and construction phase takes 4 years and the decommission time takes 1 year. Which gives a total project time of of 25 years.

H.1 Calculations Original 5MW Spar

		Total	per MW	Phasing (Years)	-4	-3	-2	-1	0
Operational phase									
Decommissioning phase					0	0	0	0	0
CAPEX					3.0%	6.6%	32.8%	27.5%	29.9%
Development and consenting	€		*208,000.00*		56%	10%	11%	11%	12%
Construction phase insurance	€		*50,000.00*		0%	25%	25%	25%	25%
Turbine	€		*1,281,000.00*		0%	0%	19%	39%	42%
Support structure (inc. tower)	€		*888,000.00*		0%	0%	19%	39%	42%
mooring (inc. installation)	€		*182,761.00*		0%	0%	0%	40%	60%
Grid cost	€		*1,097,000.00*		0%	20%	75%	5%	0%
Installation	€		*157,000.00*		0%	0%	0%	36%	64%
Total CAPEX (€)	**€**	**19,318,805.00**	**€ 3,863,761.00**		**€ 582,400.00**	**€ 1,283,713.47**	**€ 6,355,577.07**	**€ 5,328,822.00**	**€ 5,796,050.80**
OPEX				in-warranty%	100%	100%	100%	100%	100%
Operations and maintenance	€		*131,000.00*		0%	0%	0%	0%	0%
Operating phase insurance	€		-		0%	0%	0%	0%	0%
Transmission charges	€		-		0%	0%	0%	0%	0%
Total OPEX (€/MW/annum)	**€**	**655,000.00**	**€ 131,000.00**		**€ -**	**€ -**	**€ -**	**€ -**	**€ -**
Decommissioning									
Phasing									
Total Decommissioning cost (€)	**€**	**530,000.00**	**€ 106,000.00**		**€ -**	**€ -**	**€ -**	**€ -**	**€ -**
Energy Production									
Net energy production per MW (MWh)			**3,854**		3,854	3,854	3,854	3,854	3,854
% energised					0%	0%	0%	0%	0%
NET Annual Energy Production - MWh		**385,400**			-	-	-	-	-
Discount Rate (average over project lifetime)		**8.20%**		Discount factor	1.000	0.961	0.889	0.821	0.759
Discounted Cashflow									
Total CAPEX	€	16,245,440.75		€	582,400.00	€ 1,234,111.69	€ 5,646,952.03	€ 4,375,856.40	€ 4,398,825.87
Total OPEX	€	4,808,833.06		€	-	€ -	€ -	€ -	€ -
Total Decommissioning cost	€	76,861.35		€	-	€ -	€ -	€ -	€ -
Total discounted cashflow	€	21,131,135.15		€	582,400.00	€ 1,234,111.69	€ 5,646,952.03	€ 4,375,856.40	€ 4,398,825.87
Discounted net generation		141,475			-	-	-	-	-
Levelised Cost of Energy		**149.4**	**€/MWh**						

	1	2	3	4	5	6	7	8	9	10
	1	1	1	1	1	1	1	1	1	1
	0	0	0	0	0	0	0	0	0	0
	0.1%									
	1%									
	0%									
	0%									
	0%									
	0%									
	0%									
	0%									
€	**10,400.00**	**€ -**	**€ -**	**€ -**	**€ -**	**€ -**	**€ -**	**€ -**	**€ -**	**€ -**
	100%	100%	100%	100%	100%	100%	100%	100%	100%	100%
	100%	100%	100%	100%	100%	100%	100%	100%	100%	100%
	100%	100%	100%	100%	100%	100%	100%	100%	100%	100%
	100%	100%	100%	100%	100%	100%	100%	100%	100%	100%
€	**655,000.00**	**€ 655,000.00**	**€ 655,000.00**	**€ 655,000.00**	**€ 655,000.00**	**€ 655,000.00**	**€ 655,000.00**	**€ 655,000.00**	**€ 655,000.00**	**€ 655,000.00**
€	**-**	**€ -**	**€ -**	**€ -**	**€ -**	**€ -**	**€ -**	**€ -**	**€ -**	**€ -**
	3,854	*3,854*	*3,854*	*3,854*	*3,854*	*3,854*	*3,854*	*3,854*	*3,854*	*3,854*
	100%	100%	100%	100%	100%	100%	100%	100%	100%	100%
	19,270	19,270	19,270	19,270	19,270	19,270	19,270	19,270	19,270	19,270
	0.701	0.648	0.599	0.554	0.512	0.473	0.437	0.404	0.373	0.345
€	7,294.75	€ -	€ -	€ -	€ -	€ -	€ -	€ -	€ -	€ -
€	459,429.23	€ 424,611.12	€ 392,431.72	€ 362,691.05	€ 335,204.30	€ 309,800.65	€ 286,322.23	€ 264,623.13	€ 244,568.51	€ 226,033.74
€	-	€ -	€ -	€ -	€ -	€ -	€ -	€ -	€ -	€ -
€	466,723.99	€ 424,611.12	€ 392,431.72	€ 362,691.05	€ 335,204.30	€ 309,800.65	€ 286,322.23	€ 264,623.13	€ 244,568.51	€ 226,033.74
	13,516	12,492	11,545	10,670	9,862	9,114	8,424	7,785	7,195	6,650

11	12	13	14	15	16	17	18	19	20	21
1	1	1	1	1	1	1	1	1	1	0
0	0	0	0	0	0	0	0	0	0	1
€ -	**€ -**	**€ -**	**€ -**	**€ -**	**€ -**	**€ -**	**€ -**	**€ -**	**€ -**	**€ -**
100%	100%	100%	100%	100%	100%	100%	100%	100%	100%	0%
100%	100%	100%	100%	100%	100%	100%	100%	100%	100%	0%
100%	100%	100%	100%	100%	100%	100%	100%	100%	100%	0%
100%	100%	100%	100%	100%	100%	100%	100%	100%	100%	0%
€ 655,000.00	**€ 655,000.00**	**€ 655,000.00**	**€ 655,000.00**	**€ 655,000.00**	**€ 655,000.00**	**€ 655,000.00**	**€ 655,000.00**	**€ 655,000.00**	**€ 655,000.00**	**€ -**
									0%	100%
€ -	**€ -**	**€ -**	**€ -**	**€ -**	**€ -**	**€ -**	**€ -**	**€ -**	**€ -**	**€ 530,000.00**
3,854	*3,854*	*3,854*	*3,854*	*3,854*	*3,854*	*3,854*	*3,854*	*3,854*	*3,854*	*3,854*
100%	100%	100%	100%	100%	100%	100%	100%	100%	100%	0%
19,270	19,270	19,270	19,270	19,270	19,270	19,270	19,270	19,270	19,270	-
0.319	0.295	0.272	0.252	0.233	0.215	0.199	0.184	0.170	0.157	0.145
€ -	€ -	€ -	€ -	€ -	€ -	€ -	€ -	€ -	€ -	€ -
€ 208,903.65	€ 193,071.76	€ 178,439.71	€ 164,916.55	€ 152,418.25	€ 140,867.15	€ 130,191.45	€ 120,324.81	€ 111,205.93	€ 102,778.12	€ -
€ -	€ -	€ -	€ -	€ -	€ -	€ -	€ -	€ -	€ -	€ 76,861.35
€ 208,903.65	€ 193,071.76	€ 178,439.71	€ 164,916.55	€ 152,418.25	€ 140,867.15	€ 130,191.45	€ 120,324.81	€ 111,205.93	€ 102,778.12	€ 76,861.35
6,146	5,680	5,250	4,852	4,484	4,144	3,830	3,540	3,272	3,024	-

H.2 Calculations Combined 6 MW System, configuration 1

		Total	per MW	Phasing (Years)	-4	-3	-2	-1	0
Operational phase									
Decommissioning phase					0	0	0	0	0
CAPEX					3.4%	6.3%	31.8%	28.1%	30.5%
Development and consenting			€ *208,000.00*		56%	10%	11%	11%	12%
Construction phase insurance			€ *42,000.00*		0%	25%	25%	25%	25%
Turbine			€ *1,281,000.00*		0%	0%	19%	39%	42%
Support structure (inc. tower)			€ *740,000.00*		0%	0%	19%	39%	42%
mooring (inc. installation)			€ *152,301.00*		0%	0%	0%	40%	60%
Grid cost			€ *914,000.00*		0%	20%	75%	5%	0%
Installation			€ *130,000.00*		0%	0%	0%	36%	64%
Total CAPEX (€)	€	**20,803,806.00**	€ **3,467,301.00**		€ **698,880.00**	€ **1,308,856.16**	€ **6,621,584.19**	€ **5,849,942.40**	€ **6,356,311.23**
OPEX				in-warranty%	100%	100%	100%	100%	100%
Operations and maintenance	€	*150,000.00*			0%	0%	0%	0%	0%
Operating phase insurance	€	-			0%	0%	0%	0%	0%
Transmission charges	€	-			0%	0%	0%	0%	0%
Total OPEX (€/MW/annum)	€	**900,000.00**	€ **150,000.00**		€ -	€ -	€ -	€ -	€ -
Decommissioning									
Phasing									
Total Decommissioning cost (€)	€	**529,999.98**	€ **88,333.33**		€ -	€ -	€ -	€ -	€ -
Energy Production									
Net energy production per MW (MWh)			3,854		*3,854*	*3,854*	*3,854*	*3,854*	*3,854*
% energised					0%	0%	0%	0%	0%
NET Annual Energy Production - MWh		**462,528**			-	-	-	-	-
Discount Rate (average over project lifetime)		**8.20%**		Discount factor	1.000	0.961	0.889	0.821	0.759
Discounted Cashflow									
Total CAPEX	€	17,477,027.61		€ 698,880.00	€ 1,258,282.89	€ 5,883,300.27	€ 4,803,783.63	€ 4,824,027.12	
Total OPEX	€	6,607,556.87		€ -	€ -	€ -	€ -	€ -	
Total Decommissioning cost	€	76,861.34		€ -	€ -	€ -	€ -	€ -	
Total discounted cashflow	€	24,161,445.83		€ 698,880.00	€ 1,258,282.89	€ 5,883,300.27	€ 4,803,783.63	€ 4,824,027.12	
Discounted net generation		169,788		-	-	-	-	-	
Levelised Cost of Energy		**142.3**	**€/MWh**						

	1	2	3	4	5	6	7	8	9	10
	1	1	1	1	1	1	1	1	1	1
	0	0	0	0	0	0	0	0	0	0
	0.1%									
	1%									
	0%									
	0%									
	0%									
	0%									
	0%									
	0%									
€	**12,480.00**	**€ -**	**€ -**	**€ -**	**€ -**	**€ -**	**€ -**	**€ -**	**€ -**	**€ -**
	100%	100%	100%	100%	100%	100%	100%	100%	100%	100%
	100%	100%	100%	100%	100%	100%	100%	100%	100%	100%
	100%	100%	100%	100%	100%	100%	100%	100%	100%	100%
	100%	100%	100%	100%	100%	100%	100%	100%	100%	100%
€	**900,000.00**	**€ 900,000.00**	**€ 900,000.00**	**€ 900,000.00**	**€ 900,000.00**	**€ 900,000.00**	**€ 900,000.00**	**€ 900,000.00**	**€ 900,000.00**	**€ 900,000.00**
€	**-**	**€ -**	**€ -**	**€ -**	**€ -**	**€ -**	**€ -**	**€ -**	**€ -**	**€ -**
	3,854	*3,854*	*3,854*	*3,854*	*3,854*	*3,854*	*3,854*	*3,854*	*3,854*	*3,854*
	100%	100%	100%	100%	100%	100%	100%	100%	100%	100%
	23,126	23,126	23,126	23,126	23,126	23,126	23,126	23,126	23,126	23,126
	0.701	0.648	0.599	0.554	0.512	0.473	0.437	0.404	0.373	0.345
€	8,753.71	€ -	€ -	€ -	€ -	€ -	€ -	€ -	€ -	€ -
€	631,276.81	€ 583,435.13	€ 539,219.16	€ 498,354.12	€ 460,586.06	€ 425,680.28	€ 393,419.85	€ 363,604.30	€ 336,048.34	€ 310,580.72
€	-	€ -	€ -	€ -	€ -	€ -	€ -	€ -	€ -	€ -
€	640,030.52	€ 583,435.13	€ 539,219.16	€ 498,354.12	€ 460,586.06	€ 425,680.28	€ 393,419.85	€ 363,604.30	€ 336,048.34	€ 310,580.72
	16,221	14,992	13,856	12,806	11,835	10,938	10,109	9,343	8,635	7,981

11	12	13	14	15	16	17	18	19	20	21
1	1	1	1	1	1	1	1	1	1	0
0	0	0	0	0	0	0	0	0	0	1
€ -	**€ -**	**€ -**	**€ -**	**€ -**	**€ -**	**€ -**	**€ -**	**€ -**	**€ -**	**€ -**
100%	100%	100%	100%	100%	100%	100%	100%	100%	100%	0%
100%	100%	100%	100%	100%	100%	100%	100%	100%	100%	0%
100%	100%	100%	100%	100%	100%	100%	100%	100%	100%	0%
100%	100%	100%	100%	100%	100%	100%	100%	100%	100%	0%
€ 900,000.00	**€ 900,000.00**	**€ 900,000.00**	**€ 900,000.00**	**€ 900,000.00**	**€ 900,000.00**	**€ 900,000.00**	**€ 900,000.00**	**€ 900,000.00**	**€ 900,000.00**	**€ -**
									0%	100%
€ -	**€ -**	**€ -**	**€ -**	**€ -**	**€ -**	**€ -**	**€ -**	**€ -**	**€ -**	**€ 529,999.98**
3,854	*3,854*	*3,854*	*3,854*	*3,854*	*3,854*	*3,854*	*3,854*	*3,854*	*3,854*	*3,854*
100%	100%	100%	100%	100%	100%	100%	100%	100%	100%	0%
23,126	23,126	23,126	23,126	23,126	23,126	23,126	23,126	23,126	23,126	-
0.319	0.295	0.272	0.252	0.233	0.215	0.199	0.184	0.170	0.157	0.145
€ -	€ -	€ -	€ -	€ -	€ -	€ -	€ -	€ -	€ -	€ -
€ 287,043.18	€ 265,289.44	€ 245,184.33	€ 226,602.89	€ 209,429.66	€ 193,557.91	€ 178,889.01	€ 165,331.80	€ 152,802.04	€ 141,221.85	€ -
€ -	€ -	€ -	€ -	€ -	€ -	€ -	€ -	€ -	€ -	€ 76,861.34
€ 287,043.18	€ 265,289.44	€ 245,184.33	€ 226,602.89	€ 209,429.66	€ 193,557.91	€ 178,889.01	€ 165,331.80	€ 152,802.04	€ 141,221.85	€ 76,861.34
7,376	6,817	6,300	5,823	5,382	4,974	4,597	4,248	3,926	3,629	-

H.3 Calculations Combined 6 MW System, configuration 2

		Total	per MW	Phasing (Years)	-4	-3	-2	-1	0
Operational phase									
Decommissioning phase					0	0	0	0	0
CAPEX					3.4%	6.3%	31.9%	28.0%	30.4%
Development and consenting	€		*208,000.00*		56%	10%	11%	11%	12%
Construction phase insurance	€		*42,000.00*		0%	25%	25%	25%	25%
Turbine	€		*1,281,000.00*		0%	0%	19%	39%	42%
Support structure (inc. tower)	€		*740,000.00*		0%	0%	19%	39%	42%
mooring (inc. installation)	€		*137,348.00*		0%	0%	0%	40%	60%
Grid cost	€		*914,000.00*		0%	20%	75%	5%	0%
Installation	€		*130,000.00*		0%	0%	0%	36%	64%
Total CAPEX (€)	**€**	**20,714,088.00**	**€ 3,452,348.00**		**€ 698,880.00**	**€ 1,308,856.16**	**€ 6,621,353.03**	**€ 5,814,055.20**	**€ 6,302,480.43**
OPEX				in-warranty%	100%	100%	100%	100%	100%
Operations and maintenance	€		*150,000.00*		0%	0%	0%	0%	0%
Operating phase insurance	€		-		0%	0%	0%	0%	0%
Transmission charges	€		-		0%	0%	0%	0%	0%
Total OPEX (€/MW/annum)	**€**	**900,000.00**	**€ 150,000.00**		**€ -**	**€ -**	**€ -**	**€ -**	**€ -**
Decommissioning									
Phasing									
Total Decommissioning cost (€)	**€**	**529,999.98**	**€ 88,333.33**		**€ -**	**€ -**	**€ -**	**€ -**	**€ -**
Energy Production									
Net energy production per MW (MWh)			3,854		*3,854*	*3,854*	*3,854*	*3,854*	*3,854*
% energised					0%	0%	0%	0%	0%
NET Annual Energy Production - MWh			**462,528**		-	-	-	-	-
Discount Rate (average over project lifetime)		**8.20%**		Discount factor	1.000	0.961	0.889	0.821	0.759
Discounted Cashflow									
Total CAPEX	€	17,406,498.74		€	698,880.00	€ 1,258,282.89	€ 5,883,094.88	€ 4,774,314.22	€ 4,783,173.04
Total OPEX	€	6,607,556.87		€	-	€ -	€ -	€ -	€ -
Total Decommissioning cost	€	76,861.34		€	-	€ -	€ -	€ -	€ -
Total discounted cashflow	€	24,090,916.95		€	698,880.00	€ 1,258,282.89	€ 5,883,094.88	€ 4,774,314.22	€ 4,783,173.04
Discounted net generation		169,788			-	-	-	-	-
Levelised Cost of Energy		**141.9**	**€/MWh**						

	1	2	3	4	5	6	7	8	9	10
	1	1	1	1	1	1	1	1	1	1
	0	0	0	0	0	0	0	0	0	0
	0.1%									
	1%									
	0%									
	0%									
	0%									
	0%									
	0%									
	0%									
€	**12,480.00**	**€ -**	**€ -**	**€ -**	**€ -**	**€ -**	**€ -**	**€ -**	**€ -**	**€ -**
	100%	100%	100%	100%	100%	100%	100%	100%	100%	100%
	100%	100%	100%	100%	100%	100%	100%	100%	100%	100%
	100%	100%	100%	100%	100%	100%	100%	100%	100%	100%
	100%	100%	100%	100%	100%	100%	100%	100%	100%	100%
€	**900,000.00**	**€ 900,000.00**	**€ 900,000.00**	**€ 900,000.00**	**€ 900,000.00**	**€ 900,000.00**	**€ 900,000.00**	**€ 900,000.00**	**€ 900,000.00**	**€ 900,000.00**
€	**-**	**€ -**	**€ -**	**€ -**	**€ -**	**€ -**	**€ -**	**€ -**	**€ -**	**€ -**
	3,854	*3,854*	*3,854*	*3,854*	*3,854*	*3,854*	*3,854*	*3,854*	*3,854*	*3,854*
	100%	100%	100%	100%	100%	100%	100%	100%	100%	100%
	23,126	23,126	23,126	23,126	23,126	23,126	23,126	23,126	23,126	23,126
	0.701	0.648	0.599	0.554	0.512	0.473	0.437	0.404	0.373	0.345
€	8,753.71	€ -	€ -	€ -	€ -	€ -	€ -	€ -	€ -	€ -
€	631,276.81	€ 583,435.13	€ 539,219.16	€ 498,354.12	€ 460,586.06	€ 425,680.28	€ 393,419.85	€ 363,604.30	€ 336,048.34	€ 310,580.72
€	-	€ -	€ -	€ -	€ -	€ -	€ -	€ -	€ -	€ -
€	640,030.52	€ 583,435.13	€ 539,219.16	€ 498,354.12	€ 460,586.06	€ 425,680.28	€ 393,419.85	€ 363,604.30	€ 336,048.34	€ 310,580.72
	16,221	14,992	13,856	12,806	11,835	10,938	10,109	9,343	8,635	7,981

11	12	13	14	15	16	17	18	19	20	21
1	1	1	1	1	1	1	1	1	1	0
0	0	0	0	0	0	0	0	0	0	1
€ -	**€ -**	**€ -**	**€ -**	**€ -**	**€ -**	**€ -**	**€ -**	**€ -**	**€ -**	**€ -**
100%	100%	100%	100%	100%	100%	100%	100%	100%	100%	0%
100%	100%	100%	100%	100%	100%	100%	100%	100%	100%	0%
100%	100%	100%	100%	100%	100%	100%	100%	100%	100%	0%
100%	100%	100%	100%	100%	100%	100%	100%	100%	100%	0%
€ 900,000.00	**€ 900,000.00**	**€ 900,000.00**	**€ 900,000.00**	**€ 900,000.00**	**€ 900,000.00**	**€ 900,000.00**	**€ 900,000.00**	**€ 900,000.00**	**€ 900,000.00**	**€ -**
									0%	100%
€ -	**€ -**	**€ -**	**€ -**	**€ -**	**€ -**	**€ -**	**€ -**	**€ -**	**€ -**	**€ 529,999.98**
3,854	*3,854*	*3,854*	*3,854*	*3,854*	*3,854*	*3,854*	*3,854*	*3,854*	*3,854*	*3,854*
100%	100%	100%	100%	100%	100%	100%	100%	100%	100%	0%
23,126	23,126	23,126	23,126	23,126	23,126	23,126	23,126	23,126	23,126	-
0.319	0.295	0.272	0.252	0.233	0.215	0.199	0.184	0.170	0.157	0.145
€ -	€ -	€ -	€ -	€ -	€ -	€ -	€ -	€ -	€ -	€ -
€ 287,043.18	€ 265,289.44	€ 245,184.33	€ 226,602.89	€ 209,429.66	€ 193,557.91	€ 178,889.01	€ 165,331.80	€ 152,802.04	€ 141,221.85	€ -
€ -	€ -	€ -	€ -	€ -	€ -	€ -	€ -	€ -	€ -	€ 76,861.34
€ 287,043.18	€ 265,289.44	€ 245,184.33	€ 226,602.89	€ 209,429.66	€ 193,557.91	€ 178,889.01	€ 165,331.80	€ 152,802.04	€ 141,221.85	€ 76,861.34
7,376	6,817	6,300	5,823	5,382	4,974	4,597	4,248	3,926	3,629	-

Bibliography

Aqwa, ANSYS (2013). *Aqwa Users Manual*. Tech. rep. url: https://cyberships.files.wordpress.com/2014/01/wb_aqwa.pdf.

– (2015). *AQWA Reference Manual*. Tech. rep. October, pp. 724–746. url: https://www.scribd.com/document/339199621/Aqwa-Reference-Manual.

– (2016). *Introduction to Hydrodynamic Analysis with ANSYS Aqwa. Workshop 6.1: Truss Spar Including Drag Linearization*. Tech. rep., pp. 1–49.

Astariz, S., A. Vazquez, and G. Iglesias (2015). "Evaluation and comparison of the levelized cost of tidal, wave, and offshore wind energy". In: *Journal of Renewable and Sustainable Energy* 7.5. issn: 19417012. doi: 10.1063/1.4932154. url: https://aip.scitation.org/doi/10.1063/1.4932154.

Bahaj, A. S. (2011). "Generating electricity from the oceans". In: *Renewable and Sustainable Energy Reviews* 15.7, pp. 3399–3416. issn: 13640321. doi: http://dx.doi.org/10.1016/j.rser.2011.04.032.

Batten, W. M.J. et al. (2007). "Experimentally validated numerical method for the hydrodynamic design of horizontal axis tidal turbines". In: *Ocean Engineering* 34.7, pp. 1013–1020. issn: 00298018. doi: 10.1016/j.oceaneng.2006.04.008. url: https://www.sciencedirect.com/science/article/pii/S0029801806001843?via%3Dihub.

Batten, W.M.J. et al. (2006). "Hydrodynamics of marine current turbines". In: *Renewable Energy* 31.2, pp. 249–256. issn: 09601481. doi: 10.1016/j.egypro.2015.11.419. url: http://linkinghub.elsevier.com/retrieve/pii/S0960148105002314.

CIMAF (2013). *Wire Rope Technical manual*. Tech. rep., p. 62. url: http://www.cimafbrasil.com.br/down/espec_rev3_220413demo.pdf.

Curfs, C. P. M. (2015). *Dynamic behaviour of floating wind turbines. MSc Thesis*. Delft. url: https://repository.tudelft.nl/islandora/object/uuid%3Af339482a-8e0d-4827-85af-c8cf05b4260f?collection=education.

DNV (2011). *Modelling and Analysis of Marine Operations*. Tech. rep. url: https://rules.dnvgl.com/docs/pdf/DNV/codes/docs/2011-04/RP-H103.pdf.

– (2014). *Design of Offshore Wind Turbine Structures*. Tech. rep. url: https://rules.dnvgl.com/docs/pdf/DNV/codes/docs/2014-05/Os-J101.pdf.

ECN (2015). *Kosten wind op ze 2015*. Tech. rep. url: http://vrijehorizon.nl/wp-content/uploads/2016/01/ECN-042015.pdf.

European Commission (2014). *Energy Efficiency and its contribution to energy security and the 2030 Framework for climate and energy policy*. Tech. rep. Brussels: European Commission. url: https://ec.europa.eu/energy/sites/ener/files/documents/2014_eec_communication_adopted_0.pdf.

EWEA (2009). "The Economics of Wind Energy: A report by the European Wind Energy Association". In: *Renewable and Sustainable Energy Reviews* 13.6-7, pp. 1372–1382. issn: 13640321. doi: 10.1016/j.rser.2008.09.004.

GWEC (2016). *Global Wind Report 2016*. Tech. rep. url: http://gwec.net/publications/global-wind-report-2/global-wind-report-2016/.

Hasselmann, K et al. (1973). *Measurements of wind-wave growth and swell decay during the joint north sea wave project*. url: https://repository.tudelft.nl/islandora/object/uuid:f204e188-13b9-49d8-a6dc-4fb7c20562fc.

Homb, H. R. (2013). "Fatigue Analysis of Mooring Lines on the Floating Wind Turbine Hywind Demo". In: June. url: https://brage.bibsys.no/xmlui/handle/11250/2400729.

Howard, R. (2012). *Offshore Wind Cost Reduction Pathways project - Simple Levelised Cost of Energy Model*. url: http://www.thecrownestate.co.uk/media/359601/simple_lcoe_model.xlsx.

IEA (2015). *International levelised cost of energy for ocean energy technologies*. Tech. rep. url: https://www.ocean-energy-systems.org/news/international-lcoe-for-ocean-energy-technology/.

Jonkman, J. M. (2010). *Definition of the Floating System for Phase IV of OC3*. Tech. rep. url: http://scholar.google.com/scholar?hl=en&btnG=Search&q=intitle:Definition+of+the+Floating+System+for+Phase+IV+of+OC3#0.

– (2015). *Explanation additional yaw spring stiffness*. url: https://wind.nrel.gov/forum/wind/viewtopic.php?f=4&t=1357.

Jonkman, J. M. et al. (2009). *Definition of a 5-MW reference wind turbine for offshore system development*. Tech. rep. url: https://www.nrel.gov/docs/fy09osti/38060.pdf.

Jonkman, J. M. et al. (2015). "AeroDyn v15 User's Guide and Theory Manual". In: url: https://nwtc.nrel.gov/system/files/AeroDyn_Manual_V15.04a.pdf.

Journee, J. M. J., W. W. Massie, and R. H. M. Huijsmans (2015). *Offshore Hydromechanics*. Third edit. TU Delft. url: http://www.shipmotions.nl/DUT/LectureNotes/OffshoreHydromechanics.pdf.

Karimirad, M. (2011). "Stochastic Dynamic Response Analysis of Spar-Type Wind Turbines with Catenary or Taut Mooring Systems". PhD thesis. NTNU. isbn: 9788247125267. url: https://www.researchgate.net/publication/277017299_Stochastic_dynamic_response_analysis_of_spar-type_wind_turbines_with_catenary_or_taut_mooring_systems.

Karimirad, M. and T. Moan (2012). "Wave-and Wind-Induced Dynamic Response of a Spar-Type Offshore Wind Turbine". In: *Journal of Waterway, Port, Coastal, and Ocean Engineering* 138.1, pp. 9–20. doi: 10.1061/(ASCE)WW.1943-5460. url: http://scholar.google.com/scholar?hl=en&btnG=Search&q=intitle:Wave-+and+Wind-Induced+Dynamic+Response+of+a+Spar-Type+Offshore+Wind+Turbine#0.

Khair Al-Solihat, M. and M. Nahon (2015). "Nonlinear Hydrostatic Restoring of Floating Platforms". In: *Journal of Computational and Nonlinear Dynamics* 10.4, p. 041005. url: http://computationalnonlinear.asmedigitalcollection.asme.org/article.aspx?doi=10.1115/1.4027718.

Kumar, Y. et al. (2016). "Wind energy: Trends and enabling technologies". In: *Renewable and Sustainable Energy Reviews* 53, pp. 209–224. issn: 18790690. doi: 10.1016/j.rser.2015.07.200.

Lankhorst Ropes (2014). *Offshore Steel Wire Ropes*. Tech. rep. url: http://www.lankhorstropes.com/files/uploads/Offshore/brochures/Steel_Wire_Rope_brochure__72dpi____April_2014.pdf.

– (2018). *Personal correspondence between Rodrigo Oliveira Sá from Lankhorst Ropes and Joeri Haaker on the cost of mooring lines*.

Magagna, D. and A. Uihlein (2015). "Ocean energy development in Europe: Current status and future perspectives". In: *International Journal of Marine Energy* 11, pp. 84–104. issn: 22141669. doi: 10.1016/j.ijome.2015.05.001. url: http://dx.doi.org/10.1016/j.ijome.2015.05.001.

Male, P. van der (2017). *Offshore Wind Farm Design, Aerodynamic Loading*. url: https://ocw.tudelft.nl/courses/offshore-wind-farm-design/.

MSL (2001). "Appraisal of API RP 2FPS (Recommended practice for planning, designing and constructing floating production systems)". In: *Uk Hse Offshore Technology Report 2001/006*. url: http://www.hse.gov.uk/research/otopdf/2001/oto01006.pdf.

Musial, W. et al. (2004). "Feasibility of Floating Platform Systems for Wind Turbines". In: ASME 2004 Wind Energy Symposium, 476–486. url: https://www.nrel.gov/docs/fy04osti/34874.pdf.

Myhr, Anders et al. (2014). *Levelised cost of energy for offshore floating wind turbines in a lifecycle perspective*. Tech. rep., pp. 714–728. doi: 10.1016/j.renene.2014.01.017. url: http://dx.doi.org/10.1016/j.renene.2014.01.017.

NASA (2015). *Shape effects on drag*. url: https://www.grc.nasa.gov/WWW/k-12/airplane/shaped.html.

NREL (2017). *National Renewable Energy Laboratory*. url: https://www.nrel.gov/about/mission-programs.html.

NZ Electricity Commission (2005). "An Appraisal of New and Renewable Generation Technologies as Transmission Upgrade Alternatives". In: December. url: https://www.ea.govt.nz/dmsdocument/4687.

Ocean Energy Europe (2017). *Ocean energy project spotlight: Investing in tidal and wave energy*. url: https://www.oceanenergy-europe.eu/wp-content/uploads/2017/06/170228-Ocean-energy-spotlight-final.pdf.

Oh, Im Sang and Yoo Yin Kim (1992). *Wave characteristics changes under a strong tidal current influence*. url: http://www.sfjo-lamer.org/la_mer/30-3/30-3-18.pdf.

Pierson, W. J. and L. Moskowitz (1963). *A proposed spectral form for fully developed wind seas based on the similarity theory of S.A. Kitaigiridskii*. url: http://www.dtic.mil/dtic/tr/fulltext/u2/421610.pdf.

Sale, D. C. (2010). *HARP_Opt User's Guide*. Tech. rep. url: https://nwtc.nrel.gov/system/files/HARP_Opt.pdf.

Statoil (2008). *Hywind floating offshore wind turbine, Siemens 2.3 MW in North Sea, Norway. Used as cover photo.* url: https://www.sierraclub.org/sites/www.sierraclub.org/files/sce-authors/u2175/17097556_1433846703353003_1550947939394088014_o.jpg.

– (2017). *World's first floating wind farm has started production*. url: https://www.statoil.com/en/news/worlds-first-floating-wind-farm-started-production.html.

Steen, K. E. (2015). *Hywind Scotland - status and plans*. Tech. rep. url: https://www.sintef.no/globalassets/project/eera-deepwind-2015/presentations/closing/rune-yttervik_statoil.pdf.

UNFCCC (2015). *Paris Agreement*. Tech. rep. url: http://unfccc.int/paris_agreement/items/9485.php.

Velema, J. (2010). *On the Tidal Dynamics of the North Sea. MSc Thesis*. Twente. url: https://www.utwente.nl/en/et/wem/education/msc-thesis/2010/velema.pdf.

VGB PowerTech (2015). "Levelised Cost of Electricity 2015". In: url: https://www.vgb.org/lcoe2015.html?dfid=74042.

Vijfhuizen, W. (2008). *Design of Wind and Wave Power Barge. MSc Thesis*. Strathclyde. url: https://www.strath.ac.uk/.

Viré, A. (2016). *Introduction to Wind Energy, Aerodynamic theory, TU Delft*. url: http://studiegids.tudelft.nl/a101_displayCourse.do?course_id=42218.

WindEurope (2017). *Floating Offshore Wind Vision Statement*. Tech. rep. url: https://windeurope.org/wp-content/uploads/files/about-wind/reports/Floating-offshore-statement.pdf.

Zaaijer, Michiel (2017). *Introduction to Wind Energy , Strength and fatigue*. Delft. url: https://ocw.tudelft.nl/courses/offshore-wind-farm-design/?view=lectures.